FACTOR GRAPH-BASED GEOLOCATION TECHNIQUES FOR POSITION DETECTION OF UNKNOWN RADIO WAVE EMITTERS

MUHAMMAD REZA KAHAR AZIZ

in partial fulfillment of the requirements
for the degree of
Doctor of Philosophy

School of Information Science
Japan Advanced Institute of Science and Technology

June, 2016

Supervised by
Professor Tadashi Matsumoto

Reviewed by
Professor Jun-ichi Takada
Professor Takeo Ohgane
Professor Xiaobo Zhou
Professor Brian Michael Kurkoski
Professor Yuto Lim

ISBN 978-4-903092-46-1 (Paperback)

Abstract

Wireless geolocation techniques are of crucial importance for current and future dense wireless networks to support location-based services and applications requiring high accuracy. One of the challenging problems in wireless geolocation is to estimate the position of an unknown (anonymous) radio wave emitter. The location detection of unknown radio emitter is very important especially for helping people in disastrous situations; such as, finding the victims who are buried due to landslide, tsunami, and/or earthquake. It is also important for monitoring illegal radio emitter to prevent public broadcasting from being jammed.

In this research, factor graph-based techniques for geolocation techniques are considered the most promising candidates having several benefits; namely, (i) it decomposes the complex problem with many variables into a set of simple sub-problems with fewer variables, (ii) it operates in the form of mean and variance messages under the Gaussianity assumption of the measurement error, and (iii) it also requires only solving linear equations resulting significant reduction in computational complexity. It should be noticed that low computational complexity is of great importance for green technology to save the energy consumption. Furthermore, high accuracy is achieved by the factor graph because it effectively and efficiently performs statistical signal processing for probability marginalization.

The primary objective of this research is to propose novel algorithms of high accuracy and low complexity wireless geolocation techniques, based on the factor graph technique, to detect non-moving (static) position of a single unknown (anonymous) radio wave emitter. However, it should be emphasized that the proposed technique is not only applicable for unknown radio wave emitter, but also for general radio wave emitter position detections. In this research, three propagation parameters, i.e., direction of arrival (DOA), time difference of arrival (TDOA), and differential received signal strength (DRSS) are proposed, and their corresponding factor graph geolocation techniques are derived. Those techniques are suitable for solving the problems arising in each scenario for detecting the static position of single radio wave emitter.

In the presence of imperfect time synchronization with line-of-sight (LOS) condition, the DOA-based geolocation technique is known to be the best solution to the single static location detection. We consider factor graph geolocation technique, where the input is the samples of DOA measurement results sent from the sensors. This research proposes DOA-based factor graph (DOA-FG) with linear approximation of the tangent function so-called Taylor series DOA-FG (TS-DOA-FG), where the first order Taylor series expansion of the tangent is taken into account. It is shown that the accuracy of the DOA-FG geolocation algorithm can be improved by introducing approximated expressions for the mean and variance of the tangent and cotangent functions.

The TDOA-based geolocation techniques are known to be the most suitable solution in the presence of perfect time synchronization among the sensors. The proposed new technique, so-called Pythagorean TDOA-based factor graph (P-TDOA-FG), requires much less computational complexity compared to the conventional TDOA-based factor graph techniques employing hyperbolic function (H-TDOA-FG). The great improvement is due to the use of simple Pythagorean function, which is widely used in TOA-based geolocation techniques. The function is considered for the use of the conventional time of arrival (TOA)-based factor graph technique (TOA-FG). However, in practice, it is impossible for the TOA-based location identification techniques including the conventional TOA-FG to detect the position of the unknown target. This is because the TOA measurements require the knowledge of the absolute departure time of the signal, and this knowledge is unavailable.

The proposed P-TDOA-FG introduces several sets of new nodes and expressions into the conventional TOA-FG technique to convert the TDOA information from the measurements to the *equivalent* TOA information. The TDOA measurements do not require the knowledge of the absolute departure time information of the measured signal sent from the target. Hence, the *equivalent* TOA can be utilized in the modified TOA-FG to detect the position of the unknown target. The results have shown that the proposed P-TDOA-FG improves the accuracy of the conventional TOA-FG technique.

On the other hand, neither RSS-based nor DRSS-based geolocation techniques require the perfect time synchronization among the sensors and as well as between the target and sensors, array antenna, and knowledge of the absolute departure time of the signal sent from the target. In such conditions, the RSS and DRSS-based geolocation techniques are believed to be the most promising solution for the geolocation detection. However, the

conventional RSS-based factor graph RSS-FG) technique can not estimate the position of an unknown radio emitter because the technique requires the knowledge of the absolute value of the transmit power. Nevertheless, in practice, the transmit power information from the signal transmitted by the unknown target emitter is unavailable. It should be noticed that the knowledge of the transmit power is necessary for calibration/reference of linear approximation process using training signal sent from the monitoring spots. Thus, the DRSS-based factor graph (DRSS-FG) technique is proposed to solve the problem, where the necessity for the knowledge of the absolute transmit power of unknown target is eliminated. Hence, the DRSS-FG can estimate the unknown target.

Closed-form expression of the Cramer Rao lower bound (CRLB) taking into account of the number of samples, for DOA- and TOA- geolocation techniques, are also derived in this dissertation. An approximated CRLB taking into account of the number of samples, for TDOA-based technique, is also derived. The performance of the proposed technique is evaluated in terms of root-mean-square error (RMSE). The results show that the proposed techniques accurately estimate the location of unknown target, while they requires low computational complexity. It is shown that all of our proposed techniques achieve much higher accuracy compared to the conventional techniques. The achieved RMSE with the proposed techniques are also evaluated and found to be very close to the CRLB.

Keywords: Wireless Geolocation, Factor Graphs, DOA, TDOA, DRSS, TOA, RSS, CRLB, Voronoi Diagram, Unknown Radio Wave Emitter, Single Static Target

Acknowledgments

The research work presented in this Doctoral Dissertation has been supported, in part, by Doctor Research Fellow (DRF) of JAIST, and in part, by Koden Electronics Co., Ltd, Japan.

Contents

List of Figures

List of Tables

Symbols and Abbreviations

$(.)^T$	Transpose function
$(.)^{-1}$	Inverse matrix
$(.)_{\rightarrow}$	The direction of message flow in the FG
$(.)_m$	monitoring spot index
$(\cdot)_h$	Sensor index in general
$(\cdot)_i$	Sensor index in general. Primary sensor index for the case of DRSS- and TDOA-based factor graph techniques
$(\cdot)_j$	Secondary sensor index
$(\cdot)_k$	Sample index
$(\cdot)_{i,j,k}$	With the i-th and j-th sensors, and k-th sample
$(\hat{x}, \hat{y})$	Target position estimate
(x, y)	Target position
(X_i, Y_i)	Sensor position with i-th sensor
$\frac{\partial\theta}{\partial\mathbf{x}}$	The first derivation of θ over $\mathbf{x}$
$\hat{\theta}$	DOA sample
$\hat{d}_{i,j}$	Difference Euclidean distance sample, corresponding to true TDOA, between sensor i to target and sensor j to target
$\hat{P}_w$	RSS sample measurement in watt
$\mathbf{\Sigma}_\theta$	Gaussian covariance for DOA measurement error
$\mathbf{\Sigma}_d$	Gaussian covariance for TDOA measurement error

$\mathbf{\Sigma}_r$	Gaussian covariance for TOA measurement error
$\mathbf{A}$	A matrix in general
$\mathbf{A}_\theta$	Matrix for DOA-LS
$\mathbf{b}_\theta$	Vector for DOA-LS
$\mathbf{F}(\mathbf{x})$	FIM matrix
$\mathbf{J_{TDOA}}$	Jacobian matrix of TDOA
$\mathbf{J_{TOA}}$	Jacobian matrix of TOA
$\mathbf{J}$	Jacobian matrix
$\mathbf{X}$	Sensor position vector
$\mathbf{x}$	Target position vector
$\mathbf{Y}$	Monitoring spot position vector
σ_d^2	Variance of TDOA corresponding to the difference Euclidean distance
σ_r^2	Variance of TOA corresponding to the Euclidean distance
σ_θ^2	Variance of DOA measurement error
σ_d^2	Variance of measurement error of the Euclidean distance corresponding to TDOA
$\sigma_{P_w}^2$	Variance of measurement error of RSS in watt
σ_θ	Standard deviation of DOA measurement error
σ_d	Standard deviation of measurement error of the Euclidean distance corresponding to TDOA
σ_{P_w}	Standard deviation of measurement error of RSS in watt
$\sum_{\sim x_1}$	The summary operator for x_1
$\mathbf{I}_N$	$N \times N$ Identity matrix
θ	True DOA

$d_{i,j}$	True difference Euclidean distance, corresponding to true TDOA, between sensor i to target and sensor j to target
$f_A(.)$	Local function at factor node A
f_c	Carrier frequency
$g(.)$	Global function
K	Total samples
m_m	Matrix dimension index
N	Total number of sensors
n	Path-loss exponent
n_m	Matrix dimension index
n_θ	DOA measurement error
n_d	Difference Euclidean distance measurement error corresponding to TDOA
n_{P_w}	RSS measurement error in watt
$p(.)$	Probability density function
p_m	Matrix dimension index
P_{v_i}	A set of Voronoi points
P_w	True RSS in watt
r_0	denotes reference distance
r_i	Euclidean distance between target and sensor i
$r_{i,j}$	Euclidean distance between sensors i and j
RSS-FG	RSS-based factor graph geolocation technique
RSS-V	RSS-based Voronoi geolocation technique
CRLB	Cramer Rao Lower Bound
DOA	Direction of Arrival

DOA-FG	DOA-based factor graph
DRSS-FG	DRSS-based factor graph geolocation technique
E-911	Emergency or Enhanced 911
FCC	Federal Communications Commission
FG-GN	Factor Graph Gauss-Newton
FIM	Fisher Information Matrix
GPS	Global Positioning System
LOS	Line-of-sight
LS	Least Squares
MOM	Method of Moments
NLSS	Non-linear Least Square
P-TDOA-FG	Pythagorean TDOA-based factor graph geolocation technique
pdf	probability density function
RMSE	Root Mean Square Error
RSS	Received Signal Strength
SNR	Signal to Noise Ratio
TDOA	Time of Difference Arrival
TOA	Time of Arrival
TOA-FG	TOA-based factor graph geolocation technique
TS-DOA-FG	Taylor series DOA-based factor graph
WSN	Wireless Sensor Newtorks

Chapter 1

Introduction

1.1 Motivation and Method

1.1.1 Wireless Geolocation Overview

Accurate wireless geolocation has been recognized as a key technology with significant importance to supporting various location-related services and applications which require the capability of detecting the location [1–5]. Moreover, it is also expected to play important roles when location-based services are to be in practical operations on the basis of the current systems and wireless communication systems of the future [6, 7]. Wireless geolocation is defined as the process to compute the accurate geographical coordinates of radio wave emitters location by observing the precise measurement results of electromagnetic wave properties of the signal sent from the emitters. The measurements are performed by spatially separated number of sensors and/or receivers. This process is also known as positioning system, localization, and navigation [8, 9].

It should be noticed that research in global positioning system (GPS) started over four decades ago [10]. However, this research topic has attracted considerable attention over the past two decades [11–13]. This is because since 1996, U.S. Federal Communications Commission (FCC) issued the requirement of the location identification capability for Emergency 911 (E-911) applied in any wireless communication networks [14–16]. Hence, the research activity in the geolocation field has substantially increased.

In the future, high speed processing capability is required for designing dense wireless networks. This is because various services are supposed to be provided by the future mobile wireless systems. Several services

may require heavy computational complexity. Hence, geolocation-based services should not require heavy computational burden. Furthermore, high accuracy is required in wireless geolocation because it plays crucial roles to provide location-related services and applications in many aspects of human life.

The geolocation techniques are of great importance in commercial aspects, to support the location-based services and applications such as automated and location-sensitive billing [5, 6, 11, 17–19], package and parcel, cargo, and personnel tracking [5, 20], mobile yellow pages [5, 11], interactive map consultation [19], and resource management [6, 14]. Furthermore, these techniques are momentous for enabling the intelligent transport systems [11, 19] such as the vehicle navigation [6], traffic information, vehicle and fleet tracking [5, 20], accident reporting, and roadside assistance [20]. Also, in the health care and civilian services we need the position detection capability for tracking of patients requiring special care, mentally impaired people, and the elderly and/or young children [18–21].

In public safety and military applications [4, 21, 22], the wireless geolocation techniques play crucial roles to activate many services such as Emergency or Enhanced-911 (E-911) [5, 6, 11, 14, 17–19, 23, 24], fraud detection [6, 11, 17, 20, 23, 24], tracking and navigating of emergency-rescue personnel, policemen, firefighters, and soldiers in their missions [18, 21, 25]. Moreover, the location identification capability is the key to enabling the technologies, e.g., precision mobile communication networks planning [20], deployment of wireless sensor networks (WSN) supporting a variety of applications [26–30], navigating beam-forming for wireless charging [31], biologic systems [4], environment monitoring, and precision agriculture[1] [25].

Besides those described above, one of the challenging problems in wireless geolocation is to estimate the position of unknown (anonymous)[2] radio wave emitter. The location detection of unknown radio emitter is very important in helping people in disastrous situations, e.g., finding the victims who are buried due to landslide, tsunami, and/or earthquake. It is also important for detecting and identifying the presence of illegal radio emitters because of the significant increase in radio wireless communications deployment nowadays [33]. Hence, we have to seriously secure the wireless and mobile networks by geolocation detection and identification of any malicious radio wave attackers, wireless jamming, and dangerous

[1]The example of the use of geolocation techniques for precision agriculture is to observe the potentially infected zones, hence we can identify the plant disease [32].

[2]The terminology "anonymous" is omitted in the rest of the dissertation for simplicity.

intruder [34]. Those attacks tend to threaten major social events such as Olympic games and other major events. These events use wireless communication networks for several purposes, such as, broadcasting the event scenes to the public, coordination between personnel, communication among visitors, and other activities.

The primary objective of this research is to propose novel algorithms of high accuracy and low complexity wireless geolocation algorithms to detect position of a single static unknown radio wave emitter. The unknown radio wave emitter is defined as the anonymous device emitting radio wave where the sensors/receivers have no any knowledge regarding the emitter. The knowledge can be as follows: (1) There is no synchronization between the target and sensors, (2) the absolute knowledge of transmit power and time of departure of the signal are unavailable, and others. The example of unknown radio emitter can be an illegal radio or pirate radio. This problem is also known as passive radio positioning systems [35, 36]. However, it should be emphasized that the proposed techniques are not only applicable for position detection of unknown radio wave emitter, but also for known radio wave emitter in general. It should be noticed that neither the terminology of "known" nor "unknown" refers to the positions of the radio wave emitter.

1.1.2 Factor Graph-based Geolocation Tehniques

Factor graph for geolocation is considered as one of the most promising candidates. This is because the factor graph has several benefits that enable great reduction in computational complexity; because, (1) it provides a natural graphical description of the factorization of a global multivariate function into a product of several local functions, hence, it decomposes the complex problem with many variables into a set of simple sub-problems with fewer variables, (2) The message passing takes place among the nodes in the factor graph where the messages are expressed in the form of only the means and variances, owing to the Gaussianity assumption of the measurement error, (3) In most cases, the factor graph-based geolocation technique requires only solving linear functions, by which the Gaussianity assumption always holds. It should be noticed that low computational complexity is of great importance for green technology to save the energy consumption Nevertheless, high accuracy is achieved by the factor graph because it effectively and efficiently performs statistical signal processing by iteratively exchanging the messages among the nodes according to sum-product algorithm for the probabil-

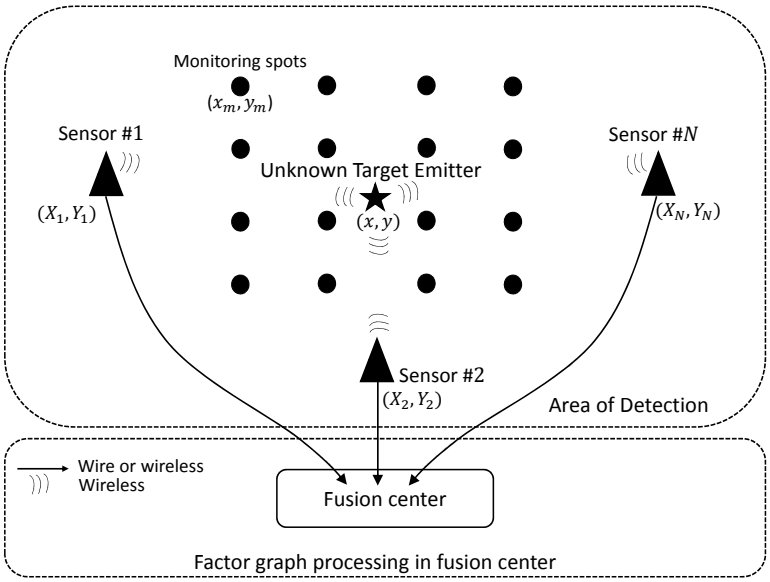

Figure 1.1. Basic structure of measured parameter-based factor graph geolocation techniques with $N = 3$ sensors consisting of a single static unknown radio wave emitter, 4 monitoring spots (monitoring spots are only required for the conventional RSS-FG and the proposed DRSS-FG technique).

ity marginalization. Since the factor graph visualizes the process of the behavior of the message passing for the probability marginalization, new view of the processing structure will likely be created to improve performance of the algorithms/techniques [4, 17, 18, 23, 37, 38].

1.2 Related Work

The use of the factor graph has been used in wireless geolocation techniques since past decade.[3] In 2003, the first geolocation technique by using the factor graph algorithm was introduced in [39], which was a few years after the mathematical framework of the factor graph was first introduced in [37]. Currently, several factor graph techniques have been developed with different types of measured parameters such as time of ar-

[3]In this dissertation, the position identification using factor graph is simply referred to as factor graph technique. The term "techniques" in this dissertation refer to "geolocation technique" except specified.

rival (TOA) [3,5,17,19], direction of arrival (DOA)[4] [4,23], time difference of arrival (TDOA) [6], and received signal strength (RSS) [18], with the aim of detection of radio wave emitter location.

The basic structure of factor graph-based techniques is shown in Fig. 1.1. The sensors measure the signal sent from a single static unknown radio wave emitter. The DOA, TOA, and RSS samples can be processed in the sensor, however, as a consequence, the sensors require the capability for processing. Alternatively, the measured signal is directly sent to the fusion center. In this case, the process to obtain the measured samples is performed at the fusion center. While, the TDOA and difference received signal strength (DRSS) samples to be processed in the fusion center because the processing requires the difference of TOA and RSS samples, respectively, between two sensors. After the measured parameter samples are obtained, the factor graph algorithm is performed in the fusion center to estimate the position of the unknown target. It should be noticed that technical details of the measurement process is not discussed in this research because it is out of scope.

However, it is impossible for the TOA-based factor graph technique identification techniques in [5, 17, 19] to detect the position of the unknown target because absolute departure time of the unknown signal is unavailable. As shown in Fig. 1.2, TOA measurements need the knowledge of absolute departure time of the signal[5]. Furthermore, the conventional received signal strength (RSS)-based factor graph technique (RSS-FG) in [18] cannot estimate the position of an unknown radio emitter because the knowledge of absolute value of the transmit power is also unavailable. In practice, however, the transmit power information from the signal transmitted by the unknown target emitter is unavailable. It should be noticed that the knowledge of the transmit power is necessary for calibration/reference of linear approximation process using training signal sent from the monitoring spots.[6] For clarity, the configuration of monitoring spots can be seen in Fig. 1.1.

The conventional DOA-based factor graph (DOA-FG) techniques in [23] has incorrect expression as explained in [17]. Furthermore, the expression in another conventional DOA-FG [4] is not provided in complete

[4]In this dissertation, we use terminology DOA instead of Angle of Arrival (AOA) for better expression.

[5]Absolute departure time of the signal is also known as time of departure (TOD). This information can be extracted from the time stamp (if available) in the signal transmitted by the target.

[6]In this dissertation, monitoring spot is used instead of training point in [18] for better expression.

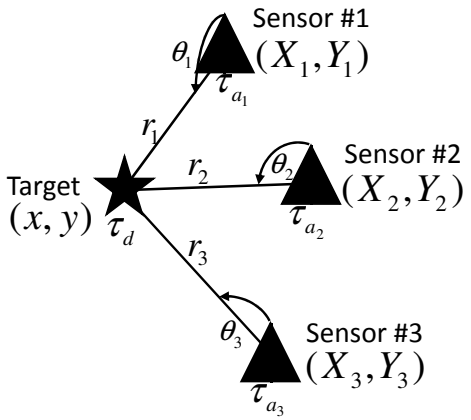

$$i = 1,2, \dots, N$$

$$j = 2,3, \dots, N$$

$$\theta_i = \tan^{-1}\left(\frac{Y_i - y}{X_i - x}\right)$$

$$\tau_i = \tau_{a_i} - \tau_d$$

$$\tau_{i,j} = \tau_{a_i} - \tau_{a_j}$$

$$r_i = v_c \cdot \tau_i$$

$$r_i = \sqrt{(X_i - x)^2 + (Y_i - y)^2}$$

Figure 1.2. General insight of the measurement parameters in wireless geolocation. θ_i denoting the DOA in i-th sensor, i, $i = 1, 2, ..., N$, denoting the sensor index or the primary sensor index, j, $j = 2, 3, ..N$, denoting the secondary sensor index, N denoting number of sensors in total, τ_i denoting the TOA in i-th sensor, $\tau_{i,j}$ denoting the TDOA between i-th primary sensor and j-th secondary sensor, v_c denoting velocity of the light $3 \cdot 10^8$ m/s, r denoting the Euclidean distance, (x, y) denoting the target position, and (X_i, Y_i) denoting the sensor position. It should be noticed that the τ_d is unavailable in the signal sent from unknown radio emitter.

form. The detailed discussion of conventional DOA-FG can be found in Chapter 2. Moreover, the conventional TDOA-based factor graph technique in [6] requires high computational complexity. This is because the conventional technique performs twice conversion as the initial process; i.e., (i) the conversion of TDOA values and known sensor positions into hyperbolic functions, then (ii) the conversion of hyperbolic functions into general quadratic equations. It also involves the use of rotation, shifting, and mapping equations for iteration process. More detailed explanation of that conventional TDOA-based technique will be given in Chapter 2.

The problems described above have motivated us to develop several new factor graph-based algorithms to detect the position of a single static unknown radio emitter. In this work, three propagation parameters, DOA, TDOA, and DRSS are considered when developing their corresponding factor graph geolocation techniques, as summarized in Table. 1.1. These proposed techniques are suitable for solving problems arising in each scenario for detecting the position of a single static unknown radio wave emitter.

DOA samples can be measured using either antenna arrays or directional antenna [40, 41] without requiring perfect synchronization, time

Table 1.1. The Conventional vs. Proposed Factor Graph-Based Techniques.

Measured parameters	Motivation towards developing new techniques	Proposed solution
DOA	Incorrect expression in [23] and incomplete expression in [4]	TS-DOA-FG [42]
TOA	Unable to detect the position of unknown target [5, 17, 19]	P-TDOA-FG
TDOA	High computational complexity due to hyperbolic conversion [6]	
RSS	Unable to detect the position of unknown target [18]	DRSS-FG [43]
DRSS	Not found in literature	

stamp[7], or transmit power information of a single static unknown radio wave emitter. In such condition, the factor graph geolocation technique is considered, where the input is the samples of DOA measurement results sent from the sensors. This research proposes DOA-FG with a linear approximation of tangent function by using the first order Taylor series, so-called Taylor series DOA-FG (TS-DOA-FG). It is shown that the accuracy of the DOA-FG geolocation algorithm can be improved by introducing approximated expressions for the mean and variance of the tangent and cotangent functions based on the first-order Taylor series at the tangent factor nodes of the TS-DOA-FG.

On the other hand, the TOA and TDOA measurements require neither array antennas, monitoring spots, nor knowledge of transmit power. Furthermore, the presence of perfect time synchronization among target and sensors provides reliable TOA and TDOA measurements. Moreover, the presence of line-of-sight (LOS) conditions also increases the reliability of the measurements. However, the TDOA measurements have two advantages over the TOA measurements, which are: (i) TDOA parameter can be measured without requiring the knowledge of the absolute time departure of the target, while TOA measurement requires it. (ii)

[7]In DOA-based technique, time stamp may be required for multiple-target detection, however, in this work we only consider a single static target. The development of multiple-target detection is left for future work.

TDOA measurement requires time synchronization only among the sensors, while the TOA measurement requires time synchronization among the targets and the sensors. Because of the advantageous nature over the other measurement techniques, the TDOA-based techniques are the most widely investigated and in fact, it is has already been put into practice for aviation control [12, 35, 44–48]

Given the facts described above, under such conditions, the TDOA measurements are the most suitable for the factor graph-based technique. Most of the TDOA-based geolocation techniques solve the position detection problem by solving the hyperbolic functions because the TDOA values can be converted to hyperbolic functions. The conventional TDOA-based factor graph technique in [6] also utilizes hyperbolic functions. As mentioned above, even though the conventional technique is already utilizing the factor graph, it still requires high computational complexity. Hence, the Pythagorean TDOA-based factor graph (P-TDOA-FG) technique which requires much less computational complexity compared to the conventional TDOA-based factor graph techniques employing hyperbolic functions (H-TDOA-FG) in [6]. The brief hyperbolic function explanation is described in Chapter 2.

The factor graph algorithm used in the P-TDOA-FG employs a simple Pythagorean functions which is the general functions of TOA-based geolocation technique. Apparently, the conventional TOA-based factor graph technique (TOA-FG) in [17] also utilizes Pythagorean function. However, as mentioned above, the conventional TOA-FG can not be used for location detection of unknown radio wave emitter.

In this research, several sets of new factor graph nodes and expressions are introduced into the conventional TOA-FG. By using the TDOA values as the input, the nodes calculate the *equivalent* TOA values.[8] The new factor graph structure also enables the modified TOA-FG to exchange the TDOA information from the measurement. Hence, the proposed technique can perform location detection of a single static unknown radio wave emitter, where the input is TDOA from the measurement. The problem due to the necessity of having to know the absolute time stamp information needed by the conventional TOA-FG are solved by P-TOA-FG. Evidently, P-TOA-FG also improves the accuracy of the conventional TOA-FG technique.

[8]TOA and TDOA, τ_i and $\tau_{i,j}$, discussed in this paragraph refer to the corresponding Euclidean distance and difference Euclidean distance, r_i and $d_{i,j}$, respectively. This is because the TOA and TDOA can be easily converted in terms of distance/range due to the velocity of the radio propagation wave.

On the other hand, in the presence of imperfect synchronization, it is obvious that TOA and TDOA measurements are not preferable. Furthermore, without array antenna or with a small number of elements in the array antenna, for example three elements antenna array, the DOA measurement is also not desirable. Moreover, the TOA, TDOA, and DOA measurements error are increased due to insufficiency of LOS condition between the target and sensors resulting in multipath-rich propagation scenario [18]. However, the RSS and DRSS measurements require neither array antenna, perfect time synchronization, nor the time stamp. Also, RSS measurement is already standardized in IEEE 802.11 [18]. Hence, under such conditions, the RSS and DRSS measurements are probably the most suitable solution for the factor graph-based technique.

As shown in Fig. 1.3, the RSS measurements contain path-loss, shadowing variations, and instantaneous attenuation[9]. The instantaneous attenuation together with accumulation effect of many independent factors cause the measurement error [17,18]. The conventional RSS-FG technique in [18] utilizes linear approximation of the shadowing variations in indoor environments. The approximation utilizes the least square (LS) algorithm to the RSS measurement of training signals sent from monitoring spots. There are several monitoring spots deployed as shown in Fig. 1.1. Then, the pattern-recognition technique, i.e., RADAR,[10] is used by the conventional RSS-FG [18] to find four appropriate monitoring spots covering the target. However, the process to select the monitoring spots is not explained in detail in [18]. Moreover, because of the reason discussed before, the RSS-FG technique in [18] can not be used to estimate the position of unknown radio wave emitter.

In order to overcome the shortcomings of the conventional RSS-FG in [18], several research works are addressed as follows: (A) DRSS-based factor graph (DRSS-FG) technique is proposed in this research to eliminate the necessity of the knowledge of the transmit power information, and hence this technique successfully estimates the position of a single static unknown radio emitter [43]. (B) The joint RSS-based Voronoi factor graph (RSS-V-FG) technique is proposed. The RSS-based Voronoi (RSS-V) algorithm is used for selecting four appropriate monitoring spots for the RSS-FG algorithm [51, 52]. Nevertheless, the development joint RSS-V and DRSS-FG technique, and joint P-TDOA-FG and DRSS-FG

[9]We use these terminologies instead of mean path-loss, shadowing, and small-scale fading used in [49] for clarity.

[10]RADAR is a radio-frequency (RF) based system for locating and tracking users inside buildings [50].

Table 1.2. Measured parameter-based geolocation technique requirements for unknown radio position detection.

Requirements	DOA	TOA	TDOA	RSS	DRSS	Remarks
Sufficient array antenna or direction antenna	O	X	X	X	X	- The antenna is required for DOA measurement
LOS condition	O	O	O	X	X	- The DOA, TOA, and TDOA measurements suffer from harsh multipath effects [18] - The shadowing component in RSS and DRSS samples can be eliminated by long enough averaging over an area around the reference position of the sensors
Perfect time synchronization among the sensors	X	O	O	X	X	- The TDOA measurement does not require the presence of perfect time synchronization between the unknown target and sensors
Perfect time synchronization between the target and sensors	X	O	X	X	X	- It is impossible to establish perfect time synchronization between the unknown target and sensors
Knowledge of absolute time departure information (time stamp)	X	O	X	X	X	- The information is unavailable in the signal sent from the unknown target
Knowledge of absolute transmit signal power	X	X	X	O	X	- The information is unavailable in the signal sent from the unknown target
Monitoring spots (For pattern recognition technique)	X	X	X	O	O	- The monitoring spots are required by the conventional RSS- and proposed DRSS-based factor graph techniques

Note: - The category of RSS- and DRSS-based techniques discussed in this table are only the pattern recognition technique category. This is because the conventional RSS- and proposed DRSS-based factor graph techniques employ the pattern recognition technique by utilizing the monitoring spots
- The circle (O) and cross (X) marks indicate that the conditions are required and not required, respectively, by the corresponding techniques

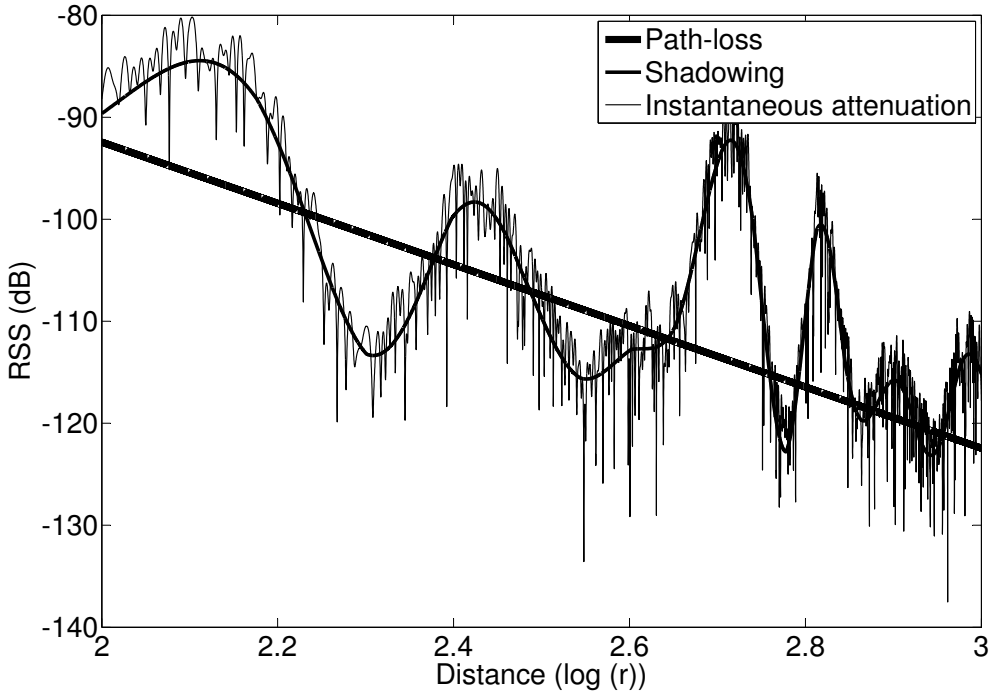

Figure 1.3. Path-loss, shadowing, and instantaneous attenuation as shown in [49]

.

are left for future work. The proposed DRSS-FG and RSS-V-FG were tested by a series computer simulations in the outdoor scenario. For this purpose, the path-loss profile is used. The outdoor scenario consists of two conditions: (i) free space or LOS environments, and (ii) Non-LOS environments. In the Non-LOS environments, the shadowing variations can be eliminated by long (in distance/range) enough averaging over the surrounding geography of the sensors. The requirements of the factor graph-based techniques are summarized in Table. 1.2 and 1.3.

It should be noticed that the area of monitoring spots can be any forms. In this research, we follow [18] to use rectangular area shaped by four monitoring spots covering the target. The size of rectangular area of monitoring spots are flexible for both environment with shadowing variations or path-loss only. The smaller size of rectangular area of the monitoring spots, the more accuracy of the linear approximation can be achieved for shadowing variations. For example, the conventional RSS-FG in [18] is successfully tested in the indoor environments, taking into account shadowing variations. The technique uses small rectangular area of monitoring spots, i.e., 6 m $\times$ 6 m, and 3 m $\times$ 3 m, to linearly approximate

Table 1.3. Summary of the factor graph-based techniques for location detection of a single static unknown radio emitter.

Measured parameters	Factor graph-based techniques for unknown radio position detection
DOA	Suitable for location detection of a single static unknown radio wave emitter if sufficient array antenna is available and also LOS condition exists
TDOA	Suitable for location detection of a single static radio wave emitter without array antenna, with LOS condition and perfect time synchronization
DRSS	Suitable for location detection of a single static unknown radio wave emitter in LOS and/or Non-LOS condition, and imperfect time synchronization
TOA	Unsuitable for location detection of unknown radio wave emitter because the knowledge of the abolute time departure of the unknown target is unavailable
RSS	Unsuitable for location detection of unknown radio wave emitter because the knowledge of absolute transmit power of the unknown target is unavailable

the shadowing variations.

On the other hand, the larger size of rectangular area of the monitoring spots, the accuracy of the linear approximation is only suitable for path-loss component. The proposed DRSS-FG in [43] and RSS-V-FG in [51, 52] are successfully tested by a series computer simulations in outdoor environments by taking into account path-loss only. The reasonable size of rectangular area of monitoring spots for linear approximation of the path-loss component is 200 m $\times$ 200 m, based on our finding in [53]. If it is not possible to perform long (in distance/range) enough averaging of the RSS measurements, the solution is by reducing the size of rectangular area of the monitoring spots. Hence, the smaller size of the area, the higher accuracy of the RSS- and DRSS-based factor graph techniques achieved. The detail discussion of the rectangular area size of the monitoring spots can be found in Chapter 5.

A closed-form expression of the Cramer Rao lower bounds (CRLBs), taking into account the number of samples, for DOA- and TOA-based geolocation techniques, as well as the approximated CRLB for TDOA-based geolocation are also derived in this dissertation. The performance of the proposed technique is evaluated in the term of root-mean-square error (RMSE). The results show that the proposed techniques accurately estimate the location of unknown target, while it requires low computational complexity. It is shown that all of the techniques proposed in this dis-

sertation can achieve much higher accuracy compared to the conventional techniques. The achieved RMSE with the proposed techniques are also evaluated, and are found to achieve very close RMSE to the CRLB. The derivation of CRLB for RSS- and DRSS-based techniques will be explored further in our future work.

1.3 Summary of Contribution

Usually, in many dissertations of this nature, the research work focuses on a single measured parameters of propagation electromagnetic waves. In this dissertaion, however, the proposal to develop new geolocation algorithms incorporates many measured parameters because our research work initially motivated by industry requirements. The focus in industrial problem is to detect the location of unknown radio wave emitter. Hence, several techniques based of factor graph algorithm and measured parameters, such as, DOA, TDOA, and DRSS, are proposed.

Such industrial background invokes the theoretical bounds; and mathematical expression of the proposed techniques are derived, where these are the part of academic research works. Furthermore, the detailed explanation of how the messages are updated at each node, and how the updated messages are exchanged between the nodes, is provided. The results of a series of simulation are presented to evaluate the convergence property and the accuracy of the proposed techniques. The focus of our research work is to develop several new mathematical formulas and/or algorithm for calculating the position of unknown radio by utilizing the samples of measured parameters. The dissertation does not cover the security issue, sensor specification, bandwidth, signal waveform, measurement issue, etc.

The contributions of this research are based on published conference paper [51, 53], accepted journal paper [52], conditional accepted journal paper [42], and accepted conference paper [43], summarized as follows:

1. For the presence of imperfect time synchronization with LOS condition, we propose a new TS-DOA-FG [42] to estimate the position of the unknown target, where the input is the samples of DOA measurement results sent from the sensors. Incorrect and incomplete algorithms of the conventional DOA-FG techniques are fixed by introducing new expressions and nodes. A linear approximation of tangent and cotangent functions by utilizing the first order Taylor expansion series is derived. It is shown that the accuracy of the proposed technique outperforms the conventional DOA-based least

squares (DOA-LS) and Gauss-Newton (DOA-GN) techniques and also achieves close to the theoretical limit.

2. In addition, with the presence of perfect time synchronization among the sensors and also LOS condition, we propose a new P-TDOA-FG technique requiring much less computational complexity compared to the conventional H-TDOA-FG techniques. The proposed technique uses simple Pythagorean function-based FG technique, which has been taken into account for the use of conventional TOA-FG technique. The establishment of several sets of formulas is to convert the TDOA (different Euclidean distance) to *equivalent* TOA (Euclidean distance). Hence, the necessity of the knowledge of the absolute time stamp information in the TOA-FG can be eliminated. It is shown that our proposed technique successfully estimates the unknown target. It is also shown that the accuracy of the proposed technique outperforms the conventional TOA-FG and also achieves close to the theoretical limit.

3. Furthermore, with the LOS and/or Non-LOS condition, where perfect time synchronization and sufficient array antenna are unavailable, we propose a new DRSS-FG technique [43]. The proposed technique solves the problem of conventional RSS-FG technique which is unable to estimate the position of a single static unknown radio wave emitter without the knowledge of absolute value of its transmit power. The necessity of the knowledge of the absolute value is eliminated by performing subtraction the RSS value (in terms of dB) among the sensors. It is shown that the accuracy of our proposed technique outperforms the conventional RSS-based FG to estimate the position of an unknown target.

4. Besides proposing above three factor graph geolocation techniques, we also propose new RSS-V-FG [51, 52] utilizing the initial point given by the conventional RSS-V technique. The initial point is required for selecting four most appropriate monitoring spots. It is shown that our proposed technique also improves the accuracy of RSS-V technique.

1.4 Dissertation Outline

The outline of this doctoral research dissertation is organized as follows.

In Chapter 1, the background, motivation, overview, and related work of this research have been described. The summary of the contributions and the organization of this dissertation has also been presented this chapter. In Chapter 2, the factor graph algorithm overview is discussed. It is followed by the description of several measured-based factor graph techniques. The Gaussianity assumption and theoretical limit in wireless geolocation are also discussed in Chapter 2.

The main contributions in this research are presented in the following three chapters. In Chapter 3, a new TS-DOA-FG technique is proposed. The derivation of linearly approximated expressions of the tangent and cotangent functions is presented. This approximation utilizes the first-order Taylor series of the tangent and cotangent functions. In Chapter 4, a new P-TDOA-FG technique is proposed. In Chapter 5, new DRSS-FG and RSS-V-FG techniques are proposed. Results of a series of simulations conducted to evaluate the size required for monitoring spots.

Finally, conclusions and future work for further development of the geolocation techniques using factor graph are presented in Chapter 6.

Chapter 2

Research Background

2.1 Overview of Factor Graph

As described in [37], A factor graph is a bipartite graph showing the factorization/decomposition structure of global function into several local function. It can be seen that the factor graph is used to derive many algorithms to be working as sum-product algorithm, e.g., low-density parity-check (LDPC) codes, turbo codes, Kalman filter, fast Fourier transform (FFT), spanning tree, and geolocation techniques. The factor graph is also well known for the LDPC code because the factor graph is applying the functions into Tanner graph, where the Tanner graph is utilized to described the LDPC code. In this dissertation, we utilize the factor graph for position detection of the unknown target.

In general, the factor graph consists of the factor and variable nodes. In Fig. 2.1, the factor node is shown by a square, while the variable node by a circle. The factor node updates the messages forwarded from the connected variable nodes by using the specific simple local function, and the result is passed to the destination variable node. The variable node combines all messages sent from the corresponding factor nodes by using sum-product algorithm.

It is alo explained in [37] that the sum-product algorithm is a generic message passing algorithm to calculate the various marginal functions. The marginal function of a variable node is the product of all incoming messages from connected factor nodes. For example, the global function for the factor graph in Fig. 2.1 is $g(x_1, x_2, x_3, x_4)$. Assume that g is the product of several simple functions as

$$g(x_1, x_2, x_3, x_4) = f_A(x_1, x_2) \cdot f_B(x_1, x_3) \cdot f_C(x_1, x_4) \cdot f_D(x_3). \qquad (2.1)$$

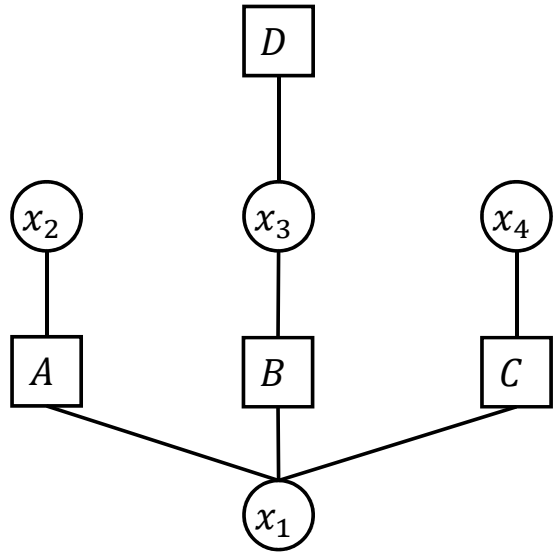

Figure 2.1. The simple structure of the factor graph.

Hence, the marginal function for x_1 can be computed by using distributive law, expressed as

$$g(x_1) = \left(\sum_{\sim x_1} f_A(x_1, x_2)\right)\left(\sum_{\sim x_1} f_B(x_1, x_3) f_D(x_3)\right)\left(\sum_{\sim x_1} f_C(x_1, x_4)\right), \quad (2.2)$$

where $\sum_{\sim x_1}$ is the summary operator for x_1, and $f_A(\cdot), f_B(\cdot), f_C(\cdot), f_D(\cdot)$ are the local function in factor nodes A, B, C, D, respectively [37].

In this research, we calculate the marginal function for coordinate position of the target (x, y). The calculation is repeated in each iteration. It should be noticed that the iteration process appears in the factor graph with cycles. In the most cases, the measured parameters-based factor graph geolocation techniques have cycles in the graph [3, 5, 6, 17–19, 23].

Fig. 2.2 shows a simple structure of the factor graph with cycles. During the iteration process, the messages sent from the source factor nodes are further combined in the variable node and passed back to the destination factor node for the next round of iteration. The messages combined in the variable node z, during the iteration process are calculated by sum-product algorithm as [37]

$$\prod_{j=1, j\neq i}^{N} \mathcal{N}(z, m_{Z_j \to z}, \sigma^2_{Z_j \to z}) \propto \mathcal{N}(z, m_{z \to Z_i}, \sigma^2_{z \to Z_i}), \quad (2.3)$$

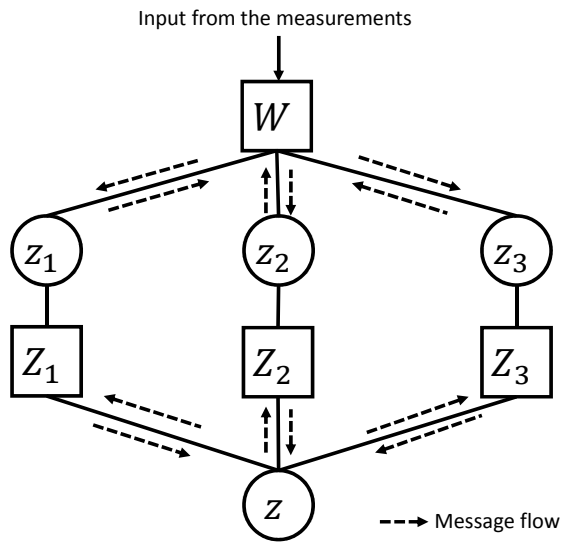

Figure 2.2. The simple structure of the factor graph with cycles.

where the fact that product of several Gaussian variables is *proportional* to Gaussian-distributed is used. z and Z indicate any variable and factor nodes, respectively. The mark $\rightarrow$ in the suffix indicates the message flow directions in the factor graph. N indicates the total edge-connecting variable node z to factor nodes Z_i. The edge-connecting indexes are indicated by i, $i = 1, 2, ...N$ and j, $i = 1, 2, ..., N$.

It should be noticed that as shown in the explanation of Fig. 1.2, N indicates the total number of sensors, $i, i = 1, 2, ..., N$ and $j, j = 2, 3, ..., N$ indicate the primary sensor and secondary sensor indexes, respectively, for the use of the discussion of the TDOA-based factor graph and DRSS-based factor graph technique. i also indicates the sensor index regardless secondary or primary sensor indexes, for the use of the discussion of the DOA-based factor graph techniques.

Furthermore, as has been derived in [37] with the Gaussianity assumption, the message passing algorithm needed to perform the sum-product algorithm can be expressed as

$$\frac{1}{\sigma^2_{z\rightarrow Z_i}} = \sum_{h=1,h\neq i}^{N} \frac{1}{\sigma^2_{Z_h\rightarrow z}}, \tag{2.4}$$

$$m_{z\rightarrow Z_i} = \sigma^2_{z\rightarrow Z_i} \sum_{h=1,h\neq i}^{N} \frac{m_{Z_h\rightarrow z}}{\sigma^2_{Z_h\rightarrow z}}. \tag{2.5}$$

Finally, when the iteration converges, the variable node z combines all incoming messages from the node Z_i, as

$$\prod_{i=1}^{N} \mathcal{N}(z, m_{Z_h \to z}, \sigma^2_{Z_h \to z}) \propto \mathcal{N}(z, m_z, \sigma^2_z), \tag{2.6}$$

where, in the similar way as above,

$$\frac{1}{\sigma^2_z} = \sum_{i=1}^{N} \frac{1}{\sigma^2_{Z_i \to z}}, \tag{2.7}$$

$$m_z = \sigma^2_z \sum_{i=1}^{N} \frac{m_{Z_i \to z}}{\sigma^2_{Z_i \to z}}. \tag{2.8}$$

The equations (2.4)–(2.8) are utilized in Chapter 3 – 5 for calculating the estimated coordinate position (x, y) of a single static unknown target. Especially in Chapter 4, these equations are also employed to calculate the *equivalent* TOA. The conventional RSS-FG in Section 2.3.1 can be used as a simple example of the factor graph-based geolocation technique .

2.2 Measurement Error in Geolocation

In this research, we directly use the samples of measurement corrupted by Gaussian noise for estimating the position of the unknown target. The mismatch between real signal with the signal model is also assumed to be included in measurement error. Hence, the signal model of the unknown radio wave emitter is not discussed. The measured samples are also corrupted by error due to spatial spread of the multipath component, impairments in measurement, and many other independent factors.

The Gaussianity assumption is used in this research because of the accumulative effects of many independent factors, as in [4, 6, 17, 18, 23]. Hence, the assumption is reasonable for many of the wireless parameter measurement-based techniques such as DOA [4, 23], TOA [17], TDOA [6], and RSS-based factor graph technique [18]. The assumption is of significant importance to simplify the operations in the factor graph so that the message exchanged among the nodes can be expressed in the form of only the means and variances. This research also uses the same assumption.

The sample equation of DOA measurements is then given by

$$\hat{\theta}_{i,k} = \theta_i + n_{\theta_{i,k}}, \quad k = \{1, 2, ..., K\}, \tag{2.9}$$

where k and i are the sample and sensor indexes, respectively. θ_i indicates the true DOA. It is reasonable to assume that $n_{i,k}$ is zero-mean Gaussian random variable where the DOA measurement is performed by using circular array antenna, hence the measurement error is in angular value. Then, $\hat{\theta}_{i,k}$ follows a Normal distribution $\mathcal{N}(\theta_i, \sigma_i^2)$ having a probability density function $p(\hat{\theta}_{i,k})$ as

$$p(\hat{\theta}_{i,k}) = \frac{1}{\sqrt{2\pi}\sigma_{\theta_i}} \exp\left(\frac{-(\hat{\theta}_{i,k} - \theta_i)^2}{2\sigma_{\theta_i}^2}\right). \tag{2.10}$$

The TOA, TDOA, RSS, and DRSS samples expression are similar to (2.9) as follows: (i) $\hat{\theta}_{i,k}$ is replaced to $\hat{r}_{i,k}$, $\hat{d}_{i,j,k}$, $\hat{P}_{w,i,k}$, and $\hat{P}_{w,i,j,k}$, (ii) $\theta_{i,k}$ is replaced to $r_{i,k}$, $d_{i,j,k}$, $P_{w,i,k}$, and $P_{w,i,j,k}$, and (iii) $n_{\theta_{i,k}}$ is replaced to $n_{r_{i,k}}$, $n_{d_{i,j,k}}$, $n_{P_{w,i,k}}$, and $n_{P_{w,i,j,k}}$, respectively. The variables indicate: (i) samples of, (ii) true value of, and (ii) measurement errors (the zero-mean Gaussian noise) of, TOA/Euclidean distance (meter), TDOA/difference Euclidean distance (meter), RSS (watt), and DRSS (watt), respectively. w indicates the unit of RSS and DRSS parameters are in watt. Thus, $\hat{r}_{i,k}$, $\hat{d}_{i,j,k}$, $\hat{P}_{w,i,k}$, and $\hat{P}_{w,i,j,k}$ follow a Normal distribution $\mathcal{N}(r_i, \sigma_{r_i}^2)$, $\mathcal{N}(d_{i,j}, \sigma_{d_{i,j}}^2)$, $\mathcal{N}(P_{w,i}, \sigma_{P_{w,i}}^2)$, and $\mathcal{N}(P_{w,i,j}, \sigma_{P_{w,i,j}}^2)$ with a probability density function $p(\hat{r}_{i,k})$, $p(\hat{d}_{i,j,k})$, $p(\hat{P}_{w,i,k})$, and $p(\hat{P}_{w,i,j,k})$, respectively.

The TOA and TDOA samples measurement, $\hat{\tau}_i$ and $\hat{\tau}_{i,j}$, can be directly converted to Euclidean distance and difference Euclidean distance samples, $\hat{r}_i$ and $\hat{d}_{i,j}$, respectively, due to the velocity of the light. Hence, in the most cases in this dissertation, the TOA and TDOA refer to Euclidean distance and difference Euclidean distance, respectively. The difference Euclidean distance $d_{i,j}$ is the difference between the Euclidean distance of primary sensors r_i and the Euclidean distance of secondary sensors r_j to the target, where $d_{i,j} = r_i - r_j$. We subtract the values in secondary sensor from the values in primary sensor to obtain the difference in values for both TDOA. The use of terminologies of primary and secondary sensors are also applied for DRSS in the same way .

However, in the conventional RSS-FG and proposed DRSS-FG, the RSS and DRSS samples in units of watt, $\hat{P}_{w,i,k}$ and $\hat{P}_{w,i,j,k}$, are converted into RSS and DRSS samples in units of dB, $\hat{P}_{i,k}$ and $\hat{P}_{i,j,k}$, respectively,

with probability density function (pdf) as [18]

$$p(\hat{P}_{i,k}) = \frac{\ln 10 \cdot 10^{\frac{\hat{P}_{i,k}}{10}}}{10 \cdot \sigma_{n_{P_{w,i}}} \cdot \sqrt{2\pi}} \cdot \exp\left(\frac{-\left(10^{\frac{\hat{P}_{i,k}}{10}} - P_{w,i}\right)^2}{2\sigma^2_{n_{P_{w,i}}}} \right). \tag{2.11}$$

The conversion from the units of watt to dB improves the linear approximation of the RSS profile . Furthermore, it has been confirmed in [18] that the pdf of (2.11) is the approximation of Gaussian distribution because the pdf shows similarity to Gaussian distribution. Hence, the Gaussianity assumption is still preserved.

2.2.1 Assumption of LOS condition

The size of area used for computer simulation in the research is $1,000 \times 1,000$ m^2. It may be difficult to achieve the LOS condition in areas with size of $1,000 \times 1,000$ m^2 especially in (sub)urban environments. However, instead, the error due to the Non-LOS components can be included to the variance of the measurement error as shown in [5, 54], where the variances are different between the sensors. For simplicity, it is assumed that the variance σ_θ^2 of the measurement error is common to all sensors as in [4, 6, 17, 18, 23]. However, it is rather straightforward to derive the algorithm where each sensor has different values of variances. In fact, in the simulation set up, the area size is much smaller than that used in other references, for example, the TOA-based factor graph in [17], TOA/DOA-based factor graph in [23], DOA-based factor graph in [4], and TDOA-based factor graph in [6], where they consider the hexagonal area with a radius of 5 km. For example, as found in the simulation results of TS-DOA-FG technique in Chapter 3, the estimation accuracy is quite high even with relatively large variance, e.g., $\sigma_\theta^2 = 45°$. This indicates that the assumption for the impact of the Non-LOS components being represented by the measurement error variance is reasonable.

2.3 Overview of Conventional Factor Graph-Based Techniques

2.3.1 RSS-Based Factor Graph

The RSS-FG presented in this section is based on the technique introduced in [18]. Fig. 2.3 shows the conventional RSS-FG with number of

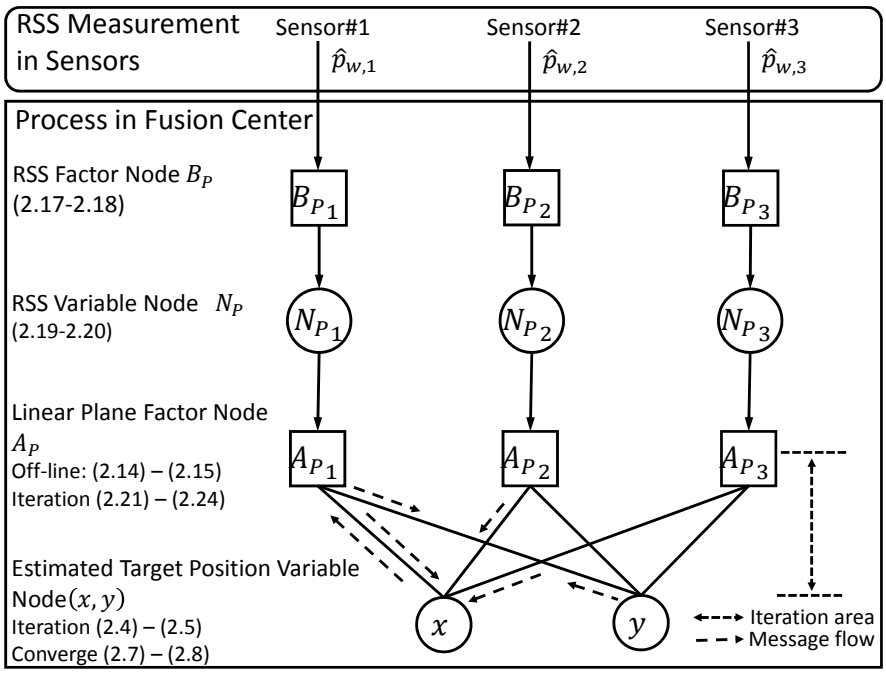

Figure 2.3. The conventional RSS-FG with number of sensors $N = 3$ [18].

sensors $N = 3$. We modify the environment from an indoor area suffering from shadowing fading [18] to an outdoor area experiencing from path-loss only [53]. The target position to be estimated is at $\mathbf{x}$. Multiple N sensors perform measurement of RSS signal sent from both the target and monitoring spots, where the position is indicated by $\mathbf{X}$ as described above. Multiple M monitoring spots send training signals to the sensors, where the position is indicated by $\mathbf{Y} = [x_m \; y_m]^T$, with $m = 1, 2, ..., M$ being the monitoring spot index. It should be noticed that monitoring spot index are also not assigned in a vector $\mathbf{Y}$.

The linear plane equation used to convert the messages of RSS from target to the coordinate is derived in [18], as

$$a_{x_i} \cdot x_j + a_{y_i} \cdot y_j + a_{p_i} \cdot P_{m,i} = c, \tag{2.12}$$

where for the i-th sensor, a_{x_i}, a_{y_i}, and a_{p_i} are the coefficients of x, y, and P_i variables of linear plane (5.3), respectively. The variables are obtained by solving the LS equation (2.15), (x_m, y_m) is the position of the

m-th monitoring spot, $P_{m,i}$ is the RSS of the m-th the monitoring spot, obtained from the training sequence, and c is a constant which is set at arbitrary value [18]. We set $c = 1$ in this research work. The matrix equation from (5.2) is expressed as below

$$\mathbf{B} \cdot \mathbf{a} = \mathbf{c}, \tag{2.13}$$

where $\mathbf{B}$ is a matrix with its elements x_j, y_j, and $P_{,m}$ as $\mathbf{a}$ is vector of a_{x_i}, a_{y_i}, and a_{p_i}, and $\mathbf{c}$ is constant vector, as

$$\mathbf{B} = \begin{bmatrix} x_1 & y_1 & P_{i,1} \\ x_2 & y_2 & P_{i,2} \\ x_3 & y_3 & P_{i,3} \\ \vdots & \vdots & \vdots \\ x_4 & y_4 & P_{i,M} \end{bmatrix}, \mathbf{a} = \begin{bmatrix} a_{x_i} \\ b_{x_i} \\ a_{p_i} \end{bmatrix}, \mathbf{c} = \begin{bmatrix} 1 \\ 1 \\ 1 \\ 1 \end{bmatrix}, \tag{2.14}$$

where $i, i = 1, 2, ..., N$ indicates sensor index, N indicates total number of sensors, $m, m = 1, 2, .., M$ indicates the monitoring spots index, and M is the total number of monitoring spots. We can use at least 3 monitoring spots. In this research, we follow [18] to use 4 monitoring spots having rectangular area shape. The use of 3 monitoring spots decreases the accuracy of the RSS-FG technique, while the use of more than 4 monitoring spots does not increase the accuracy of the RSS-FG. This is because we use linear plane to approximate the RSS profile.

The coefficient of the variables are obtained by employing a least square (LS) solution to (2.13), as

$$\mathbf{a} = \left(\mathbf{B}^T \cdot \mathbf{B}\right)^{-1} \cdot \mathbf{B}^T \cdot \mathbf{c}. \tag{2.15}$$

The coefficients in $\mathbf{a}$ from (2.15) are used for the final linear plane equation to convert the target RSS to the target coordinate (x, y) as expressed:

$$a_{x_i} \cdot x + a_{y_i} \cdot y + a_{p_i} \cdot P_i = c, \tag{2.16}$$

where P_i is the RSS of target measured by the i-th sensor. In the RSS-FG algorithm, P_i contains the information of mean and variance of the k RSS samples from the target. The node A_p uses (5.3) to convert the target RSS message to the target position in the coordinate. The summary of formulas for updating the mean and variance at each node of the RSS-FG can be found from Table I in [18], where the message flow in the RSS-FG algorithm is described below.

Now, since the equations to be calculated in the node A_P is established, we can start the factor graph algorithm. The first step in the factor graph

algorithm is conducted in *RSS measurement factor node* B_P to feed the mean $m_{B_{p_i}\to P_{R_i}}$ and variance $\sigma^2_{B_{p_i}\to P_{R_i}}$ messages extracted from k RSS samples of the target, corrupted by zero-mean Gaussian measurement error. The means and variances of the samples are calculated as

$$m_{B_{p_i}\to P_{R_i}} = \frac{1}{K}\sum_{k=1}^{K}\hat{P}_{i,k}, \tag{2.17}$$

$$\sigma^2_{B_{p_i}\to P_{R_i}} = \frac{1}{K}\sum_{k=1}^{K}\left(\hat{P}_{i,k} - m_{B_{p_i}\to P_{R_i}}\right)^2. \tag{2.18}$$

After that the messages are forwarded by the node B_P to the *averaged RSS variable node* N_P, as shown in Fig. 2.3. The variable node N_P performs sum-product algorithm (2.4) and (2.5). However, because there are only two connecting edges to the node N_P, hence the node N_P directly forwards the RSS messages of the target in the form of mean and variance, obtained from the node B_P to the node A_P, as

$$m_{P_{R_i}\to A_{P_i}} = m_{B_{P_i}\to P_{R_i}}, \tag{2.19}$$

$$\sigma^2_{P_{R_i}\to A_{P_i}} = \sigma^2_{B_{P_i}\to P_{R_i}}. \tag{2.20}$$

The messages of the mean and variance of RSS samples as well as the x and y coordinate are exchanged iteratively between the nodes A_P and the *estimated geolocation coordinate variable node* (x, y) in the factor graph as shown in Fig. 5.1. In the node A_P, the messages of mean and variance of RSS are converted to the target (x, y) coordinate, as

$$m_{A_{P_i}\to x} = \alpha_{x_i} + \beta_{x_i}\cdot m_{y\to A_{P_i}} + \gamma_{x_i}\cdot m_{P_{R_i}\to A_{P_i}}, \tag{2.21}$$

$$m_{A_{P_i}\to y} = \alpha_{y_i} + \beta_{y_i}\cdot m_{x\to A_{P_i}} + \gamma_{y_i}\cdot m_{P_{R_i}\to A_{P_i}}, \tag{2.22}$$

$$\sigma^2_{A_{P_i}\to x} = \beta^2_{x_i}\cdot \sigma^2_{y\to A_{P_i}} + \gamma^2_{x_i}\cdot \sigma^2_{P_{R_i}\to A_{P_i}}, \tag{2.23}$$

$$\sigma^2_{A_{P_i}\to y} = \beta^2_{y_i}\cdot \sigma^2_{x\to A_{P_i}} + \gamma^2_{y_i}\cdot \sigma^2_{P_{R_i}\to A_{P_i}}, \tag{2.24}$$

where

$$\begin{aligned} \alpha_{x_i} &= c/a_{x_i}, & \alpha_{y_i} &= c/a_{y_i}, \\ \beta_{x_i} &= -a_{y_i}/a_{x_i}, & \beta_{y_i} &= -a_{x_i}/a_{y_i}, \\ \gamma_{x_i} &= -a_{P_i}/a_{x_i}, & \gamma_{y_i} &= -a_{P_i}/a_{y_i}. \end{aligned} \tag{2.25}$$

During the iteration, the node (x, y) forwards the messages, obtained as the result of the sum-product algorithm performed in the node (x, y),

Table 2.1. The Operations Required for Each Node in The Conventional RSS-FG [18].

Message Flow (Nodes)	Samples ($\hat{}$) and/or (Means, Variances)	
	Inputs	Outputs
$B_{P_i} \rightarrow N_{P_i}$	$\hat{P}_{w,i}$	$\left(m_{\hat{P}_i}, \sigma^2_{\hat{P}_i}\right)$
$N_{P_i} \rightarrow A_{P_i}$	$\left(m_{\hat{P}_i}, \sigma^2_{\hat{P}_i}\right)$	$\left(m_{\hat{P}_i}, \sigma^2_{\hat{P}_i}\right)$
$A_{P_i} \rightarrow x$	$\left(m_{\hat{P}_i}, \sigma^2_{\hat{P}_i}\right)$ $\left(m_{y_i}, \sigma^2_{y_i}\right)$	$\left(\frac{c_i - a_{y_i} m_{y_i} - a_{P_i} m_{\hat{P}_i}}{a_{x_i}}, \frac{a^2_{y_i}\sigma^2_{y_i} + a^2_{P_i}\sigma^2_{\hat{P}_i}}{a^2_{x_i}}\right)$
$A_{P_i} \rightarrow y$	$\left(m_{\hat{P}_i}, \sigma^2_{\hat{P}_i}\right)$ $\left(m_{x_i}, \sigma^2_{x_i}\right)$	$\left(\frac{c_i - a_{x_i} m_{x_i} - a_{P_i} m_{\hat{P}_i}}{a_{y_i}}, \frac{a^2_{x_i}\sigma^2_{x_i} + a^2_{P_i}\sigma^2_{\hat{P}_i}}{a^2_{y_i}}\right)$
$x \rightarrow A_{P_i}$ $y \rightarrow A_{P_i}$	$\left(m_j, \sigma^2_j\right)$ $j \neq i$	$\left(\sigma^2_i \sum_{j \neq i} \frac{m_j}{\sigma^2_j}, \sigma^2_i = \frac{1}{\sum_{j \neq i} \frac{1}{\sigma^2_j}}\right)$
x and y	(m_i, σ^2_i)	$\left(\sigma^2_\Lambda \sum_i \frac{m_i}{\sigma^2_i}, \sigma^2_\Lambda = \frac{1}{\sum_i \frac{1}{\sigma^2_i}}\right)$

back to the node A_P as in (2.4) and (2.5). When the iteration converges, the mean value (m_x, m_y) obtained from (2.8) indicates the final estimate of the target position, where m_z indicates m_x and m_y. We summarize the operation required at each node in Table. 2.1.

In [53], we have investigated the RSS-FG in outdoor environments, where solely path-loss taken into account. The shadowing and instantaneous fading components are eliminated by assuming averaging over a long enough range. We also found that the accuracy of the RSS-FG depends on the width size of monitoring spot area[1] where the target is inside. Furthermore, if the target is surrounded by four monitoring spots, adding more monitoring spots does not increase the accuracy.

Path-Loss Model

The only path-loss remains due to the free space loss assumption. In addition, when the free space loss condition in outdoor environment is unavailable, the condition that the only path-loss component remains can also be achieved by performing measurement around the initial sensor position

[1]We use the terminology "monitoring spot area" instead of "training cell" mentioned in [18].

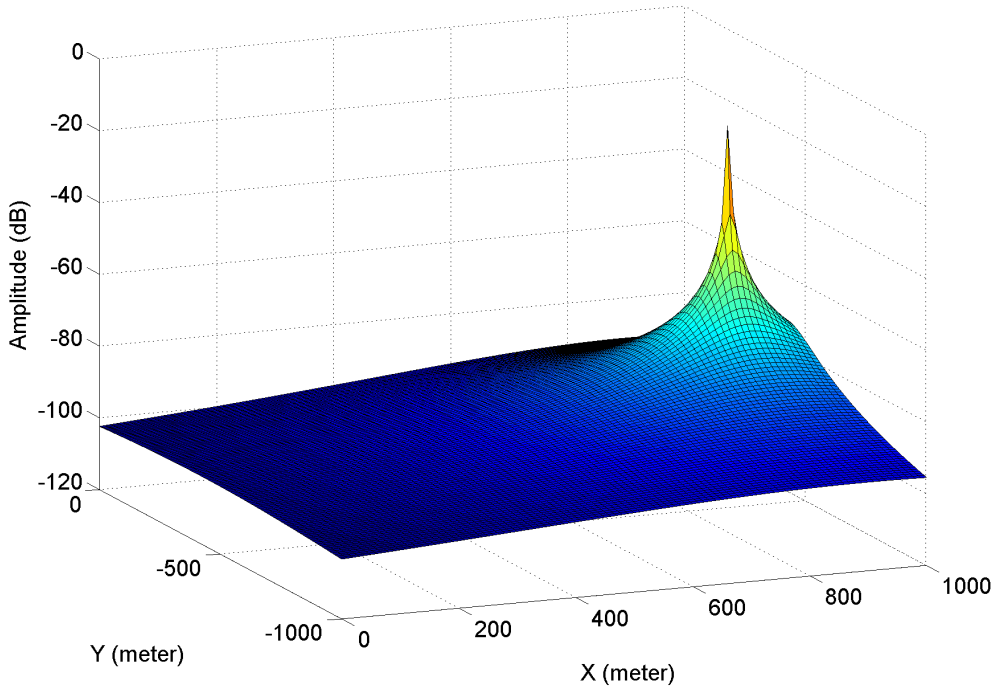

Figure 2.4. RSS profile of path-loss model with sensor position at $(901, -421)$ m, $n = 3$ for urban area, $f_c = 1$ GHz, and $r_0 = 100$ m.

$(X_i, Y_i), i = 1, 2, ..., N$. The areas for the averaging by each sensor are large enough to eliminate the shadowing components in the RSS samples. The samples of measured signal of monitoring spots and a single static unknown target are sent to the fusion center. The averaging is performed in the fusion center to obtain the average RSS samples which indicate the path-loss only. The profile of RSS at sensor position $(901, -41)$ m is shown in Fig. 2.4, where the path-loss exponent model is used as

$$P_i(r_i) = 20 \log \left(\frac{4\pi r_0 f_c}{c} \right) + 10n \log \left(\frac{r_i}{r_0} \right), \tag{2.26}$$

where r_0 denotes reference distance, f_c denotes carrier frequency, and n denotes path-loss exponent. r_i denotes Euclidean distance from target or monitoring spot to the i-th sensor [49, 53]. We use P_i instead of $P_i(r_i)$ in the rest of this dissertation for simplicity, where P_i is in unit of dB.

Monitoring Spot Area in Outdoor Area Scenario

In [53], we investigates the accuracy of RSS-based FG geolocation technique in outdoor environment. We consider the path-loss fading channel by averaging RSS samples of each monitoring spot and target, where the

averaging is long enough to eliminate the shadowing and small-scale fading component of RSS. This chapter shows the effect of the number and wide area of monitoring spot to the accuracy of RSS-based FG geolocation technique in outdoor environment.

Area of investigation in this simulation is $1,000 \times 1,000$ m^2. The square wide area of monitoring spot is evaluated from 100×100 m^2 until 800×800 m^2. The configuration of location in the simulation as follow, initial point of iteration is at $(0, 0)$ m, and three sensors location is at $(100, 0), (1100, 0), (600, -1000)$ m. Target location is randomly permuted 800×800 m^2 where the grid is every 10 m and $(600, -500)$ m is the center. The position of the sensor, target, and monitoring spots are shown in Figs. 2.5(a) and 2.5(b). The exponential path-loss model P_L is expressed as in (2.26), where frequency carrier f_c is 1 GHz, reference distance r_0 is 100 m, path-loss exponent n is 3 for urban area, and r is distance from sensor to target or monitoring spot. The RSS-based FG geolocation technique in this simulation is same as in [18]. The simulation is conducted in $10,000$ realizations, where each realization contains 10 iterations and 100 samples of RSS target. Each sample is from path-loss exponent (in watt), which is added zero-mean Gaussian noise as error measurement with SNR of 0 to 45 dB.

RSS-based FG geolocation technique employs the equation of linear plane derived in [18] as expressed as $a_x x + a_y y + a_p p = c$, where x and y is coordinate position, a_p is the RSS of target, and c is constant which we set 1. a_x, a_y, and a_p are the variable coefficients obtained by applying the leased square (LS) to the RSS monitoring spot. Therefore, the accuracy is depending on how the RSS profile of linear plane matches the actual RSS profile (RSS profile model).

Fig. 2.5(a) shows the trajectory reaches the target position after several iterations in monitoring spot area 200×200 m^2 because the RSS profile of model and the RSS profile of the equation are almost fitted each other as shown in Fig. 2.6(a). In other hand, Fig. 2.5(b) shows the trajectory can not reach the target position accurately after several iterations in monitoring spot area 800×800 m^2 because the RSS profile of model and the RSS profile of the equation are separated far away each other as shown in Fig. 2.6(b).

Fig. 2.7 shows that the accuracy increases when the area of monitoring spot is getting smaller. The accuracy of RSS-based FG geolocation technique is not depending the number of monitoring spot due to the LS property. If the monitoring spot number increases and spreads, then the accuracy is depending on how close the monitoring spot to the target.

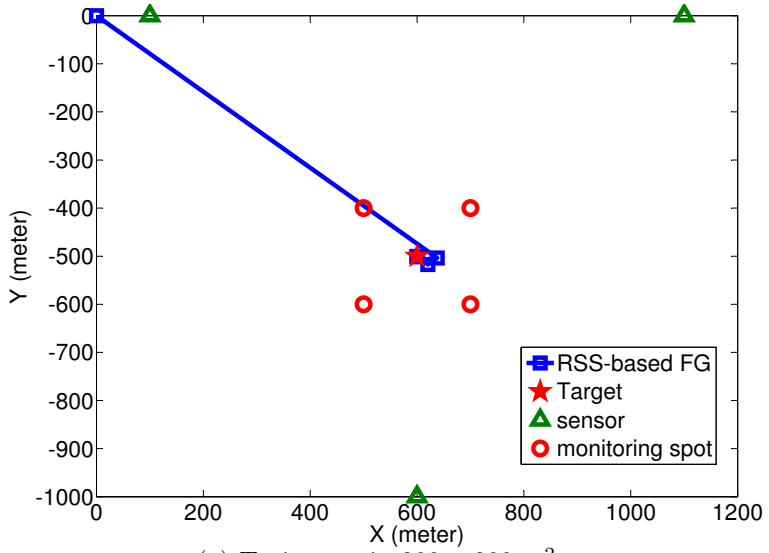

(a) Trajectory in 200×200 m^2.

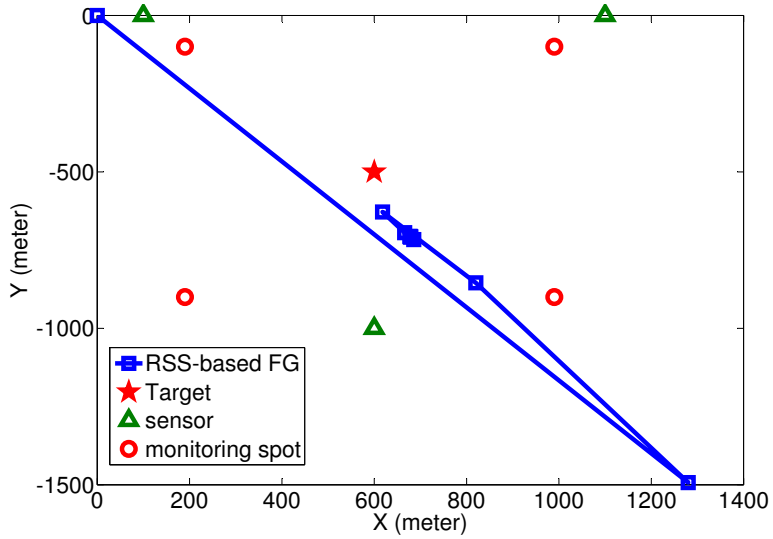

(b) Trajectory in 800×800 m^2.

Figure 2.5. Trajectory of RSS-based FG with 3 sensors.

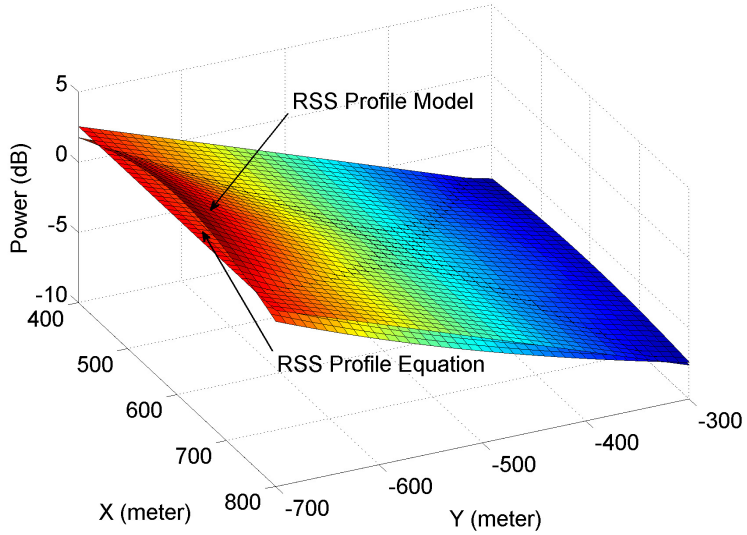

(a) RSS profile in 200×200 m^2.

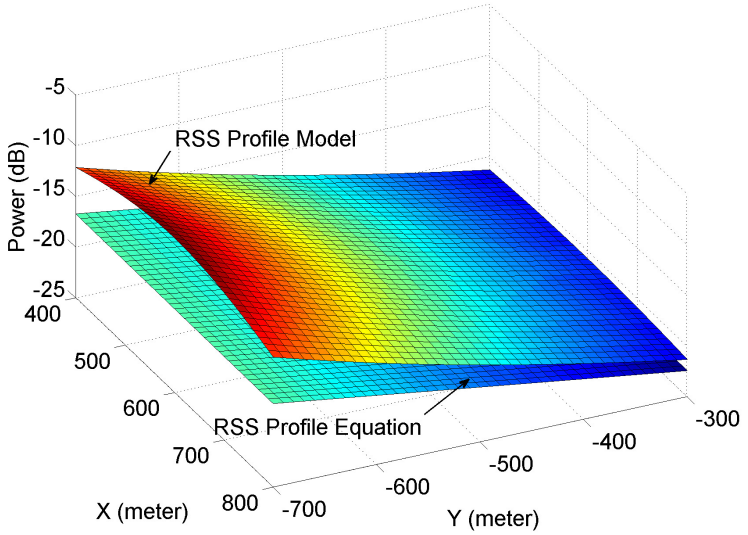

(b) RSS profile in 800×800 m^2.

Figure 2.6. RSS profile vs RSS plan equation of RSS-based FG at sensor #3.

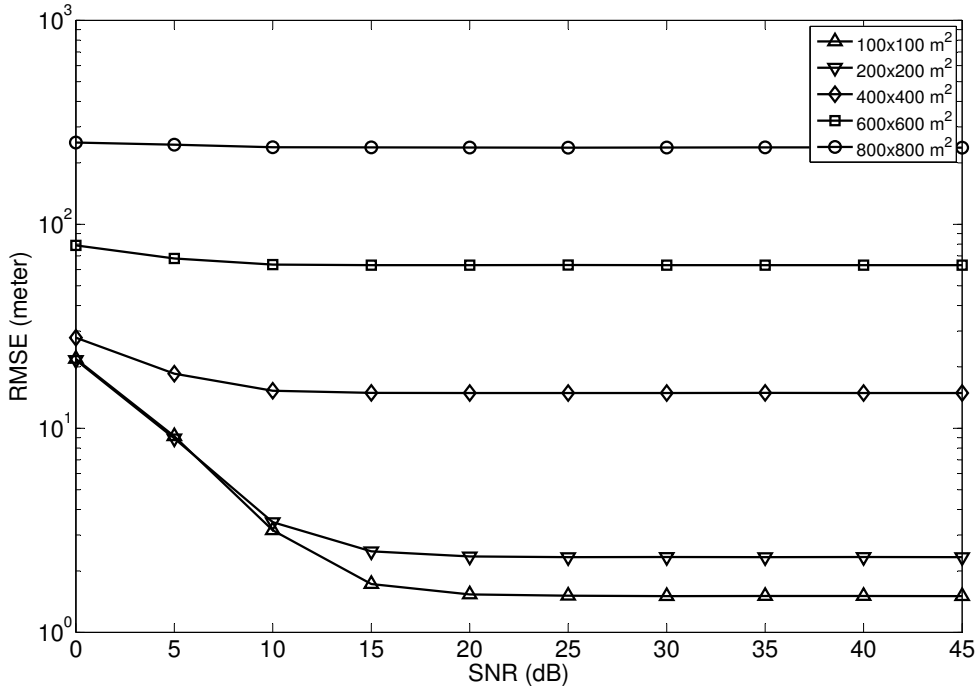

Figure 2.7. Fig. 2. RMSE vs. σ_{RSS} for each wide area of monitoring spot.

2.3.2 DOA-Based Factor Graph

A lot of work in DOA-based geolocation techniques has been proposed over the past 30 years [55, 56]. However, it was quite recently that the factor graph-based techniques using DOA were proposed, where the measurement data related to the DOA parameters are used as the input to the algorithms. A Joint TOA-DOA-based factor graph geolocation algorithm was proposed in [23], where the measured samples are efficiently used in factor graph to estimate the position accurately.

The factor graph geolocation technique derived in [23] is improved in [4] as suggested in [17]. It also removes the necessity of measuring the TOA data from the joint TOA-DOA-based factor graph geolocation algorithm shown in [23] to obtain a simple DOA-based factor graph technique. After the DOA-based factor graph technique reaches a convergence point, the position estimate results are used as the initial position for the Gauss-Newton (GN) algorithm as the second step of the algorithm, so-called factor graph - Gauss-Newton (FG-GN) geolocation technique in [4], to achieve even higher accuracy.

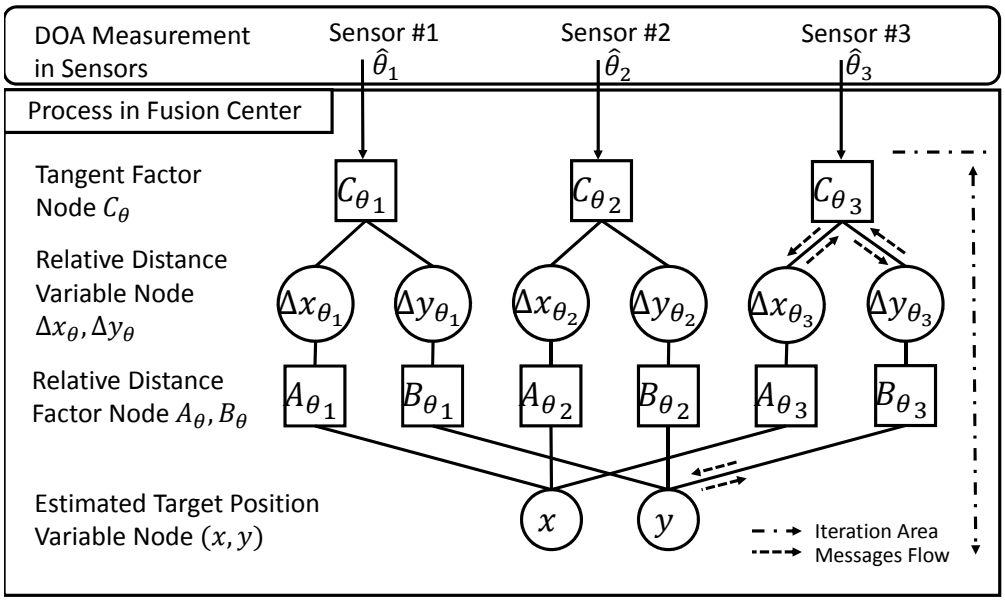

Figure 2.8. The conventional DOA-FG geolocation with number of sensors $N = 3$. The line with the arrow means the messages flow only in one direction, while the line without the arrow means the messages flow into two directions [4, 23].

We found that: (i) The joint TOA-DOA-based factor graph geolocation algorithm shown in [23] is still not fully correct because the message to be exchanged, the information of measurement error derived from the measurement results, enters the factor graph at improper node as identified by [17]. Furthermore, the derivation of the formula in *tangent factor node* C_θ in [23] is not provided. (ii) The mean formula at node C_θ [4] is not completely written. Furthermore, the derivation of the formula is unavailable. Hence, we are unable to complete the formula. (iii) The factor node used for collecting the samples is not available in DOA-based factor graph geolocation techniques in [4,23]. Fig. 2.8 shows the conventional factor graph for DOA-based geolocaiton technique. The mathematical expressions of the conventional DOA-FG in [4,23] are not shown in this dissertation because we proposed new expressions with detailed derivation in Chapter 3.

2.3.3 TOA-Based Factor Graph

The conventional TOA-FG in [17] is shown in Fig. 2.9. The required mathematical operations in the conventional TOA-FG are summarized in Table. 2.2, where the (m_i, σ_i^2) indicates the updated messages for each iteration in general. We replace (m_i, σ_i^2) with $\left(m_{x_i}, \sigma_{x_i}^2\right)$ and $\left(m_{y_i}, \sigma_{y_i}^2\right)$ for the messages forwarded from the node Δx and Δy to the node C_i, respectively, to provide more clarity. As we has described before in Chapter 1, the conventional TOA-FG technique can not be used to detect the position of unknown target because knowledge of the absolute departure time in the signal sent from the unknown target is unavailable. In Chapter 4, we present the proposed P-TDOA-FG with the detailed discussion of modification of the conventional TOA-FG in [17]. Hence, the modified TOA-FG can detect the position of a single static unknown radio wave emitter with TDOA parameters as the input.

2.3.4 Hyperbolic TDOA-Based Factor Graph

The conventional hyperbolic TDOA-Based Factor Graph (H-TDOA-FG) technique [6] uses a set of hyperbolic functions to obtain the target position estimate from TDOA samples. The measured TDOA samples and the information of sensor positions are converted into hyperbolic geometric parameters, e.g., the central point between the sensors, and the distances between the two points related to the hyperbolic curves where all the combinations of the hyperbolic curves in the set have to be taken into account. Only after that, the general quadratic hyperbolic function can

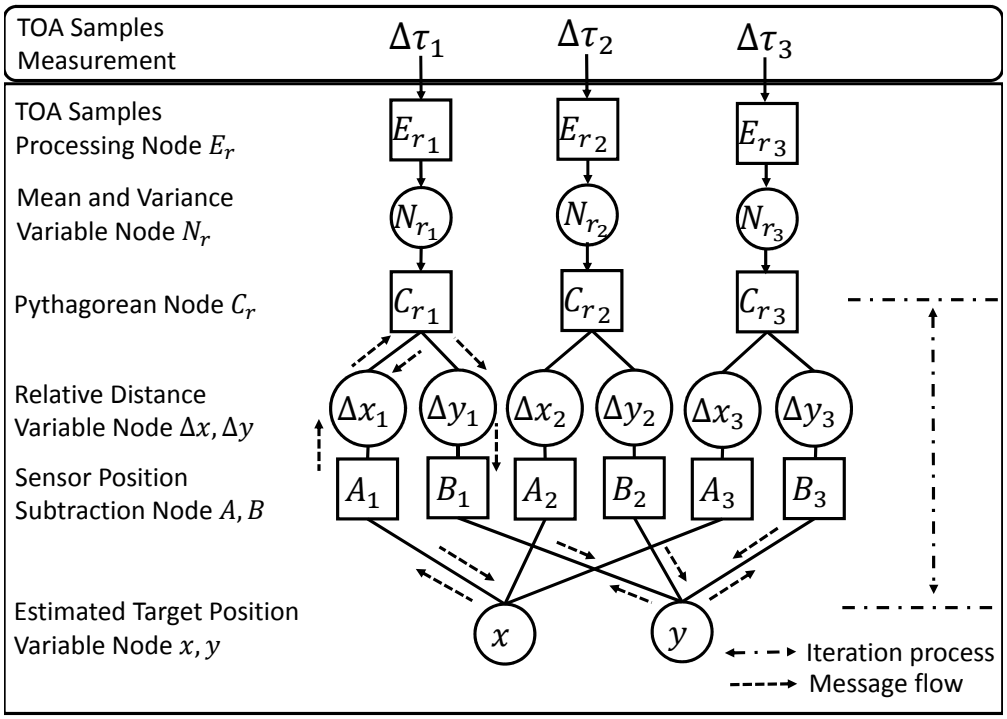

Figure 2.9. The conventional TOA-FG technique [17] with number of sensors $N = 3$.

Table 2.2. The operations required for each node in the conventional TOA-FG [17].

Messages Flow	Samples ($\hat{}$) and/or (Means, Variances)	
	Inputs	Outputs
$E_{r_i} \rightarrow N_{r_i}$	$\hat{r}_i$ samples	$\left(m_{\hat{r}_i}, \sigma^2_{\hat{r}_i}\right)$
$N_{r_i} \rightarrow C_{r_i}$	$\left(m_{\hat{r}_i}, \sigma^2_{\hat{r}_i}\right)$	$\left(m_{\hat{r}_i}, \sigma^2_{\hat{r}_i}\right)$
$C_{r_i} \rightarrow \Delta y_i$	$\left(m_{x_i}, \sigma^2_{x_i}\right)$ $\left(m_{\hat{r}_i}, \sigma^2_{\hat{r}_i}\right)$	$\left(\pm\sqrt{m^2_{\hat{r}_i} - m^2_{x_i}}, \frac{m^2_{\hat{r}_i}\sigma^2_{\hat{r}_i} + m^2_{x_i}\sigma^2_{x_i}}{m^2_{\hat{r}_i} - m^2_{x_i}}\right)$
$C_{r_i} \rightarrow \Delta x_i$	$\left(m_{y_i}, \sigma^2_{y_i}\right)$ $\left(m_{\hat{r}_i}, \sigma^2_{\hat{r}_i}\right)$	$\left(\pm\sqrt{m^2_{\hat{r}_i} - m^2_{y_i}}, \frac{m^2_{\hat{r}_i}\sigma^2_{\hat{r}_i} + m^2_{y_i}\sigma^2_{y_i}}{m^2_{\hat{r}_i} - m^2_{y_i}}\right)$
$C_{r_i} \leftarrow \Delta x_i \rightarrow A_i$ $C_{r_i} \leftarrow \Delta y_i \rightarrow B_i$	(m_i, σ^2_i)	(m_i, σ^2_i)
$\Delta x_i \leftarrow A_i \rightarrow x$	(m_i, σ^2_i)	$(X_i - m_i, \sigma^2_i)$
$\Delta y_i \leftarrow B_i \rightarrow y$	(m_i, σ^2_i)	$(Y_i - m_i, \sigma^2_i)$
$x \rightarrow A_i$ $y \rightarrow B_i$	$\left(m_j, \sigma^2_j\right)$ $j \neq i$	$\left(\sigma^2_i \sum_{j \neq i} \frac{m_j}{\sigma^2_j}, \sigma^2_i = \frac{1}{\sum_{j \neq i} \frac{1}{\sigma^2_j}}\right)$
x and y	(m_i, σ^2_i)	$\left(\sigma^2_\Lambda \sum_i \frac{m_i}{\sigma^2_i}, \sigma^2_\Lambda = \frac{1}{\sum_i \frac{1}{\sigma^2_i}}\right)$

be obtained. It should be noticed that hyperbolic function depends on the type, i.e., horizontal or vertical [57].

The coefficient of the general quadratic formula is used to obtain unitary matrix and its eigenvalues. Finally, the values are used by the nodes in the H-TDOA-FG nodes to perform hyperbolic rotation and shifting before obtaining the target coordinate position. Hence the conventional H-TDOA-FG technique is not compared to the proposed P-TDOA-FG technique because: (i) The conventional H-TDOA-FG technique has high computational complexity, even compared to the Gauss-Newton technique, as described before in Chapter 1. (ii) The derivation of conversion the TDOA parameters into hyperbolic functions and then converted again to the general quadratic functions are unavailable. Hence, it is quite difficult to fully investigate the conventional H-TDOA-FG technique. The detailed equations of the conventional H-TDOA-FG can be found in [6].

The brief explanation of hyperbolic function is provided in this section. There are two types of hyperbolic equations, i.e., horizontal and vertical hyperbolic equations. We discuss horizontal hyperbolic expressed as

$$\frac{(x - h_{i,j})^2}{a^2_{i,j}} - \frac{(y - k_{i,j})^2}{b^2_{i,j}} = 1, \tag{2.27}$$

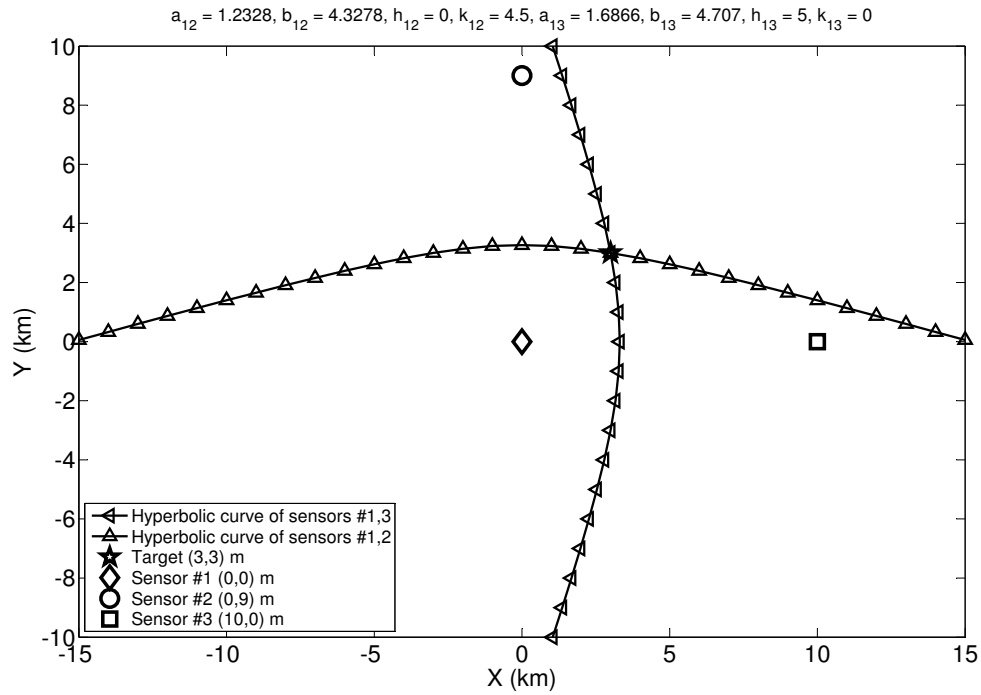

Figure 2.10. Intersection of at least two hyperbolic curves indicates the position of the unknown target.

with $a_{i,j} = \frac{d_{i,j}}{2}$, $c_{i,j} = \frac{r_{i,j}}{2}$, $b_{i,j} = \sqrt{c_{i,j}^2 - a_{i,j}^2}$, $h_{i,j} = \frac{X_i + X_j}{2}$, and $k_{i,j} = \frac{Y_i + Y_j}{2}$. $d_{i,j}$ is the different Euclidean distance, where we can directly obtain from TDOA conversion as $d_{i,j} = \tau_{i,j} \cdot v_c$. Euclidean distance between sensor i and j is denoted by $r_{i,j}$. This hyperbolic equation can be converted to general quadratic equation as

$$A_{i,j}x^2 + B_{i,j}xy + C_{i,j}y^2 + D_{i,j}x + E_{i,j}y + F_{i,j} = 0, \tag{2.28}$$

with $A_{i,j} = b_{i,j}^2$, $B_{i,j} = 0$, $C_{i,j} = -a_{i,j}^2$, $D_{i,j} = -2b_{i,j}^2 h_{i,j}$, $E_{i,j} = 2a_{i,j}^2 k_{i,j}$, and $F_{i,j} = -a_{i,j}^2 b_{i,j}^2 - a_{i,j}^2 k_{i,j}^2 + b_{i,j}^2 h_{i,j}^2$. The intersection of at least two hyperbolic curves is the position of the unknown target radio wave emitter as shown in Fig. 2.10.

2.3.5 Convergence Analysis of Factor Graph-Based Geolocation Technique

Since the factor graph-based geolocation was introduced more than 10 years ago by [39], various derivative algorithms using different wireless parameters have been proposed [3, 5, 6, 17–19, 23]. However, the proof of

the algorithm convergence in fully mathematical way has not yet been given. This is because of the difficulty in the analysis due to the cycles appearing inside the factor graph as mentioned in [6]. Despite the controversy of the convergence analysis, the functions in the factor graph-based techniques in many cases well behave as mentioned in [17]. Hence, it can be concluded that the factor graph techniques are near-optimum solution as mentioned also in [6,18] for wireless geolocation problems. Fully mathematical analysis of the convergence property of the factor graph techniques is also left as a future work.

2.4 Other Conventional Geolocation Techniques

2.4.1 RSS-based Voronoi

The algorithm of RSS-V [58] is briefly described in [59]. According to the technique shown in [58], the target receives the RSS information from several beacons, hence the target processes the RSS information to detect its own position estimate. The beacon in [58] is defined as the transmitter with fixed position, such as base station, wireless access point, etc. The position estimate is obtained by accumulating the measured RSS belonging to each Voronoi region. In [58], the Voronoi region is defined as $V(P_{v_i}) = x \in V(P_{v_i}) | r(x, P_{v_i}) \leq r(x, P_{v_j})$, where x and P_{v_i} indicate any point and a set of Voronoi point in the whole region, respectively, $r(x, P_{v_i})$ indicates the Euclidean distance between x and P_{v_i}, $i, i = 1, 2, ..., N, j, j = 1, 2, ..., N, j \neq i$, indicate the Voronoi point indexes. The Voronoi points can be the position of beacons, sensors, access points, and base stations. After that, the algorithm was improved in [59] by employing the triangle algorithm between two sensors and the target to obtain the straight line. The several crossing points made by several straight lines are close to the target position. The measured RSS value is included to the expectation of the crossing points as weighting factor in calculating the position estimate. In the RSS-V, high accuracy is achieved with the large number of sensors.

The RSS-V technique is used to select four monitoring spots for RSS-FG algorithm. The following process of RSS-V algorithm is modified from [59] so that it can be performed in the fusion center: 1) Create the Voronoi diagram based on sensors position. 2) Sort the sensors based on RSS value, where sensor with the highest RSS value is in the first position.

3) Add plots having the highest RSS value to the first Voronoi region. 4) Remove the first sensor from the system. 5) Re-create the Voronoi region based on the rest of the sensors, where the second sensor works as the new first sensor. 6) Add the plots having the second largest RSS value to the new Voronoi region of the next first sensor. 7) Repeat the processes of 3) to 6) until the calculation of the last sensor completed. 8) Obtain the target position by calculating the expectation of the coordinate positions with the highest accumulated RSS value.

2.4.2 RSS-Based RADAR and LANDMARC

Other well-known techniques in RSS-based geolocation are the RADAR [50] and the LANDMARC[2] [60]. The RADAR estimates the position by averaging several location of monitoring spots having the RSS measurement values close to the RSS measurement values of the signal sent from target. The LANDMARC, on the other hand, improves RADAR by introducing a weighting factor. The weighting factor is obtained from the Euclidean distance between RSS measurements of the signal sent from monitoring spots and the target. It is indicated in [18] that stochastic properties of RSS measurement errors are not taken into account by both conventional techniques. Moreover, the Euclidean distance used in the LANDMARC is not geometrically representing the actual distance. Similar to the conventional RSS-FG, the conventional RSS-based RADAR and LANDMARC also can not be used for the location detection of the unknown radio wave emitter because all of those three conventional techniques require the knowledge of the absolute transmit power of the unknown signal.

2.4.3 DOA-Based Least Squares

The conventional DOA-based least squares DOA-LS technique in [61] is summarized below:

$$\begin{bmatrix} m_{y_{LS}} \\ m_{x_{LS}} \end{bmatrix} = \left(\mathbf{A}_\theta^T \mathbf{A}_\theta\right)^{-1} \mathbf{A}_\theta^T \mathbf{b}_\theta, \tag{2.29}$$

[2]LANDMARC is a location sensing prototype system that uses Radio Frequency Identification (RFID) technology [60].

where

$$\mathbf{A}_\theta = \begin{bmatrix} 1 & -\tan\left(m_{N_{\theta_1}\to C_{\theta_1}}\right) \\ 1 & -\tan\left(m_{N_{\theta_2}\to C_{\theta_2}}\right) \\ \vdots & \vdots \\ 1 & -\tan\left(m_{N_{\theta_3}\to C_{\theta_3}}\right) \end{bmatrix}, \mathbf{b}_\theta = \begin{bmatrix} Y_1 - X_1\tan\left(m_{N_{\theta_1}\to C_{\theta_1}}\right) \\ Y_2 - X_2\tan\left(m_{N_{\theta_2}\to C_{\theta_2}}\right) \\ \vdots \\ Y_N - X_N\tan\left(m_{N_{\theta_3}\to C_{\theta_3}}\right) \end{bmatrix},$$

with $(m_{x_{LS}}, m_{y_{LS}})$ being the target position estimate.

2.4.4 DOA-Based Gauss-Newton

The Gauss-Newton algorithm is one of the most popular iterative algorithms for solving non-linear equations. Hence, the algorithm can be used for the estimation the target position, in principle. The algorithm is very fast to converge in terms of iteration number with given good initial value [6]. The Gauss-Newton algorithm for geolocation is summarized as below [6, 62]

$$\begin{bmatrix} x^{(q+1)} \\ y^{(q+1)} \end{bmatrix} = \begin{bmatrix} x^{(q)} \\ y^{(q)} \end{bmatrix} + \left(\left(\mathbf{J}^{(q)}\right)^T \mathbf{\Sigma}_\theta^{-1}\left(\mathbf{J}^{(q)}\right)\right)^{-1}\left(\mathbf{J}^{(q)}\right)^T \mathbf{\Sigma}_\theta^{-1}\left(\mathbf{m}_\theta - \theta^{(q)}\right), \quad (2.30)$$

where for the DOA-based Gauss-Newton (DOA-GN) geolocation technique, $\mathbf{J}^{(q)} = \frac{\partial\theta}{\partial\mathbf{x}}$ denotes Jacobian matrix at q-th iteration given by [4]

$$\mathbf{J}^{(q)} = \mathbf{J_{DOA}}^{(q)} = \begin{bmatrix} \frac{Y_1 - y^{(q)}}{(r_1^{(q)})^2} & -\frac{X_1 - x^{(q)}}{(r_1^{(q)})^2} \\ \frac{Y_2 - y^{(q)}}{(r_2^{(q)})^2} & -\frac{X_2 - x^{(q)}}{(r_2^{(q)})^2} \\ \vdots & \vdots \\ \frac{Y_N - y^{(q)}}{(r_N^{(q)})^2} & -\frac{X_N - x^{(q)}}{(r_N^{(q)})^2} \end{bmatrix} \quad (2.31)$$

with the r_N denoting the Euclidean distance between the target and the sensors, Σ_θ^{-1} and $\mathbf{m}_\theta$ indicates the covariance matrix and mean of DOA samples, respectively, and $\theta^{(q)} = \arctan\left(\frac{Y_i - y^{(q)}}{X_i - x^{(q)}}\right)$ in units of radiant. As indicated in [6], The Gauss-Newton algorithm faces convergence problems for the conditions as follows: (i) the target is at the undesirable locations, for example, very near to the sensors, and (ii) the initial value for the iteration process of the Gauss-Newton has to be correctly chosen. This is because rank deficiency in those conditions results in failure to inverse the matrix.

2.5 Complexity Analysis Overview of Conventional Techniques

The complexity analyses of conventional factor graph geolocation techniques are provided in [6, 17, 18] for TOA-FG [17], RSS-FG [18], and H-TDOA-FG [6]. It is mentioned in [17, 18] that the conventional TOA-FG [17] and RSS-FG [18] have computational complexity/load *linearly* proportional to N. This is because the both factor graph techniques only require to solve linear functions. The linear approximation is of great importance in the factor graph techniques to preserve the Gaussianity assumption so that the messages in the factor graph algorithm can only be in the form of means and variances. This approximation also provides simple mathematical operations in each factor node. Hence, it results in significant reduction of computational complexity.

Even though other geolocation techniques without using factor graph, such as, Newton's method, Gauss-Newton aglorithm, nonlinear least squares (NLSS), and method of moments (MOM), have been able to achieve CRLB, those techniques require high computational complexity for solving non-linear equations [6, 19, 63]. It is indicated in [17, 18] that the number of derivative alone required in the Newton's method, the popular method to solve the non-linear functions, is proportional to $(2N)^2$.

2.6 Geolocation Theoterical Limit

The CRLB is widely used for evaluation and benchmarking of the performance of the estimator including the accuracy of position estimate of geolocation techniques [64, 65]. In this section we derived the CRLB for DOA- and TOA-based technique taking into account the number of samples. We also derive the approximated CRLB for TDOA-based technique. Accurate derivations for CRLB for TDOA-, RSS- and DRSS-based geolocation techniques are left for future work.

Among the existing variance bounds, the CRLB is the easiest lower bound on the variance of any unbiased estimator to determine whether an estimator can achieve the bound [64]. The measured parameter-based geolocation technique is also an estimator that is used for calculating the position estimate of the radio emitter by utilizing the measured parameter. As shown in [65], the errors of target position estimation due to the variance are included in the RMSE as

$$\text{RMSE} = \sqrt{E[(x-\hat{x})^2 + (y-\hat{y})^2]}, \tag{2.32}$$

where $(\hat{x}, \hat{y})$ is the target position estimate. The CRLB provides a lower bound to the RMSE as

$$\text{RMSE} \geq \text{CRLB}, \tag{2.33}$$

where the variance inside the CRLB is from the given parameter measurement errors.

In the CRLB, the lowest achievable variance as well as the relationship between the variance of the parameter measurement errors and the target position can be seen from the Fisher Information Matrix (FIM) as [10, 64, 65]

$$\mathbf{F}(\mathbf{x}) = E\left[\left(\frac{\partial}{\partial \mathbf{x}} \ln p(\hat{\theta})\right)^2\right], \tag{2.34}$$

where the sensor index i is omitted. Hence, the CRLB is expressed as

$$\text{CRLB} = \sqrt{\text{trace}(\mathbf{F}^{-1}(\mathbf{x}))}. \tag{2.35}$$

The detailed derivation of the CRLB refers to Appendix A.

2.6.1 CRLB for DOA-based Geolocation

This section derives the CRLB for DOA-based geolocation, taking into account the number of samples. The CRLB for DOA-based geolocation is presented in [4], however, it does not take into account the number of samples. Assume that the unknown radio wave emitter is located at coordinate position $\mathbf{x} = [x\ y]^T$, where $(\cdot)^T$ is the transpose function. Sensors are located at positions $\mathbf{X} = [X_i\ Y_i]^T$, where i, $i = \{1, 2, ..., N\}$, is the sensor index. It should be noticed that the sensor index is not assigned in a vector $\mathbf{X}$.

The likelihood for K identically independently distributed (i.i.d.) samples, each following the Gaussian distribution is presented in [64], as

$$p(\hat{\theta}_i) = \prod_{k=0}^{K-1} \frac{1}{\sqrt{2\pi\sigma_{\theta_i}^2}} \exp\left(-\frac{1}{2\sigma_{\theta_i}^2}\left(\hat{\theta}_{i,k} - \theta_i\right)^2\right),$$

where $\hat{\theta}_k,\ k = \{1, 2, ..., K\}$, indicates the DOA samples, $\theta_i = \arctan\left(\frac{Y_i - y}{X_i - x}\right)$ indicates the true DOA. After several mathematical manipulations shown in Appendix A, a closed-form of the second-order derivative of log-likelihood function (LLF) is expressed as [64]

$$\frac{\partial^2}{\partial \theta_i^2} \ln p(\hat{\theta}_i) = -\frac{K}{\sigma_{\theta_i}^2}. \tag{2.36}$$

A closed-form CRLB for DOA-based geolocation technique taking into account the number of samples is found to be

$$\text{CRLB} = \sqrt{\text{trace}\left(\left(\mathbf{J}^T \Sigma_\theta^{-1} \mathbf{J}\right) K\right)^{-1}}, \tag{2.37}$$

where $\mathbf{\Sigma}_\theta = \sigma_\theta^2 \mathbf{I}_N$ denotes Gaussian covariance, $\mathbf{I}_N$ denotes an $N \times N$ identity matrix, $(.)^{-1}$ is the inverse matrix of its argument, and $\mathbf{J}$ denotes Jacobian matrix given by

$$\mathbf{J} = \mathbf{J_{DOA}} = \begin{bmatrix} \frac{Y_1 - y}{r_1^2} & -\frac{X_1 - x}{r_1^2} \\ \frac{Y_2 - y}{r_2^2} & -\frac{X_2 - x}{r_2^2} \\ \vdots & \vdots \\ \frac{Y_N - y}{r_N^2} & -\frac{X_N - x}{r_N^2} \end{bmatrix} \tag{2.38}$$

with the r_N denoting the Euclidean distance between the target and the sensors.

2.6.2 CRLB for TOA-based Geolocation

The CRLB for TOA-based geolocation as the same with (2.37). $\mathbf{\Sigma}_\theta$ is replaced by $\mathbf{\Sigma}_r = \sigma_r^2 \mathbf{I}_N$ indicating Gaussian covariance for TOA measurement error vectors with the multiple sensors. $\mathbf{I}_N$ indicates an $N \times N$ identity matrix. N denotes the number of sensors, and K the number of samples.

The CRLB for the TOA-based estimates in [6] do not take into account the number of samples. The CRLB for the TOA-based technique in [66] takes into account the number of samples, but it is not in the closed form.

$\mathbf{J}$ denotes Jacobian matrix as described in [6, 64], given by

$$\mathbf{J} = \mathbf{J_{TOA}} = \begin{bmatrix} \frac{x - X_1}{r_1} & \frac{y - Y_1}{r_1} \\ \frac{x - X_2}{r_2} & \frac{y - Y_2}{r_2} \\ \cdots & \cdots \\ \frac{x - X_N}{r_N} & \frac{y - Y_N}{r_N} \end{bmatrix}, \tag{2.39}$$

2.6.3 Approximated CRLB for TDOA-based Geolocation

Since the calculation of TDOA samples involves the subtraction of the arrival time of the signal of the target at two sensors, the TDOA samples

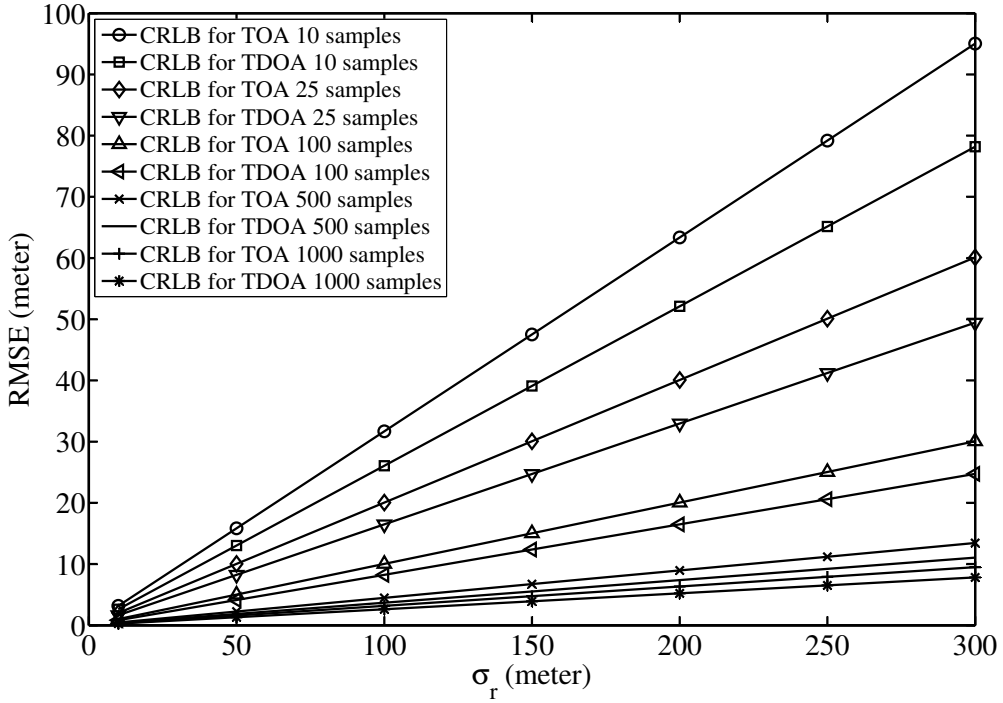

Figure 2.11. RMSE of CRLBs for TOA and TDOA geolocation vs. σ_r

are correlated. However, the CRLB for TDOA-based geolocation technique is needed for comparison purpose. For simplicity, we follow [6] to use the approximation of CRLB for TDOA-based geolocation technique in this research. As mentioned in [6], the approximated CRLB assumes perfect power control to obtain the TDOA measurement is linearly independent. Hence, the noise covariance matrix of TDOA measurement error is diagonal matrix.

The approximated CRLB of position estimate for TDOA-based geolocation in [6] does not take into account the number of samples. Hence, we use (2.37) to derive the approximated CRLB by replacing $\mathbf{\Sigma}_\theta$ with $\mathbf{\Sigma}_d = \sigma_d^2 \mathbf{I}_N$. $\mathbf{\Sigma}_d$ indicates Gaussian covariance for TDOA measurement error vectors with the multiple sensors. $\mathbf{J}$ denotes Jacobian matrix as described in [6, 64], given by

$$\mathbf{J} = \mathbf{J_{TDOA}} = \begin{bmatrix} \frac{x-X_2}{r_2} - \frac{x-X_1}{r_1} & \frac{y-Y_2}{r_2} - \frac{y-Y_1}{r_1} \\ \frac{x-X_2}{r_2} - \frac{x-X_1}{r_1} & \frac{y-Y_3}{r_3} - \frac{y-Y_1}{r_1} \\ \cdots & \cdots \\ \frac{x-X_N}{r_N} - \frac{x-X_1}{r_1} & \frac{y-Y_N}{r_N} - \frac{y-Y_1}{r_1} \end{bmatrix}. \tag{2.40}$$

Fig. 2.11 shows that the higher number of samples, the lower of the CRLB

of and the approximated CRLB for TOA- and TDOA-based geolocation, respectively, can be achieved. It is also shown in the figure that the approximated CRLB for TOA-based geolocation always (in most cases) higher than that for TDOA, which is consistent to [6].

It should be noticed that the CRLB for TDOA-based geolocation is only one. However, beside the approximation as described above, other works related to the approximated CRLB for TDOA-based gelocation are: (i) The CRLB for TOA-based geolocation shown in [67] is always (in most cases) lower than that for TDOA. This is because the noise covariance matrix for TDOA is non-diagonal matrix due to the correlation of TDOA measurement. ii) The CRLB of position estimate by using the TDOA and the TOA measurement computed in [68] shows that the CRLBs are identical for both TOA-based and TDOA-based geolocation. Given the facts described above, the further study of the CRLB of position estimate for TDOA-based geolocation is left for future work.

2.7 Summary

In this section we have presented the factor graph overview, Gaussianity assumption for measurement error, the overview of several geolocation techniques, computational complexity analysis, and the CRLB for geolocation. The overview of conventional factor graph-based technique discussed in this chapter covers the RSS-FG, DOA-FG, TOA-FG, and H-TDOA-FG. We also describe the path-loss model within the RSS-FG description. The other conventional techniques briefly discussed in this chapter are the RSS-V, RADAR and LANDMARC, DOA-LS, and DOA-GN techniques.

Chapter 3

Taylor Series DOA-Based Factor Graphs Geolocation

This chapter provides a description of our technique using the first order of Taylor-series expansion to established the new TS-DOA-FG technique for position detection of unknown target. Clear understanding of the DOA-based geolocation techniques using FG, where the detail explanation of how the messages are updated at each node, and how the updated messages are exchanged between the nodes is presented in this chapter. The primary objectives of this chapter are as follows: (A) The Taylor-series expansion used for linear approximation at the tangent and cotangent factor nodes is introduced. This approximation maintains the Gaussianity of the messages. (B) Results of a series of simulations are presented to evaluate the convergence property of the proposed technique, where the trajectory of the iterative estimation process is presented. Comparison between the RMSE of the proposed technique and the new CRLB is also provided. It is shown that the proposed algorithm can achieve close-CRLB accuracy, where the number of the samples, the number of the sensors, and the standard deviation of measurement error, are used as a parameter.

Since the detailed description of the algorithm for the DOA-FG geolocation techniques presented in [4, 23] have improper expression as mentioned above in Chapter 2, the accuracy of the proposed technique is not compared with that of [23] and [4]. Instead, the accuracy comparison is between the proposed technique and the (DOA-LS) geolocation [61] and DOA-GN [6, 62]. The factor-graph proposed in this chapter includes the DOA *measurement factor node* E_θ as shown in Fig. 3.1, according to [17]. It is also shown in this section that with the proposed technique, the accuracy of the target position estimation outperforms the conven-

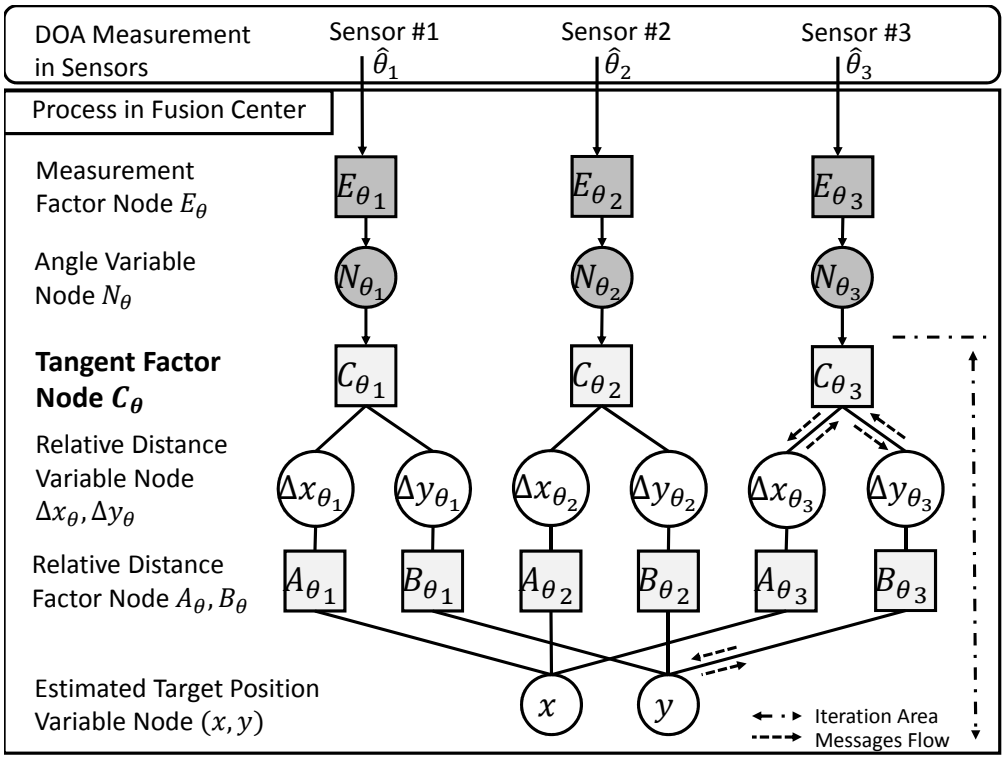

Figure 3.1. The proposed TS-DOA-FG for Geolocation Technique . We propose new expression/functions in lightgray nodes, mainly in node C_θ, and new nodes in darkgray nodes

tional DOA-LS geolocation technique, and the results are also very close to theoretical CRLB for the DOA-based geolocation.

3.1 System Model

The orientation of the sensors is assumed to be known to ensure that the sensors measure the angle with respect to the global coordinate system. The sensor-to-fusion center transmission is perfect via wired or wireless connections. $\mathbf{\Delta_x} = [\Delta y_{\theta_i}\ \Delta x_{\theta_i}]^T$ is the relative distance between the sensor position (X_i, Y_i) and target position (x, y), given by

$$\begin{bmatrix} \Delta x_{\theta_i} \\ \Delta y_{\theta_i} \end{bmatrix} = \begin{bmatrix} X_i \\ Y_i \end{bmatrix} - \begin{bmatrix} x \\ y \end{bmatrix}, \tag{3.1}$$

with the θ_i being the true DOA. For the notation simplicity, the sensor index i is omitted from the equations common to all the sensors, while it is included when needed, in the rest of the dissertation.

The relative distance in (3.1) in the (X, Y) coordinate and the true DOA θ are connected by the tangent and cotangent functions, as [4, 23]

$$\Delta y_\theta = \Delta x_\theta \cdot \tan(\theta), \tag{3.2}$$
$$\Delta x_\theta = \Delta y_\theta \cdot \cot(\theta). \tag{3.3}$$

Even though (3.2) and (3.3) are self-referenced point equation, which can be solved by iterative techniques, the iteration needs proper initialization of the mean and variance of the argument variables $\Delta\hat{x_\theta}$ and $\Delta\hat{y_\theta}$ which are corresponding to $\hat{x}$ and $\hat{y}$ by (3.1) and (2.9), where the detail of initializations are described in Section 5. The true values of θ, Δx_θ, Δy_θ, x, and y, are not known, however, the message needed in the factor graph is the mean and variance of samples $\hat{\theta}$, $\Delta x_{\hat{\theta}}$, $\Delta y_{\hat{\theta}}$, $\hat{x}$, and $\hat{y}$, which can be produced from the angle messages in the form of mean and variance of samples $\hat{\theta}$, $(m_{E_\theta \to N_\theta}, \sigma^2_{E_\theta \to N_\theta})$. The details of entire process are described in next section.

3.2 Proposed Technique

Each sensor does not know the needed values of θ and σ_θ. Hence, Each sensor in the proposed TS-DOA-FG geolocation technique first calculates the mean $m_{E_\theta \to N_\theta}$ and the variance $\sigma^2_{E_\theta \to N_\theta}$ from the K measured samples. The node E_θ forwards the messages $(m_{E_\theta \to N_\theta}, \sigma^2_{E_\theta \to N_\theta})$ to the *angle variable node* N_θ and then the messages $(m_{N_\theta \to C_\theta}, \sigma^2_{N_\theta \to C_\theta})$ are directly forwarded to the *tangent factor node* C_θ, where $m_{N_\theta \to C_\theta} = m_{E_\theta \to N_\theta}$ and $\sigma^2_{N_\theta \to C_\theta} = \sigma^2_{E_\theta \to N_\theta}$. The angle messages $(m_{N_\theta \to C_\theta}, \sigma^2_{N_\theta \to C_\theta})$ are converted to relative distance messages $(m_{C_\theta \to \Delta x_\theta}, \sigma^2_{C_\theta \to \Delta x_\theta})$ and $(m_{C_\theta \to \Delta y_\theta}, \sigma^2_{C_\theta \to \Delta y_\theta})$ in the node C_θ.

The messages corresponding to Δy_θ and Δx_θ of (3.2) and (3.3), respectively, are the mean and variance, i.e., $(m_{C_\theta \to \Delta x_\theta}, \sigma^2_{C_\theta \to \Delta x_\theta})$ and $(m_{C_\theta \to \Delta y_\theta}, \sigma^2_{C_\theta \to \Delta y_\theta})$, where $m_{C_\theta \to \Delta x_\theta}$ and $m_{C_\theta \to \Delta y_\theta}$ are the means of $\Delta x_{\hat{\theta}}$ and $\Delta y_{\hat{\theta}}$, respectively; $\sigma^2_{C_\theta \to \Delta x_\theta}$ and $\sigma^2_{C_\theta \to \Delta y_\theta}$ are the variances of $\Delta x_{\hat{\theta}}$ and $\Delta y_{\hat{\theta}}$, respectively. The messages for (3.2) and (3.3), are derived based on the formula for the product of two independent random variables $(a \cdot b)$ as [69]

$$m_{a \cdot b} = m_a \cdot m_b, \tag{3.4}$$
$$\sigma^2_{a \cdot b} = m_a^2 \cdot \sigma_b^2 + m_b^2 \cdot \sigma_a^2 + \sigma_a^2 \cdot \sigma_b^2, \tag{3.5}$$

where m_x and σ_x^2, $x \in \{a, b, a \cdot b\}$, are the mean and variance of x, respectively. It should be noticed from (3.2)–(3.5) that the means and variances of $\tan(\hat{\theta})$ and $\cot(\hat{\theta})$, $m_{\tan(\hat{\theta})}$ and $\sigma^2_{\tan(\hat{\theta})}$, and $m_{\cot(\hat{\theta})}$ and $\sigma^2_{\cot(\hat{\theta})}$, are required. However, there arises a problem because $\tan(\hat{\theta})$ and $\cot(\hat{\theta})$ in (3.3) and (3.2) are both nonlinear functions, that violates the Gaussianity assumption to express the messages only by the mean and variance in the FG. This motivates us to use the first-order Taylor series to derive linear approximation of the tangent and cotangent functions to obtain the messages corresponding to the relative distance, as $(m_{C_\theta \to \Delta x_\theta}, \sigma^2_{C_\theta \to \Delta x_\theta})$ and $(m_{C_\theta \to \Delta y_\theta}, \sigma^2_{C_\theta \to \Delta y_\theta})$. The detailed derivation is described below.

The first-order Taylor series is expressed as [70]

$$f(\hat{\theta}) \approx f(m_{\hat{\theta}}) + f'(m_{\hat{\theta}})(\hat{\theta} - m_{\hat{\theta}}), \tag{3.6}$$

where $f(\hat{\theta})$ is either $\tan(\hat{\theta})$ or $\cot(\hat{\theta})$, $\hat{\theta}$ is the DOA sample, $m_{\hat{\theta}}$ is the mean of $\hat{\theta}$, $f(m_{\hat{\theta}})$ is either the $\tan(m_{\hat{\theta}})$ or $\cot(m_{\hat{\theta}})$, and $f'(m_{\hat{\theta}})$ is the first derivative of $f(m_{\hat{\theta}})$. The condition for that approximation is working well for $\hat{\theta} - m_{\hat{\theta}}$ approaching 0 (zero). It is shown in Fig. 3.5 showing that the lower standard deviation of measurement error, the higher accuracy is achieved. We obtain the linear approximation as

$$\tan(\hat{\theta}) \approx \tan(m_{\hat{\theta}}) - m_{\hat{\theta}} \sec^2(m_{\hat{\theta}}) + \sec^2(m_{\hat{\theta}})(\hat{\theta}), \tag{3.7}$$

$$\cot(\hat{\theta}) \approx \cot(m_{\hat{\theta}}) - m_{\hat{\theta}} \csc^2(m_{\hat{\theta}}) + \csc^2(m_{\hat{\theta}})(\hat{\theta}). \tag{3.8}$$

It can be seen that (3.7) and (3.8) are linear equations with respect to $\hat{\theta}$ variable, where $m_{\hat{\theta}}$, $\tan(m_{\hat{\theta}})$, $\cot(m_{\hat{\theta}})$, $\sec^2(m_{\hat{\theta}})$, and $\csc^2(m_{\hat{\theta}})$ are constants.

It should be noticed that (3.6) is a linear approximation for function of $\hat{\theta}$, and hence it is found that $f(\hat{\theta})$ can be approximated by a Gaussian variable. The mean $m_{f(\hat{\theta})}$ and variance $\sigma^2_{f(\hat{\theta})}$ can then be approximated using (3.6) as [70]

$$m_{f(\hat{\theta})} \approx f(m_{\hat{\theta}}), \tag{3.9}$$

$$\sigma^2_{f(\hat{\theta})} \approx (f'(m_{\hat{\theta}}))^2 \cdot \sigma^2_{\hat{\theta}}, \tag{3.10}$$

where $\sigma^2_{\hat{\theta}}$ is the variance of $\hat{\theta}$. The mean and variance of $\tan(\hat{\theta})$ and $\cot(\hat{\theta})$ are obtained from (3.9) and (3.10) as below:

$$m_{\tan(\hat{\theta})} \approx \tan(m_{\hat{\theta}}), \tag{3.11}$$

$$m_{\cot(\hat{\theta})} \approx \cot(m_{\hat{\theta}}), \tag{3.12}$$

$$\sigma^2_{\tan(\hat{\theta})} \approx \sec^4(m_{\hat{\theta}}) \cdot \sigma^2_{\hat{\theta}}, \tag{3.13}$$

$$\sigma^2_{\cot(\hat{\theta})} \approx \csc^4(m_{\hat{\theta}}) \cdot \sigma^2_{\hat{\theta}}. \tag{3.14}$$

The approximation of (3.8), (3.12), and (3.14) works very well over relatively large value range of the angle except for mean of angle around 0°. This exception is because $\cot(0)$ and $\csc(0)$ are infinity. Hence, we can solve the infinity problem by empirically setting a limit value of m_θ. We found that $m_{\hat{\theta}} \geq |0.1|$ in units of radiant is reasonable. It should be noticed, that in our computer simulation, the tangent and cotangent functions are with argument angle in units of radiant. By setting the limit value properly, unstable behavior of the algorithm can be avoided. Theoretically, we also require to set the limit value of $m_{\hat{\theta}}$ for (3.7), (3.11), and (3.13) to avoid the infinity value. It should be noticed that, in practice, tangent function for $m_{\hat{\theta}} = \{\pi/2, 3\pi/2\}$ does not result in the infinity value. This is because the π value in the computer simulation is also an approximated value.

The node C_θ calculates relative distance messages, $(m_{C_\theta \to \Delta x_\theta}, \sigma^2_{C_\theta \to \Delta x_\theta})$ and $(m_{C_\theta \to \Delta y_\theta}, \sigma^2_{C_\theta \to \Delta x_\theta})$, according to (3.2)–(3.5) and (3.11)–(3.14), as:

$$
\begin{aligned}
m_{C_\theta \to \Delta y_\theta} &\approx m_{\Delta x_\theta \to C_\theta} \cdot \tan(m_{N_\theta \to C_\theta}), && (3.15)\\
m_{C_\theta \to \Delta x_\theta} &\approx m_{\Delta y_\theta \to C_\theta} \cdot \cot(m_{N_\theta \to C_\theta}), && (3.16)\\
\sigma^2_{C_\theta \to \Delta y_\theta} &\approx \sigma^2_{\Delta x_\theta \to C_\theta} \cdot \tan^2(m_{N_\theta \to C_\theta}) && (3.17)\\
&\quad + m^2_{\Delta x_\theta \to C_\theta} \cdot \sigma^2_{N_\theta \to C_\theta} \cdot \sec^4(m_{N_\theta \to C_\theta})\\
&\quad + \sigma^2_{\Delta x_\theta \to C_\theta} \cdot \sigma^2_{N_\theta \to C_\theta} \cdot \sec^4(m_{N_\theta \to C_\theta}),\\
\sigma^2_{C_\theta \to \Delta x_\theta} &\approx \sigma^2_{\Delta y_\theta \to C_\theta} \cdot \cot^2(m_{N_\theta \to C_\theta}) && (3.18)\\
&\quad + m^2_{\Delta y_\theta \to C_\theta} \cdot \sigma^2_{N_\theta \to C_\theta} \cdot \csc^4(m_{N_\theta \to C_\theta})\\
&\quad + \sigma^2_{\Delta y_\theta \to C_\theta} \cdot \sigma^2_{N_\theta \to C_\theta} \cdot \csc^4(m_{N_\theta \to C_\theta}).
\end{aligned}
$$

The node C_θ forwards the messages $(m_{C_\theta \to \Delta x_\theta}, \sigma^2_{C_\theta \to \Delta x_\theta})$ obtained from (3.16) and (3.18) to the *relative distance variable node* Δx_θ for the X-coordinate, while the messages $(m_{C_\theta \to \Delta y_\theta}, \sigma^2_{C_\theta \to \Delta y_\theta})$ obtained from (3.15) and (3.17) is forwarded to the *relative distance variable node* Δy_θ for the Y-coordinate. The variable node Δx_θ directly forwards the messages $(m_{\Delta x_\theta \to A_\theta}, \sigma^2_{\Delta x_\theta \to A_\theta})$ to the *relative distance factor node* A_θ, where $(m_{\Delta x_\theta \to A_\theta}, \sigma^2_{\Delta x_\theta \to A_\theta}) = (m_{C_\theta \to \Delta x_\theta}, \sigma^2_{C_\theta \to \Delta x_\theta})$. The node Δy_θ forwards the messages $(m_{\Delta y_\theta \to B_\theta}, \sigma^2_{\Delta y_\theta \to B_\theta})$ to the *relative distance factor node* B_θ, where $(m_{\Delta y_\theta \to B_\theta}, \sigma^2_{\Delta y_\theta \to B_\theta}) = (m_{C_\theta \to \Delta y_\theta}, \sigma^2_{C_\theta \to \Delta y_\theta})$.

The messages in the nodes A_θ and B_θ are finally converted to the

coordinate variable node, as [4, 17, 23]

$$(m_{A_\theta \to \Delta x_\theta}, \sigma^2_{A_\theta \to \Delta x_\theta}) = (X - m_{x \to A_\theta}, \sigma^2_{x \to A_\theta}), \tag{3.19}$$

$$(m_{B_\theta \to \Delta y_\theta}, \sigma^2_{B_\theta \to \Delta y_\theta}) = (Y - m_{y \to B_\theta}, \sigma^2_{y \to B_\theta}), \tag{3.20}$$

$$(m_{A_\theta \to x}, \sigma^2_{A_\theta \to x}) = (X - m_{\Delta x_\theta \to A_\theta}, \sigma^2_{\Delta x_\theta \to A_\theta}), \tag{3.21}$$

$$(m_{B_\theta \to y}, \sigma^2_{B_\theta \to y}) = (Y - m_{\Delta y_\theta \to B_\theta}, \sigma^2_{\Delta y_\theta \to B_\theta}). \tag{3.22}$$

As shown in Fig. 3.1, the messages of (3.21) and (3.22), $(m_{A_\theta \to x}, \sigma^2_{A_\theta \to x})$ and $(m_{B_\theta \to y}, \sigma^2_{B_\theta \to y})$, produced by the nodes A_θ and B_θ, respectively, are forwarded to the *estimated target position variable node* x and y. According to the message passing principle, now the reverse process is invoked. Recall that the sensor index was omitted in the equations, however to derive the message sent from the variable nodes x and y, the sensor index has to be introduced. All the messages coming from the nodes $A_{\theta_j}, j = \{1, ..., N\}$, except for the message sent back to the node A_{θ_i}, are used in the node x. It can be easily found by invoking the fact that the products of multiple Gaussian pdfs having different means and variances are also Gaussian pdf, the messages sent back from the variable node x to the factor node A_{θ_i} is given by $(m_{x \to A_{\theta_i}}, \sigma^2_{x \to A_{\theta_i}})$ [4,17,23,37] by using sum-product algorithm in (2.5) and (2.4), where $m_{z \to Z_i}$ indicates $m_{x \to A_{\theta_i}}$ and $\sigma^2_{z \to Z_i}$ indicates $\sigma^2_{x \to A_{\theta_i}}$. The messages $(m_{y \to B_{\theta_i}}, \sigma^2_{y \to B_{\theta_i}})$ can be obtained in the same way as $(m_{x \to A_{\theta_i}}, \sigma^2_{x \to A_{\theta_i}})$ calculated by (2.5) and (2.4).

The messages $(m_{x \to A_{\theta_i}}, \sigma^2_{x \to A_{\theta_i}})$ of (2.5) and (2.4) sent to the node A_{θ_i} is used by (3.19) to calculate the messages $(m_{A_{\theta_i} \to \Delta x_{\theta_i}}, \sigma^2_{A_{\theta_i} \to \Delta x_{\theta_i}})$, and in the same way, the messages $(m_{B_{\theta_i} \to \Delta y_{\theta_i}}, \sigma^2_{B_{\theta_i} \to \Delta y_{\theta_i}})$ is calculated by (3.20) using $(m_{y \to B_{\theta_i}}, \sigma^2_{y \to B_{\theta_i}})$. The messages $(m_{A_{\theta_i} \to \Delta x_{\theta_i}}, \sigma^2_{A_{\theta_i} \to \Delta x_{\theta_i}})$ of (3.19) is forwarded from the node A_{θ_i} to the node Δx_{θ_i} and then the messages $(m_{\Delta x_{\theta_i} \to C_{\theta_i}}, \sigma^2_{\Delta x_{\theta_i} \to C_{\theta_i}})$ is directly forwarded to the node C_{θ_i}, where $(m_{\Delta x_{\theta_i} \to C_{\theta_i}}, \sigma^2_{\Delta x_{\theta_i} \to C_{\theta_i}}) = (m_{A_{\theta_i} \to \Delta x_{\theta_i}}, \sigma^2_{A_{\theta_i} \to \Delta x_{\theta_i}})$. The messages $(m_{B_{\theta_i} \to \Delta y_{\theta_i}}, \sigma^2_{B_{\theta_i} \to \Delta y_{\theta_i}})$ of (3.20) is forwarded from the node B_{θ_i} to the node Δy_{θ_i} and then the messages $(m_{\Delta y_{\theta_i} \to C_{\theta_i}}, \sigma^2_{\Delta y_{\theta_i} \to C_{\theta_i}})$ is forwarded to the node C_{θ_i}, where $(m_{\Delta y_{\theta_i} \to C_{\theta_i}}, \sigma^2_{\Delta y_{\theta_i} \to C_{\theta_i}}) = (m_{B_{\theta_i} \to \Delta y_{\theta_i}}, \sigma^2_{B_{\theta_i} \to \Delta y_{\theta_i}})$. The entire process is repeated iteratively.

When the iteration converges or maximum iteration is reached, all messages from the node A_{θ_i} and B_{θ_i} are combined in the nodes x and y by using sum-product algorithm in (2.7) and (2.8) [4, 17, 23, 37]. Finally, the estimated coordinate position (x, y) of unknown radio wave emitter is determined by (m_x, m_y). To provide more comprehensive understanding, all equations operating at each node of the factor graph are summarized

Table 3.1. The operations required for each node in the proposed TS-DOA-FG.

Nodes	(Means, Variances)			
	Inputs	Outputs	Flops	Remarks
$E_{\theta_i} \rightarrow N_{\theta_i}$	$\hat{\theta}_i$ samples	$\left(m_{\hat{\theta}_i}, \sigma^2_{\hat{\theta}_i}\right)$	$4K$	- New nodes proposed - Similar as in the conventional TOA-FG [17] - K indicating total samples
$N_{\theta_i} \rightarrow C_{\theta_i}$	$\left(m_{\hat{\theta}_i}, \sigma^2_{\hat{\theta}_i}\right)$	$\left(m_{\hat{\theta}_i}, \sigma^2_{\hat{\theta}_i}\right)$	–	
Iteration Process				
$C_{\theta_i} \rightarrow \Delta y_{\theta_i}$	$\left(m_i, \sigma_i^2\right)$ $\left(m_{\hat{\theta}_i}, \sigma^2_{\hat{\theta}_i}\right)$	$\left(m_i \cdot \tan\left(m_{\hat{\theta}_i}\right),\right.$ $\sigma_i^2 \cdot \tan^2\left(m_{\hat{\theta}_i}\right) +$ $\left(m_i^2 + \sigma_i^2\right) \cdot$ $\left.\sigma^2_{\hat{\theta}_i} \cdot \sec^4\left(m_{\hat{\theta}_i}\right)\right)$	$^\star 13$ $^{\star\star} 6$	- New expressions proposed - Derived by using first order Taylor series - $^\star 13$ indicating first iteration - $^{\star\star} 6$ indicating next iteration
$C_{\theta_i} \rightarrow \Delta x_{\theta_i}$	$\left(m_i, \sigma_i^2\right)$ $\left(m_{\hat{\theta}_i}, \sigma^2_{\hat{\theta}_i}\right)$	$\left(m_i \cdot \cot\left(m_{\hat{\theta}_i}\right),\right.$ $\sigma_i^2 \cdot \cot^2\left(m_{\hat{\theta}_i}\right) +$ $\left(m_i^2 + \sigma_i^2\right) \cdot$ $\left.\sigma^2_{\hat{\theta}_i} \cdot \csc^4\left(m_{\hat{\theta}_i}\right)\right)$	$^\star 13$ $^{\star\star} 6$	
$A_{\theta_i} \rightarrow \Delta x_i$ $A_{\theta_i} \rightarrow x$	$\left(m_i, \sigma_i^2\right)$	$\left(X_i - m_i, \sigma_i^2\right)$	1	- New expressions proposed - Similar as in the conventional TOA-FG [17]
$B_{\theta_i} \rightarrow \Delta y_i$ $B_{\theta_i} \rightarrow y$	$\left(m_i, \sigma_i^2\right)$	$\left(Y_i - m_i, \sigma_i^2\right)$	1	
$\Delta x_i \rightarrow C_{\theta_i}$ $\Delta x_i \rightarrow A_{\theta_i}$ $\Delta y_i \rightarrow C_{\theta_i}$ $\Delta y_i \rightarrow B_{\theta_i}$	$\left(m_i, \sigma_i^2\right)$	$\left(m_i, \sigma_i^2\right)$	–	- Similar to conventional TOA-FG [17] and DOA-FG [4,23] - N indicating total number of sensors
$x \rightarrow A_{\theta_i}$ $y \rightarrow B_{\theta_i}$	$\left(m_j, \sigma_j^2\right)$ $j \neq i$	$\left(\sigma_i^2 \sum_{j \neq i} \frac{m_j}{\sigma_j^2},\right.$ $\left.\sigma_i^2 = \frac{1}{\sum_{j \neq i} \frac{1}{\sigma_j^2}}\right)$	$4(N-1)$	
Iteration Converges				
x and y	$\left(m_i, \sigma_i^2\right)$	$\left(\sigma_\Lambda^2 \sum_i \frac{m_i}{\sigma_i^2},\right.$ $\left.\sigma_\Lambda^2 = \frac{1}{\sum_i \frac{1}{\sigma_i^2}}\right)$	$4N$	- Similar to conventional TOA-FG [17] and DOA-FG [4,23]

in Table 3.1, where the directions of the message flow is shown in the left column. m_i and σ_i^2 in the Table. 3.1 indicate updated messages at each node in general.

3.2.1 Computational Complexity Analysis

In this section, the computational complexity is analyzed by using number of floating-point operations (flops). It should be noticed that flops can also defined as floating-point operations per second. In this dissertation, we follow the definition of floating-point operations without "per second" as mentioned in [18, 66, 71, 72]. Each operation for addition, subtraction, multiplication, division, tangent, cotangent, secant, and cosecant is calculated as one flop which is similar to as shown in [5, 66]. We also calculate the number of flops for matrix operations with the same formula as in [5], where the number of flops of the matrix multiplication, $\mathbf{A}_{n_m \times m_m}\mathbf{A}_{m_m \times p_m}$, and inverse matrix, $(\mathbf{A}_{n_m \times n_m})^{-1}$, are $n_m m_m p_m$ and $2n_m^3 + n_m^2 + n_m$, respectively, with $\mathbf{A}$ being a matrix, and n_m, m_m, p_m, being the matrix dimension indexes.

We summarize the the number of flops of each arithmetic operation at the nodes of the TS-DOA-FG technique in Table. 3.1. The first iteration of one messages flow of the TS-DOA-FG, $x_i \rightarrow A_{\theta_i} \rightarrow \Delta x_i \rightarrow C_{\theta_i} \rightarrow \Delta y_i \rightarrow B_{\theta_i} \rightarrow y$, requires $4(N-1)+1+13+1 = 15+4(N-1) = 4N+11$ flops. The second iteration requires $4N+4$ flops because the number of flops for $C_{\theta_i} \rightarrow \Delta y_i$ are 6 after first iteration. It should be noticed that, as described above, $\tan(m_{\hat{\theta}})$, $\cot(m_{\hat{\theta}})$, $\sec^2(m_{\hat{\theta}})$, and $\csc^2(m_{\hat{\theta}})$ are constants. The required number of flops for N messages flow, two coordinates (X, Y), are $4N^2+11N$ and $4N^2+4N$ for the first iteration and the second iteration (or after first iteration), respectively. The total number of flops required when the iteration converges after first iteration are $8N + 4N = 12N$.

In the DOA-GN technique (2.30), the operation to calculate $\mathbf{J}$ matrix requires $8N$ flops. $\mathbf{J}$, $\mathbf{\Sigma}_\theta$, and $\mathbf{m}_\theta$ has dimension $N \times 2$, $N \times N$, and $N \times 1$, respectively. The highest computational load is required to inverse the covariance matrix, where $\mathbf{\Sigma}_\theta^{-1}$ requires $2N^3 + N^2 + N$ flops. The multiplication operation of $(\mathbf{J}\mathbf{\Sigma}_\theta^{-1})$ require $2N^2$ flops (without the number of flops for matrix inversion operation). Hence, the total number of flops required by DOA-GN for each iteration is $8N+2(2N^3+N^2+N)+2(2N^2)+4N+22+2N = 4N^3+6N^2+16N+22$ flops.

Furthermore, in the DOA-LS (2.29), $\mathbf{A}_\theta$ and $\mathbf{b}_\theta$ require N and $3N$ flops. The inversion of matrix with dimension 2×2 requires 22 flops. The matrix multiplication of $(\mathbf{A}_\theta^T \mathbf{A}_\theta)$ requires $4N$ flops. The total number of

flops required by DOA-LS are $22 + 2(4N) + 2N = 10N + 22$.

For example, let we take $N = 3$. The TS-DOA-FG requires 69, 48, and 36 flops for the first iteration, second iteration, and when the iteration converges. The DOA-GN requires 232 flops for each iteration. The DOA-LS requires 42 flops. The computational complexity of TS-DOA-FG is proportional to N when the iteration converge. The formula of each factor node is also proportional to N. In iteration process, the computational complexity of sum-product algorithm in the factor graph is proportional to N^2. The computational complexity of the DOA-GN is proportional to N^3. Hence, the computational complexity of the TS-DOA-FG is much lower than the DOA-GN.

The DOA-LS has low computational complexity, this is because this technique only works for mean of the samples. The DOA-LS does not take into account the variance and/or covariance value of the samples. The DOA-LS also does not have iteration process. Hence, the DOA-LS can not achieve the theoretical limit. It is shown in the next section the higher N value, the accuracy of DOA-LS does not increase. It can also be seen in the next section that the accuracy of DOA-LS technique is lower than the proposed TS-DOA-FG technique.

3.3 Simulation Results

The performance of the proposed technique was verified via computer simulations, where the simulation round consists of $1,000$ single target locations randomly chosen from the area of $1,000 \times 1,000$ m^2, where each target location is tested in 100 trials. It should be noted here that the scope in this dissertation is to estimate only one target position. The case of unknown multiple-target detection is left for future work. It is assumed that the illegal radio, as an example of unknown radio emitter, emits the radio wave with strong enough transmit power covering the area of $1,000 \times 1,000$ m^2. The values of the measurement error were $\sigma_\theta = \{1^\circ, 5^\circ, 10^\circ, 15^\circ, \cdots, 45^\circ\}$. As mentioned in Chapter 2, it is assumed that the DOA measurement is performed by using circular array antenna, hence the measurement error is in angular value. In this simulation we directly use the DOA samples from the model. The DOA samples is calculated as follows: (1) calculate the true DOA between sensor and target, $\theta_i = \frac{Y_i - y}{x_i - x}$, (2) after that we add Gaussian noise with standard deviation of angle, σ_θ, in units of degree and also with 25 to $1,000$ samples. It was assumed that the simulation does not contain outliers in angular measurement because we do not consider the interference and non-Gaussian noise [73].

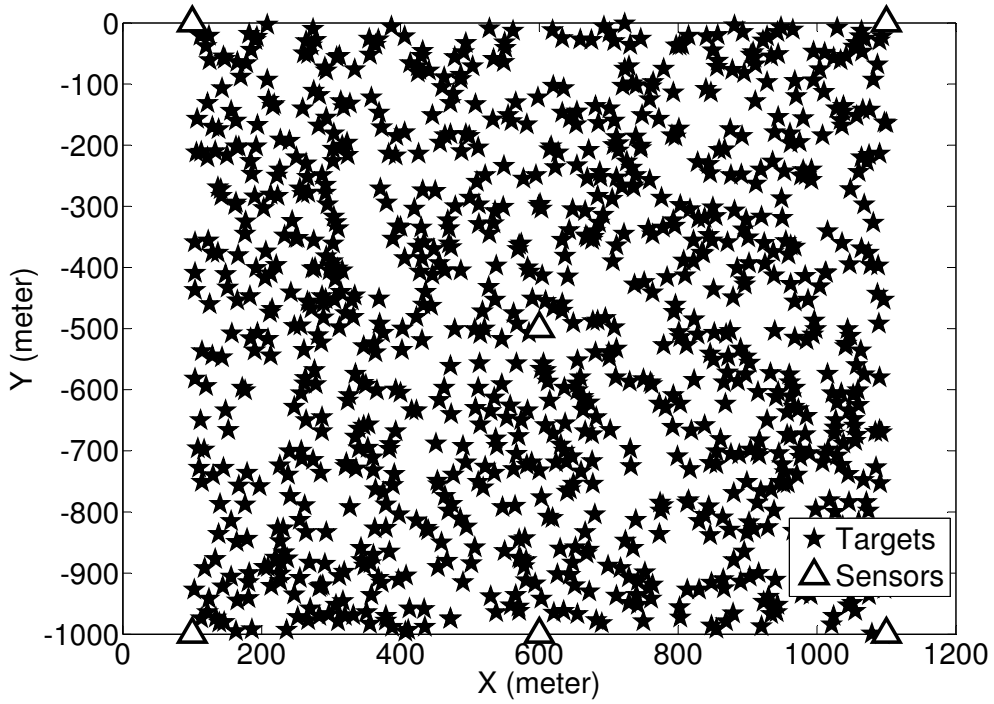

Figure 3.2. 1,000 target and 6 sensor positions in area $1,000 \times 1,000$ m^2.

As shown in Fig. 3.2, six sensors were assumed in total, indicated by the Δ mark. The sensors were set at the positions $(100, 0)$, $(100, -1000)$, $(600, 500)$, $(600, -1000)$, $(1000, 0)$, and $(1000, -1000)$ m in the (X, Y) coordinate. The simulation for various position of sensors is not needed because the randomly chosen of targets position in each trial as mentioned above is already sufficient to evaluate the effectiveness of the proposed technique. The accuracy of proposed technique was evaluated by using the following parameters: a) 3 to 5 sensors taken from the total of 6 sensors, b) 10 and 20 times of iterations for each trial. The initialization point is set at $(0, 0)$ for $m_{x \to A_\theta}$ and $m_{y \to B_\theta}$, and at $(1, 1)$ for $\sigma^2_{x \to A_\theta}$ and $\sigma^2_{y \to B_\theta}$. It should be noted that the initialization point can be set arbitrary inside the area of the expected target detection. Regardless of the target positions ($1,000$ points tested), with the initialization of mean and variance being set at $(0, 0)$ and $(1, 1)$, respectively, final estimate of the target position is quite accurate. Conversely, this observation should be understood in a way that the estimation result is less sensitive to the initial values.

To demonstrate the convergence property of the proposed technique, trajectory of a detection trail is shown in Fig. 4.7(b). It shows clearly that the target position estimate successfully reaches the true target position

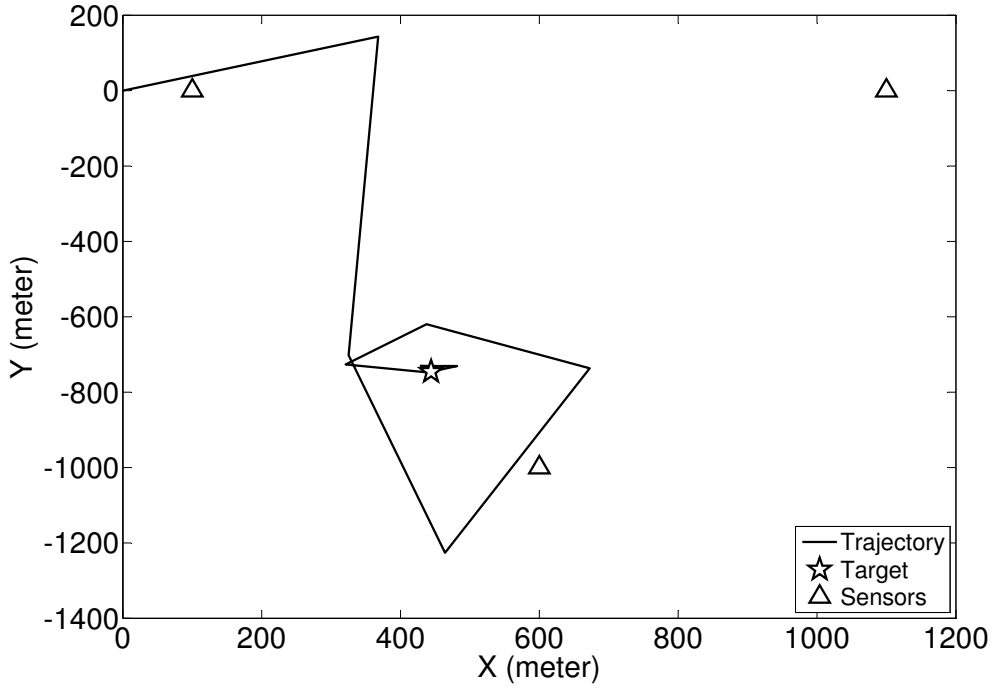

Figure 3.3. Trajectory of the proposed technique with 3 sensors, 10 iterations, 100 samples, $\sigma_\theta = 10^\circ$, and target at $(444, -746)$ m.

at $(x, y) = (444, -746)$ m in 10 iterations, where the iteration process is started from the initial point $(0, 0)$ m. The estimate target position is calculated in each iteration by using sum-product algorithm as (2.8). It should be noticed that only with 7 iterations, the position estimate of the proposed technique reaches a point close to the true target position by using 3 sensors.

Fig. 3.4 shows that even though with the target position being exactly 90° relative to a sensor position, the proposed TS-DOA-FG technique can still detect the position of the target. As described above, the π value is an approximated value so that the mathematical operations of $\tan(\pi/2)$ and $\sec(\pi/2)$ in the computer simulation do not result in infinity value. Hence, sum-product algorithm in the factor graph still can process this value to accurately estimate the target position.

Fig. 3.5 shows the RMSE versus the iteration times with the standard deviation σ_θ of the measurement error as a parameter. The RMSE of the proposed technique converges after 9 iterations for $\sigma_\theta = 1^\circ$, while it converges after 5 iterations for $\sigma_\theta = 20^\circ$ and $\sigma_\theta = 45^\circ$ as shown in Fig. 3.5. Hence, the iteration converges faster with higher standard deviation of

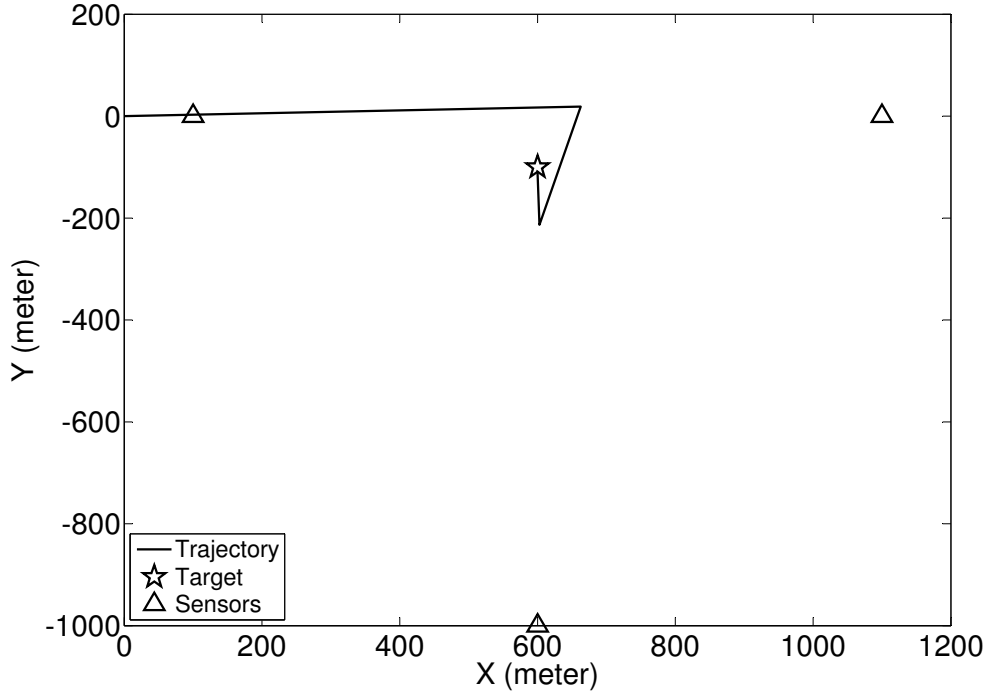

Figure 3.4. Trajectory of the proposed technique with 3 sensors, 10 iterations, 100 samples, $\sigma_\theta = 10°$, and target at $(600, -100)$ m. The target position is 90^o from sensor position at $(600, -1000)$ m.

the measurement error because lower σ_θ need more times to achieve better accuracy. Although the RMSE with $\sigma_\theta = 1°$ is worse with less than 5 iterations, the RMSE with smaller σ_θ is lower when the iterations converges.

The RMSEs achieved by the proposed and the conventional DOA-LS techniques are then compared with the CRLB. In each round of simulations, the both techniques used the same parameter values as described before. Fig. 3.6 shows that the RMSE versus the standard deviation σ_θ of the measurement error with the number of sensor as a parameter. It is found that the more sensors, the smaller RMSE. The larger the standard deviation of measurement error, the higher improvement of the accuracy is achieved by adding more sensors. It is shown that the accuracy is improved for around 10 and 30 m at $\sigma_\theta = 10°$ and $\sigma_\theta = 45°$, respectively, by adding 2 sensors. Figs. 3.6 and 3.8 show that with the conventional DOA-LS technique, the RMSE with 3 sensors yields better performance than that of with 4 sensors for $\sigma_\theta = 1°$; and the RMSE with 5 sensors is almost the same as that with 4 sensors. This is because the RMSE is

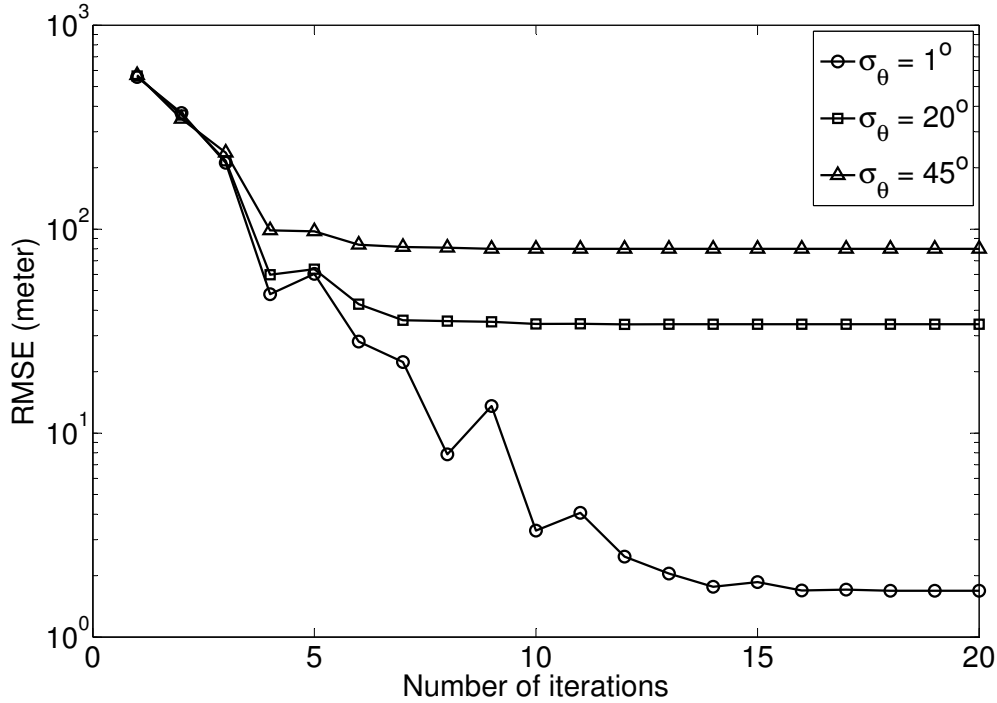

Figure 3.5. RMSE vs. iteration times of TS-DOA-FG geolocation technique with 3 sensors, 20 iterations, 100 samples, 1,000 locations, 100 trials, and $\sigma_\theta = \{1^\circ, 20^\circ, 45^\circ\}$.

calculated for 10 iterations. However, it is shown in Fig. 3.7 that with 20 iterations the RMSE of the proposed TS-DOA-LS outperforms the conventional DOA-LS. It should be noticed, the TS-DOA-FG algorithm with $\sigma = 1^\circ$ converges after 15 iterations as shown in Fig. 3.5.

Fig. 3.8 shows number of the sensors versus the RMSE with the standard deviation σ_θ of the measurement error as a parameter. It is found from the figure that there is a clear difference in the tendency of the RMSE between the proposed technique and the conventional DOA-LS technique. The RMSE decreases by increasing the number of sensors for $\sigma_\theta = \{1^\circ$, 20°, and $45^\circ\}$ with the proposed technique, and such tendency is consistent to the CRLB. It can be concluded that the geolocation accuracy in terms of RMSE with the proposed technique outperforms the reference conventional DOA-LS technique.

Fig. 3.9 shows the effect of number of samples to the accuracy of DOA-based geolocation techniques with σ_θ as a parameter. The RMSE of both the proposed and reference conventional techniques [61] as well as the CRLB of the DOA-based geolocation decrease when more samples are used. It is shown in the Fig. 3.9 that with RMSE 24 m, the proposed

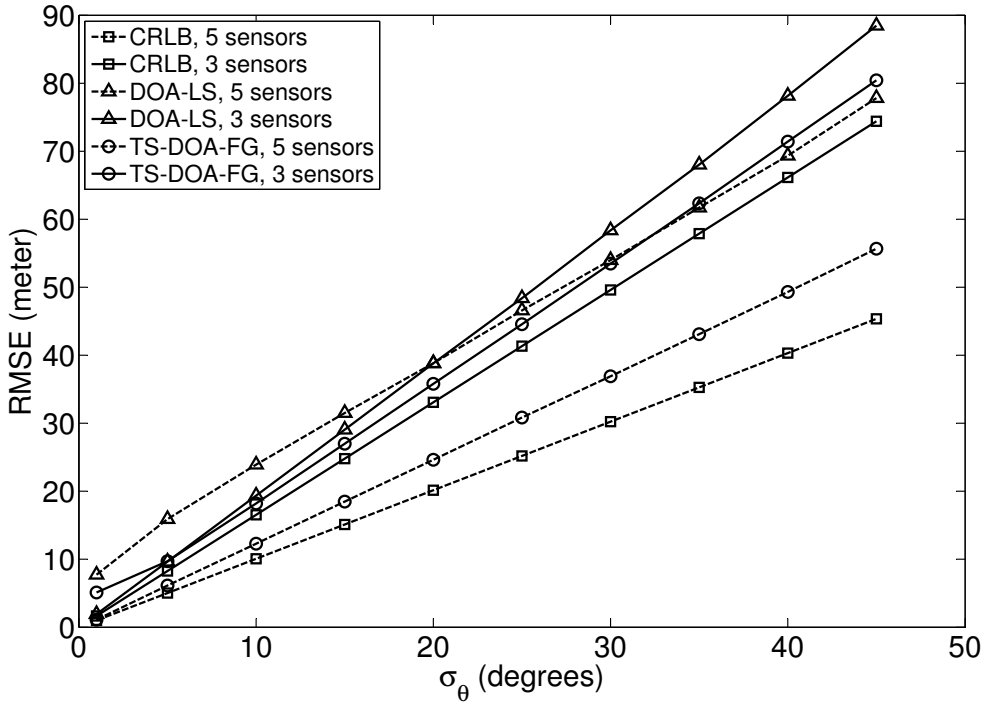

Figure 3.6. RMSE vs. σ_θ with 3 and 5 sensors, 10 iterations, 100 samples, $1,000$ locations, and 100 trials.

technique requires around 525 samples, while the conventional technique requires around 630 samples. The accuracy of the proposed technique always outperforms the reference technique with the same number of samples used. Obviously, by increasing of the number of samples, the gap to the CRLB decreases with the both proposed and reference techniques. It is also found from the figure that the smaller the measurement error, the smaller the gap to the CRLB. The gap with different σ_θ values decreases when the number of samples increases.

As described before, the Gauss-Newton algorithm may diverge with unsuitable initial points and the position of the target. In this computer simulation, when the DOA-GN diverges resulting in the position estimate with no available value (NAN) or very far from the target, we replace the position estimate with the average of the sensor positions. The initial points are fixed $(0, 0)$ m for both the proposed TS-DOA-FG and conventional DOA-GN. Figs. 3.10 and 3.11 show that the DOA-GN has RMSE of around 500 m in target position area of $1,000 \times 1,000$ m^2. It means that there are several target positions having the initial value too far. Also, the target position has bad geometric position for the DOA-GN resulting in rank deficiency. It is also shown that for the target position are of 800×800 m^2, the accuracy of DOA-GN outperforms the proposed TS-DOA-FG for

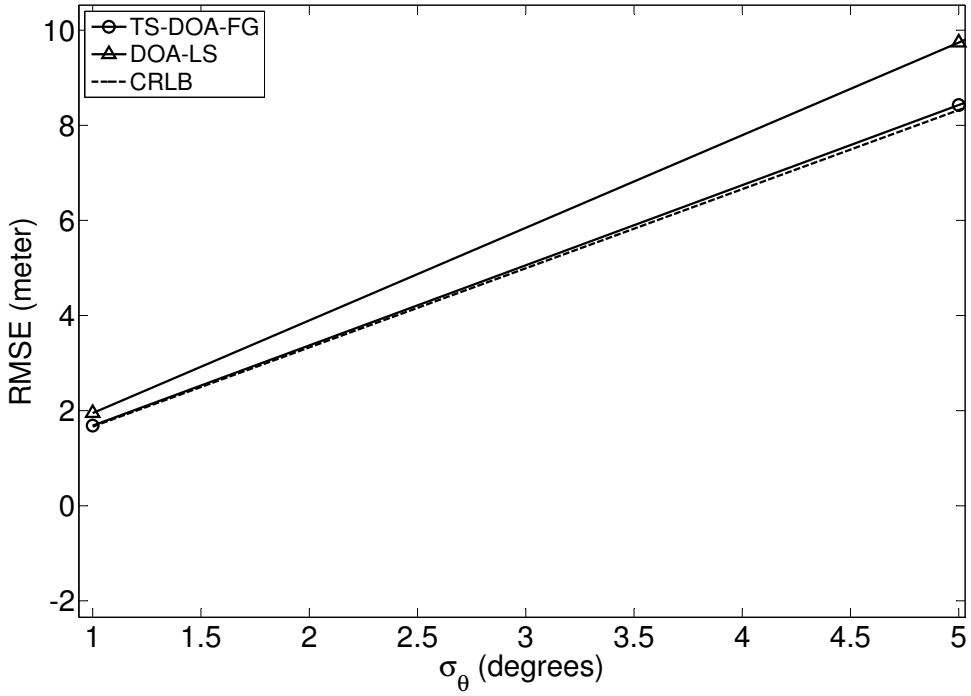

Figure 3.7. RMSE vs. σ_θ with 3 sensors, 20 iterations, 100 samples, 1,000 locations, and 100 trials.

σ_θ at 1° to 20°.

3.4 Summary

A new FG-based geolocation technique using DOA information for a single static unknown (anonymous) radio emitter with accuracy improvement of the position estimate has been proposed. A set of new approximated expression for the mean and variance of the tangent and cotangent functions has been derived based on the first-order Taylor series to hold the Gaussianity assumption. The simulation results confirmed that the proposed technique provides: (a) better accurate position estimate with number of samples and sensors, and standard deviation of measurement error, as parameters, with RMSE lower than 8 m for $\sigma_\theta < 5^\circ$, (b) fast convergence, and (c) keep low computational complexity, which are suitable for the future geolocation techniques requiring high accuracy and low complexity in imperfect synchronization condition. The development of TS-DOA-FG technique for multiple-target detection is left as future work.

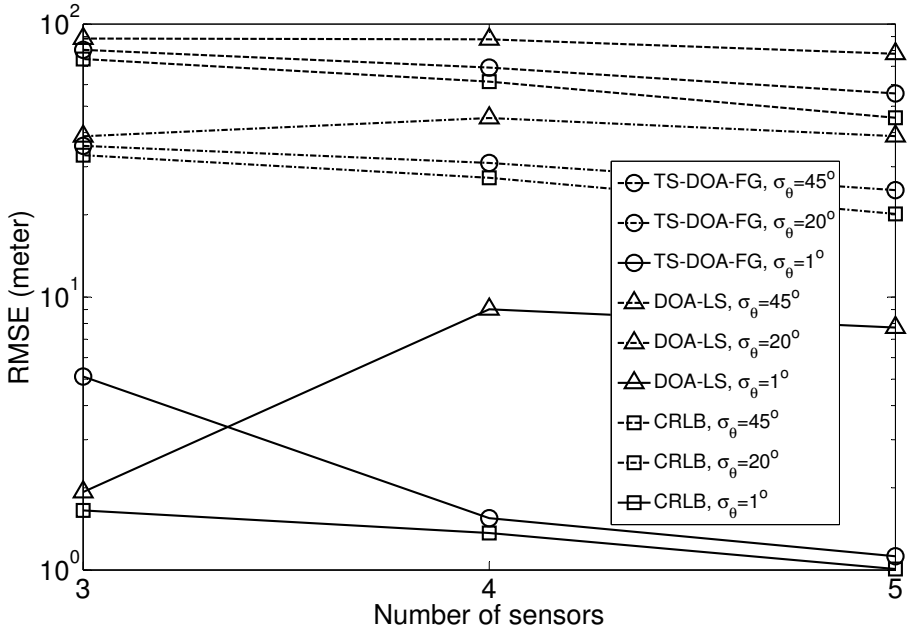

Figure 3.8. RMSE vs. number of sensors with 10 iterations, 1,000 locations, 100 trials, and $\sigma_\theta = \{1°, 20°, 45°\}$.

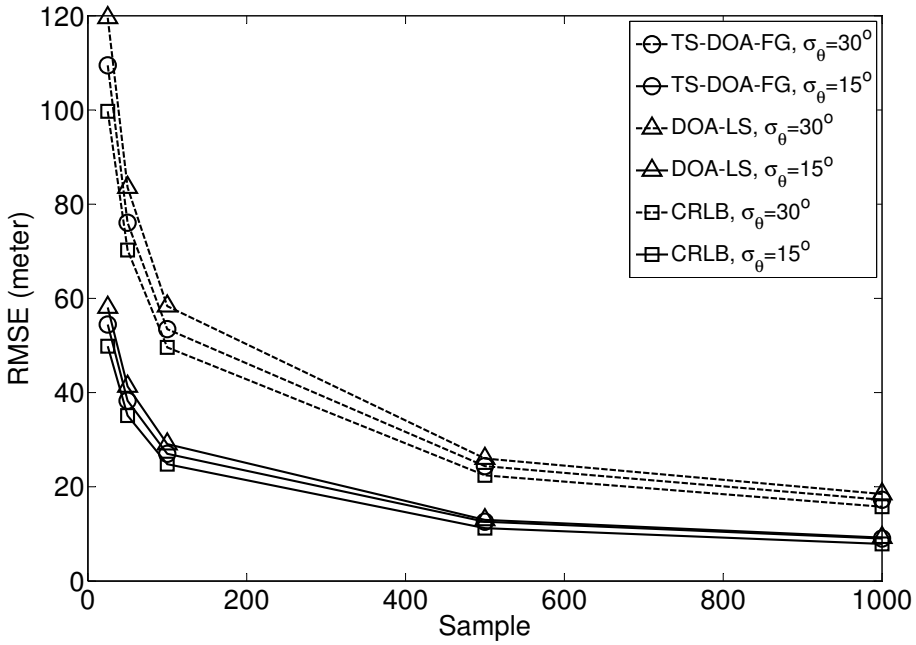

Figure 3.9. RMSE vs. number of samples with 3 sensors, 10 iterations, 1,000 locations, 100 trials, and $\sigma_\theta = \{15°, 30°\}$.

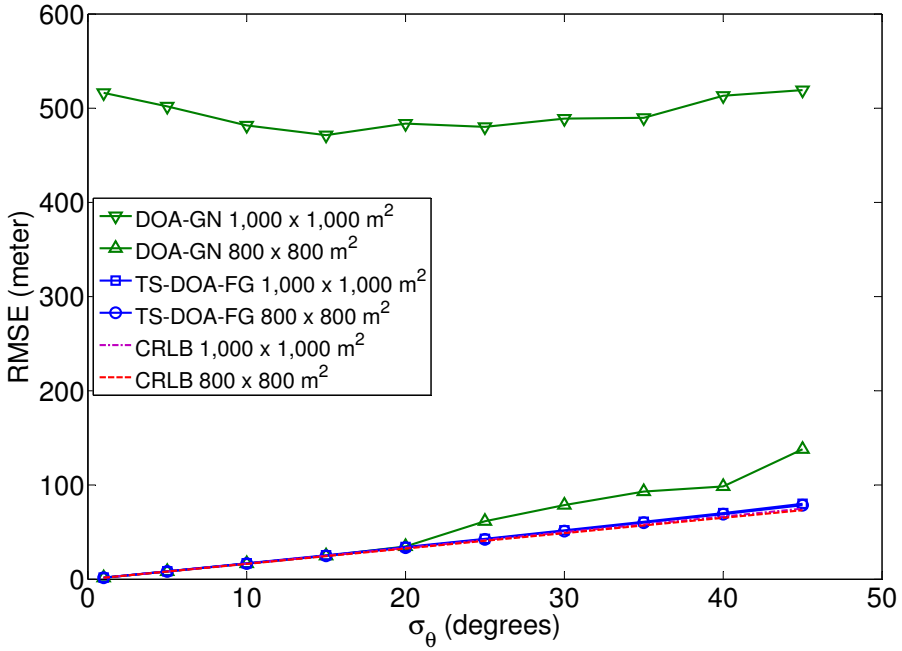

Figure 3.10. RMSE of the proposed TS-DOA-FG and conventional DOA-GN with 3 sensors, 20 iterations, 1,000 locations, and 100 trials.

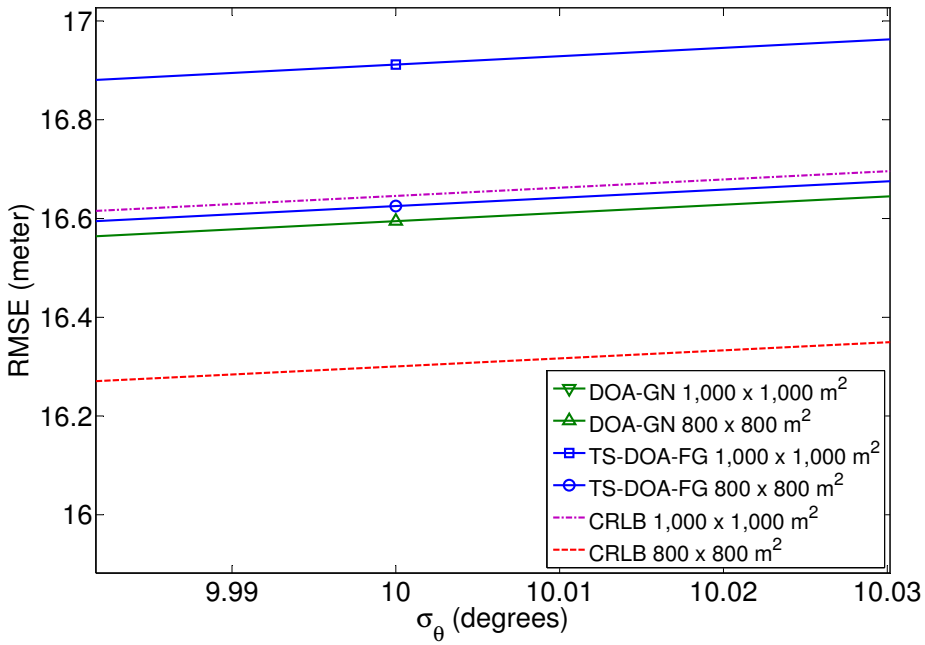

Figure 3.11. Zoom of RMSE of the proposed TS-DOA-FG and conventional DOA-GN with 3 sensors, 20 iterations, 1,000 locations, and 100 trials.

Chapter 4

Pythagorean TDOA-Based Factor Graphs Geolocation

In this chapter, the Pythagorean TDOA-FG technique is described. A simple Pythagorean function is used instead of the hyperbolic function. Fig. 4.1 illuminates the difference between Pythagorean and hyperbolic approaches. The Pythagorean function is used by the factor node to convert the Euclidean distance into relative distance. The target coordinate is obtained by subtracting the relative distances to the known sensor position. Currently, the Pythagorean function is used in TOA-based FG technique. However, as mentioned above, the TOA-based FG technique requires the absolute time stamp of the unknown signal emission. To eliminate the necessity of the knowledge of the absolute time stamp information, several sets of new nodes are introduced into the TOA-based FG, by which the TDOA is converted into equivalent TOA-based. Hence, the simple Pythagorean function approach can be used on the equivalent TOA-based FG, converted from the TDOA-FG. It is shown that the proposed technique successfully estimates the unknown target position with high accuracy without requiring heavy computational complexity. The simulation results show that the accuracy of the position estimate with the proposed technique outperforms the Pythagorean TOA-based FG technique with much higher accuracy because the proposed technique has more averaging processes conducted in the additional nodes to calculate probability marginals. The performance of the proposed technique in terms of RMSE is then compared to the CRLBs. It is shown that the achieved RMSE performance of the proposed technique is very close to TDOA-based CRLB and also is better than the TOA-based CRLB.

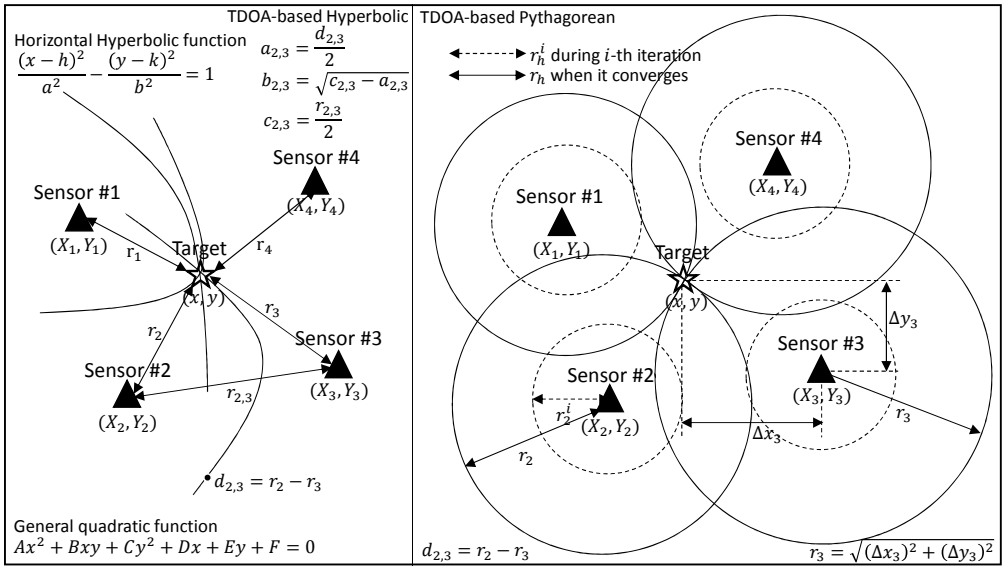

Figure 4.1. A complicated TDOA-based hyperbolic vs. a simple TDOA-based Pythagorean concept.

4.1 System Model

The system contains one unknown (anonymous) radio wave emitter, referred to as target. The target position is assumed to be fixed and no mobility assumed. The position of the target is $\mathbf{x} = [x\ y]^T$, where T indicates the transposition of the argument vector, is the objective of positioning algorithm. The system also contains multiple, N, sensors. The sensor position is indicated by $\mathbf{X} = [X_h\ Y_h]^T$, where h is the sensor index.

The terminologies, primary and secondary sensors, are used in this chapter because the TDOA information is the time difference between two sensors, where the TOA information at secondary sensor is subtracted from the TOA information at the primary sensor. Hence, we use the subscripts h, i, j in the equations to identify the sensor type. The subscript h, $h = \{1, 2, ...N\}$, in regardless of either the primary or secondary sensors, where the value of h can be either $h = i$ or $h = j$. The subscript i, $i = \{1, 2, ..., N-1\}$, is used to denote the index for the primary sensor, while the subscript j, $j = \{2, 3, ..., N\}$, is used to denote the secondary sensor. The sensor indexes for the primary and secondary sensors always satisfy $i < j$.

The TOA information indicates the the range of time from the signal

departure to it arrival at the sensors. The TOA information measured by the sensor h is given by

$$\tau_h = \tau_{a_h} - \tau_d, \tag{4.1}$$

where τ_{a_h} denotes the time when the signal of the target arrives in the sensor h. The subscript τ_d, so called TOD, denotes the time when the signal departs from the target. We notice from (4.1) that the TOA-based technique needs the TOD information τ_d provided by an absolute time stamp. However, the TOD information is not available in the signal from unknown target, as mentioned above. The TDOA information $\Delta\tau_{i,j}$ eliminates the necessity of TOD information τ_d, as

$$\begin{aligned} \Delta\tau_{i,j} &= \tau_i - \tau_j & (4.2)\\ &= (\tau_{a_i} - \tau_d) - (\tau_{a_j} - \tau_d) \\ &= \tau_{a_i} - \tau_{a_j}, & (4.3) \end{aligned}$$

hence the TDOA information can be obtained from the signal of unknown target. Therefore, the TDOA of the unknown target is the difference of the times when the signal arrives at two different sensors.

Since the radio signal is an electromagnetic wave, the TOA[1] and TDOA information, in unit of second, can be directly converted to Euclidean distance information, in unit of meter. Hence, the TOA and TDOA sample arrived in the fusion center is directly converted to the Euclidean distance and difference of Euclidean distance, given by $r_h = \tau_h \cdot c$, and $d_{i,j} = \Delta\tau_{i,j} \cdot c$, respectively, where $c = 3 \cdot 10^8$ m/s is the velocity of electromagnetic wave propagation. The Euclidean distance r_h between the sensor and the target is expressed as

$$r_h = \sqrt{(X_h - x)^2 + (Y_h - y)^2}. \tag{4.4}$$

The converted TDOA information corresponds to the difference Euclidean distance between the primary and secondary sensors, given by

$$d_{i,j} = r_i - r_j. \tag{4.5}$$

Substituting (4.4) with $h = i$ for primary sensor and $h = j$ for secondary sensor into (4.5) yields

$$\begin{aligned} d_{i,j} &= \sqrt{(X_i - x)^2 + (Y_i - y)^2} \\ &\quad - \sqrt{(X_j - x)^2 + (Y_j - y)^2}. & (4.6) \end{aligned}$$

[1]Even though the TOA is not available in the radio signal of the unknown target, we still use the TOA terminology to derive the Euclidean distance. The Euclidean distance is used in the derivation of converted TDOA to difference Euclidean distance.

Fig. 4.1 illustrates the sensors, a target, and Euclidean distance.

Now, notice that since the value of (X_i, Y_i) and (X_j, Y_j) are known, $d_{i,j}$ is obtained from the measurement, where $(x,\ y)$ are the coordinate position of the target to be estimated. The FG solves the global function (4.6) by decomposing it into several simple local functions. The process of obtaining the measurement data is out of the scope in this dissertation. The proposed technique assumes that the TDOA samples are the input to the FG algorithm performed at the fusion center.

However, the sensors have no knowledge of $d_{i,j}$ and $\sigma_{d_{i,j}}$. Hence, the proposed technique first converts K measured samples of the TDOA information to the difference Euclidean distance information, and then calculates the mean $m_{E_{i,j}\to d_{i,j}}$ and the variance $\sigma^2_{E_{i,j}\to d_{i,j}}$. The mean and variance of the difference Euclidean distance are then used as the input for iterative processing among the nodes between the *Euclidean distance estimator node* $D_{i,j}$ and *Estimated target position variable node* x and y as shown in Fig. 4.2.

4.2 Proposed Technique

Currently, the TDOA-based techniques use the hyperbolic to convert the TDOA parameter to the difference Euclidean distance based on the hyperbolic curves representing the geometric relationship of the sensors. The TDOA-based FG technique in [6] converts the hyperbolic function to a general quadratic formula before using it in the FG algorithm. It is mentioned in [6] that the TDOA-FG with hyperbolic function is more complicated than TOA-based FG technique with Pythagorean functions, because of the property of the functions.

The P-TDOA-FG technique proposed in this dissertation eliminates the necessity of the use of the complicated hyperbolic function. Since the converted TDOA corresponds to the difference Euclidean distance, we can further convert the information back to the *equivalent* Euclidean distance. The *equivalent* Euclidean distance is then used as the input to the Pythagorean TOA-based FG technique in [17]. Hence, the Pythagorean TOA-based technique can be extended to the Pythagorean TDOA-FG technique.

Our Pythagorean TDOA-FG technique consists of the factor nodes $A_h, B_h, C_h, D_{i,j}, E_{i,j}$, and variable nodes $d_{i,j}, r_h, x, y, \Delta x_h, \Delta y_h$, as shown in Fig. 4.2. The factor nodes calculate the functions to update the messages. The variable nodes in the FG combine the messages from the factor nodes, according to the sum-product algorithm, then forward the messages to

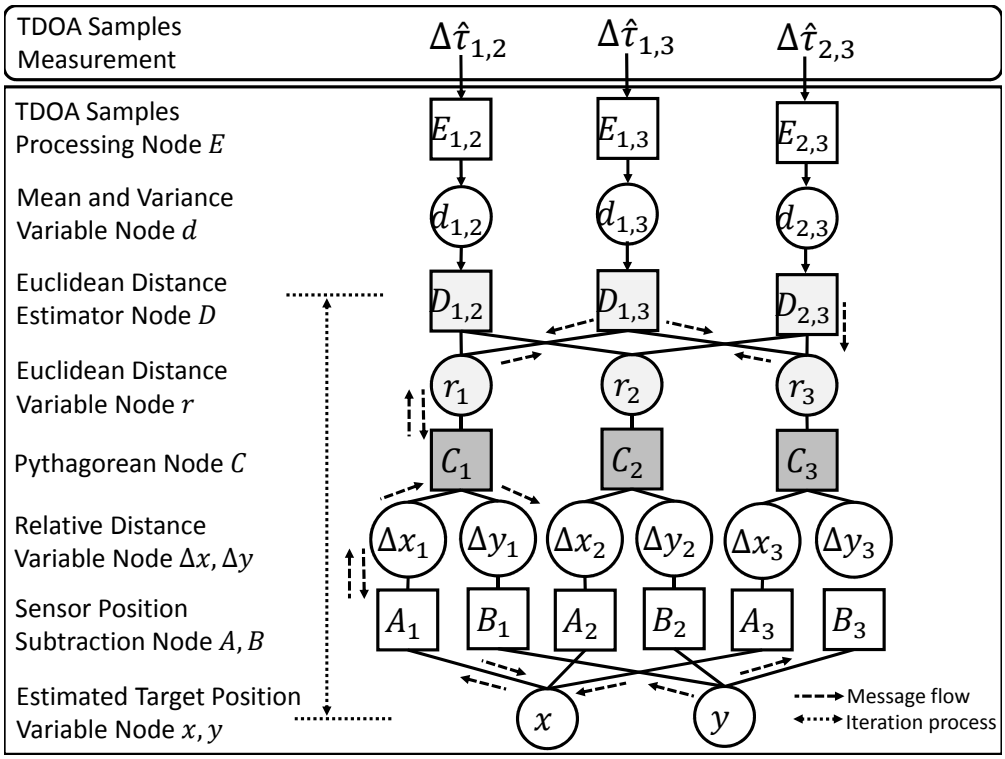

Figure 4.2. The proposed P-TDOA-FG geolocation with number of sensors $N = 3$. The node with lightgray color is the proposed new nodes and expression. The nodes with darkgray color is added with new proposed expressions.

the other factor nodes. The nodes between the *Pythagorean node* C_h and the nodes x and y are equivalent to those used in [17]. Originally in [17], the Euclidean distance information is directly obtained from the measurement and input into the node C_h. In our proposed technique, the Euclidean distance input into the node C_h is the *equivalent* Euclidean distance. The main contribution of this chapter is three folds, which are related to the introductions of the new nodes to *equivalent* TOA convert back from the TDOA information: (a) new factor nodes $D_{i,j}$ (*Euclidean distance estimator node*), (b) new variable node r_h (*Euclidean distance variable node*), and (c) additional functions in the node C_h (*Pythagorean node*), as indicated by the lightgray boxes for (a) and (b), darkgray boxes for (c), in the Fig. 4.2.

The process performed in the additional nodes (a)-(c) are summarized

as follows:

(a) *Euclidean distance estimator node*: The node converts the difference Euclidean distance to the *equivalent* Euclidean distance. The equations calculated in the node $D_{i,j}$ are very simple, which are only a summation or subtraction operations, as shown in (4.8)-(4.11).

(b) *Euclidean distance variable node*: The node r_h connects the edge from node r_h to the node $D_{i,j}$ by using (4.12)-(4.15). Information passed between node $D_{i,j}$ and the node r_h is the *equivalent* TOA values which is already in the form of the *equivalent* Euclidean distance.

(c) *Pythagorean node*: In [17], no information is passed from the node C_h to the node r_h. Hence, we modify the function at the node C_h by introducing additional Pythagorean functions (4.16) and (4.17) corresponding to the information from the node C_h to the node r_h. Finally, we introduce three constraints in the message update performed by (4.22)-(4.24) at the node C_h to ensure the stability of proposed technique. Constraint (A): to avoid the value of the node r_h to diverge in (4.22). Constraint (B): to prevent the value of the node r_h to shrink to zero in (4.23). Constraint (C): to avoid negative value in the square root of the Pythagorean function in the nodes C_h in (4.24).

The Pythagorean TOA-based FG technique in [17] requires good initial point before the iteration process begin. We modify the Pythagorean functions at the node C_h for the messages sent to *Relative distance variable nodes* Δx and Δy, hence the initial position of target can start from anywhere. The improvement in this case is obtained by introduction Constraint (C). All detailed mathematics for nodes (a)-(c) and Constraints (A)-(C) are shown in Section 4.2.2.

4.2.1 Local Functions in the FG Algorithm

It is found from (4.6) that the TDOA FG algorithm contains the subtraction of two Pythagorean functions. The proposed TDOA-based technique uses Pythagorean function instead of the Hyperbolic function, which requires complicated process for solving the global function (4.6) to obtain position estimate (x, y) of target. However, The FG algorithm factors the global function (4.6) into several simple local function as follows: 1) $(X_h - x), (Y_h - y)$, either $h = i$ or $h = j$, and $i < j$, are extracted from (4.6), hence the functions are decoupled into simple local functions, so called relative distance, given by (3.1), where x_{θ_i} and y_{θ_i} are replaced by x_{r_h} and y_{r_h}, then the functions are calculated in the nodes A_h, B_h, respectively. 2) The relative functions are used in the Pythagorean functions to

obtain the Euclidean distance for both the primary and secondary sensors, expressed as

$$r_h = \sqrt{\Delta x_{r_h}{}^2 + \Delta y_{r_h}{}^2}, \tag{4.7}$$

where the calculation for the functions are performed at the node C_h, respectively. 3) The simple function of (4.5) representing the relationship between the difference Euclidean distance $d_{i,j}$ and Euclidean distance (r_i and r_j) is calculated at the node $D_{i,j}$. The three groups of functions described above can avoid the use of the hyperbolic function.

The messages exchanged between the nodes are in the form of mean and variance because of the Gaussianity assumption of the measurement error. Hence, the messages, the result of the local functions and the sum-product algorithm, are in the form of mean $m_{a\to b}$ and variance $\sigma^2_{a\to b}$ with the suffix a and b indicates the source and destination nodes, respectively. We describe the messages exchanged between the nodes in the next Subsection.

4.2.2 Messages Exchanged in the Proposed Algorithm

The input to the node $E_{i,j}$ is the samples of difference Euclidean distance information $\hat{d}_{i,j}$. K samples are collected before starting the FG processing to obtain the position estimate of the target. The node $E_{i,j}$ calculates the mean $m_{E_{i,j}\to d_{i,j}}$ and variance $\sigma^2_{E_{i,j}\to d_{i,j}}$ from the collected samples, where it is assumed that the collected samples follow Normal distribution as mentioned in the previous Section. The node $E_{i,j}$ then forwards the messages $m_{E_{i,j}\to d_{i,j}}$ and $\sigma^2_{E_{i,j}\to d_{i,j}}$ to the node $d_{i,j}$, where the messages are directly forwarded to the node $D_{i,j}$ because the messages arriving in the node $d_{i,j}$ come from only one node $E_{i,j}$. Hence, the messages forwarded by node $d_{i,j}$ to node $D_{i,j}$ are $m_{d_{i,j}\to D_{i,j}}$ and $\sigma^2_{d_{i,j}\to D_{i,j}}$, where $m_{d_{i,j}\to D_{i,j}} = m_{E_{i,j}\to d_{i,j}}$ and $\sigma^2_{d_{i,j}\to D_{i,j}} = \sigma^2_{E_{i,j}\to d_{i,j}}$. The processes performed in the nodes $E_{i,j}$ and $d_{i,j}$ are similar to that shown in [6, 17].

The iterative processing is initiated from the node $D_{i,j}$. The processes in the node $D_{i,j}$ convert the difference Euclidean distance messages into the estimated Euclidean distance messages as mentioned before. The input messages $m_{d_{i,j}\to D_{i,j}}$ and $\sigma^2_{d_{i,j}\to D_{i,j}}$ to the node $D_{i,j}$ does not change during the iteration because the messages are obtained from the measurement. The node $D_{i,j}$ improves the accuracy of the *equivalent* Euclidean distance estimate by utilizing the messages $m_{d_{i,j}\to D_{i,j}}$ and $\sigma^2_{d_{i,j}\to D_{i,j}}$ as well

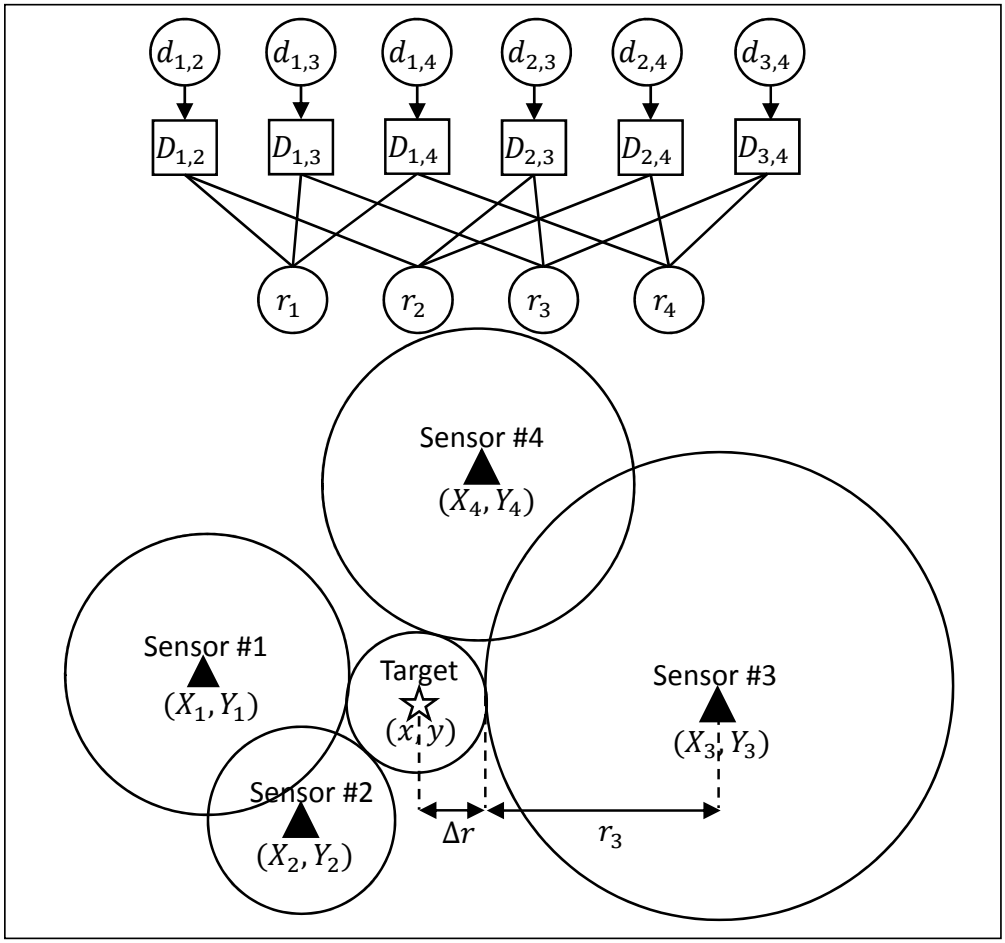

(a) The estimated Euclidean distance when the node r_h is disconnected with the node C_h.

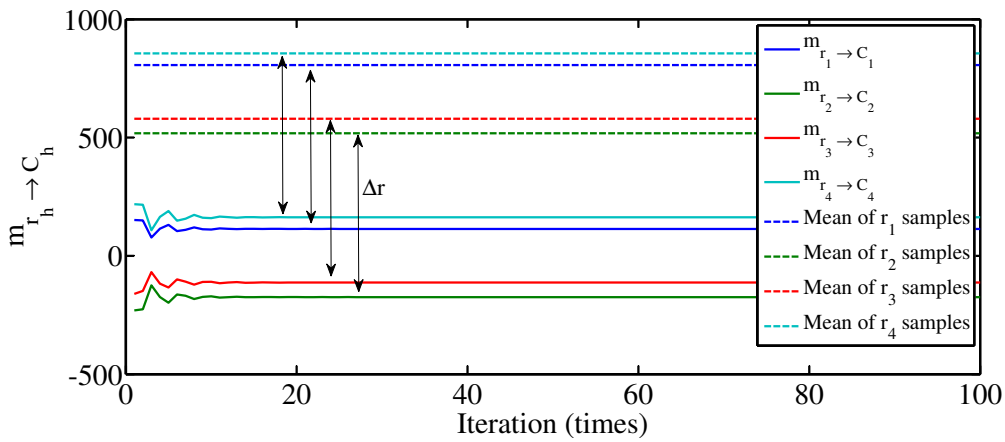

(b) $m_{r_h \to C_h}$ vs. iteration (times) with Δr error.

Figure 4.3. Disconnected r_h to C_h

as the other messages forwarded from the node r_h, $h = i, j$, which performs fine tuning of the radius of the circle having the updated Euclidean distance as shown in Fig. 4.1. The message updating function of the node $D_{i,j}$ is given by:

$$
\begin{aligned}
m_{D_{i,j}\to r_i} &= m_{d_{i,j}\to D_{i,j}} + m_{r_j\to D_{i,j}}, && (4.8)\\
m_{D_{i,j}\to r_j} &= -m_{d_{i,j}\to D_{i,j}} + m_{r_i\to D_{i,j}}, && (4.9)\\
\sigma^2_{D_{i,j}\to r_i} &= \sigma^2_{d_{i,j}\to D_{i,j}} + \sigma^2_{r_j\to D_{i,j}}, && (4.10)\\
\sigma^2_{D_{i,j}\to r_j} &= \sigma^2_{d_{i,j}\to D_{i,j}} + \sigma^2_{r_i\to D_{i,j}}, && (4.11)
\end{aligned}
$$

where $(m_{D_{i,j}\to r_i}, \sigma^2_{D_{i,j}\to r_i})$ are the messages forwarded by the node $D_{i,j}$ to node the r_i, and $(m_{D_{i,j}\to r_j}, \sigma^2_{D_{i,j}\to r_j})$ are the messages forwarded by the node $D_{i,j}$ to the node r_j. $(m_{r_i\to D_{i,j}}, \sigma^2_{r_i\to D_{i,j}})$ and $(m_{r_j\to D_{i,j}}, \sigma^2_{r_j\to D_{i,j}})$ are the messages forwarded from both the nodes r_i and r_j to the node $D_{i,j}$, respectively, where the value of the messages are set arbitrary for the first iteration.

We notice that (4.5) at the factor node $D_{i,j}$ is connected to (4.7) at the factor node C_h, where $h = i$ is for primary sensor and $h = j$ for secondary sensor. Hence, we propose a new variable node r_h to update the messages from the nodes D_h and C_h and then forward the result of updated message to the destination nodes, according to the sum-product algorithm. The messages from both the node r_i and r_j to the node $D_{i,j}$, from the node r_i to the node C_i, and from the node r_j to the node C_j are expressed as

$$
\begin{aligned}
\frac{1}{\sigma^2_{r_h\to D_{i,j}}} &= \left(\sum_{n=1,n\neq i,n\neq j}^{N} \frac{1}{\sigma_a^2}\right) + \frac{1}{\sigma^2_{C_h\to r_h}}, && (4.12)\\
m_{r_h\to D_{i,j}} &= \sigma^2_{r_h\to D_{i,j}} \cdot && (4.13)\\
&\quad \left(\left(\sum_{n=1,n\neq i,n\neq j}^{N} \frac{m_a}{\sigma_a^2}\right) + \frac{m_{C_h\to r_h}}{\sigma^2_{C_h\to r_h}}\right),\\
\frac{1}{\sigma^2_{r_h\to C_h}} &= \sum_{n=1,n\neq h}^{N} \frac{1}{\sigma_a^2}, && (4.14)\\
m_{r_h\to C_h} &= \sigma^2_{r_h\to C_h}\left(\sum_{n=1,n\neq h}^{N} \frac{m_a}{\sigma_a^2}\right), && (4.15)
\end{aligned}
$$

where either $h = i$ or $h = j$, $a = D_{h,n} \to r_h$ for $h < n$, and $a = D_{n,h} \to r_h$ for $h > n$. It should be noticed that in the first iteration, we need to use any initial values for both the messages $m_{C_h\to r_h}$ and $\sigma^2_{C_h\to r_h}$, while the

messages in the following iteration use the new function proposed in this chapter. We describe the messages $m_{C_h \to r_h}$ and $\sigma^2_{C_h \to r_h}$ later in (4.16) and (4.17) when we derived the functions at the node C_h.

The messages $m_{r_h \to C_h}$ and $\sigma^2_{r_h \to C_h}$ containing the estimated Euclidean distance information are forwarded by the node r_h to the node C_h. The proposed technique obtains the estimated Euclidean distance messages extracted from difference Euclidean distance messages at the node r_h by exchanging the messages between the nodes $D_{i,j}$ and r_h, which eliminates the necessity of the knowledge of the absolute time stamp, on the contrary, the TOA-based FG technique in [17] obtains Euclidean distance messages at the node r_h directly from the measurement of TOA samples, which requires the absolute time stamp information.

However, it is not sufficient to estimate the Euclidean distance by having knowledge of only the TDOA samples. It is shown in Figs. 4.3(a) and 4.3(b), that the difference Euclidean distance messages from TDOA samples are exchanged between the nodes $D_{i,j}$ and r_h without receiving messages from the node C_h resulting in the error Δr between the target position and the circle of Euclidean distance of each sensor. This is because process performed in the original node C_h in [17] does not take into account the input to node r_h from the node C_h, resulting in the error Δr of Euclidean distance, when the node r_h send the Euclidean distance messages to the original node C_h of the TOA-based FG.

To avoid the bias, the information of the known sensor positions at both the nodes A_h and B_h, is also utilized in the nodes $D_{i,j}$ and r_h. The known sensor positions information is converted to Euclidean distance message by using Pythagorean function forwarded from the node C_h to the node r_h. We propose modifications of the function at the node C_h in [17], of which result appears in the messages $m_{C_h \to r_h}$ and $\sigma^2_{C_h \to r_h}$ from the node C_h to the node r_h. The modifications are summarized below:

$$m_{C_h \to r_h} = \sqrt{m^2_{\Delta x_h \to C_h} + m^2_{\Delta y_h \to C_h}}, \tag{4.16}$$

$$\sigma^2_{C_h \to r_h} = \frac{m^2_{\Delta x_h \to C_h} \sigma^2_{x_h \to C_h} + m^2_{\Delta y_h \to C_h} \sigma^2_{\Delta y_h \to C_h}}{m^2_{\Delta x_h \to C_h} + m^2_{\Delta y_h \to C_h}}, \tag{4.17}$$

where the messages $(m_{\Delta x_h \to C_h}, \sigma_{x_h \to C_h})$ and $(m_{\Delta y_h \to C_h}, \sigma_{\Delta y_h \to C_h})$ are forwarded from the nodes Δx_h and Δy_h, respectively, to the node C_h, as described later in (4.26) and (4.28).

The Pythagorean function is also used at the node C_h to obtain the messages of relative distance $(m_{C_h \to \Delta x_h}, \sigma^2_{C_h \to \Delta x_h})$ and $(m_{C_h \to \Delta y_h}, \sigma^2_{C_h \to \Delta y_h})$ for both the nodes Δx_h and Δy_h, respectively, in the same way as in [17],

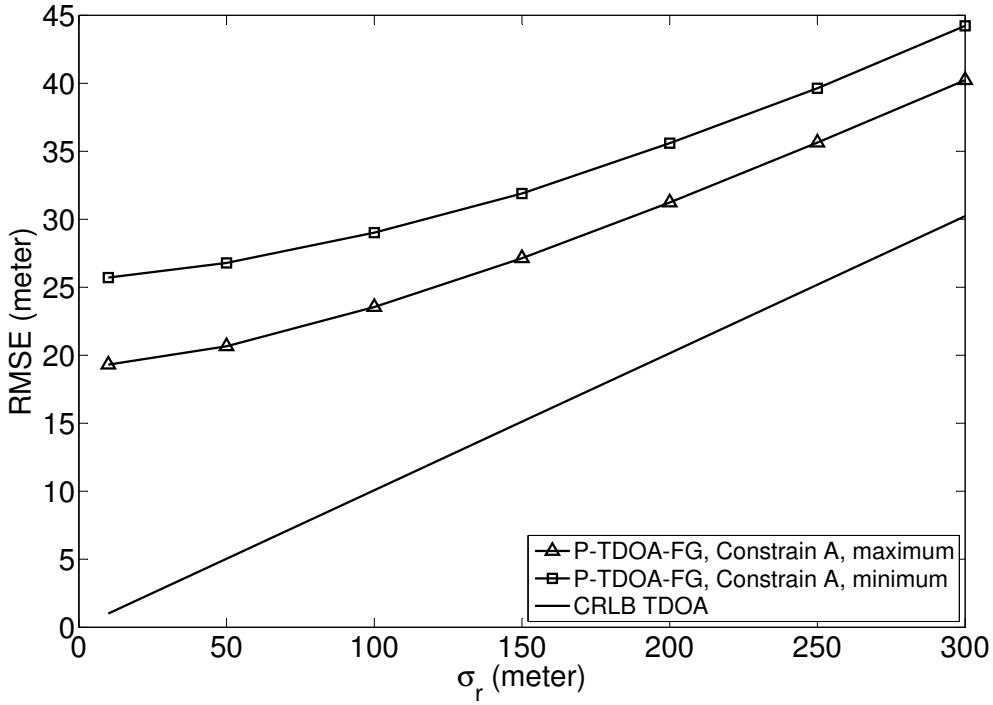

Figure 4.4. The RMSE of P-TDOA-FG for Constraint (A) of the use maximum or minimum value of the $\sigma^2_{D\to r}$ value with 3 sensors, 10,000 trials, and 100 samples.

as

$$m_{C_h\to\Delta x_h} = \pm\sqrt{m^2_{r_h\to C_h} - m^2_{\Delta y_h\to C_h}}, \tag{4.18}$$

$$m_{C_h\to\Delta y_h} = \pm\sqrt{m^2_{r_h\to C_h} - m^2_{\Delta x_h\to C_h}}, \tag{4.19}$$

$$\sigma^2_{C_h\to\Delta x_h} = \frac{m^2_{r_h\to C_h}\sigma^2_{r_h\to C_h} + m^2_{\Delta y_h\to C_h}\sigma^2_{\Delta y_h\to C_h}}{m^2_{r_h\to C_h} - m^2_{\Delta y_h\to C_h}}, \tag{4.20}$$

$$\sigma^2_{C_h\to\Delta y_h} = \frac{m^2_{r_h\to C_h}\sigma^2_{r_h\to C_h} + m^2_{\Delta x_h\to C_h}\sigma^2_{\Delta x_h\to C_h}}{m^2_{r_h\to C_h} - m^2_{\Delta x_h\to C_h}}. \tag{4.21}$$

It should be noticed that the signs plus and minus ($\pm$) of $m_{C_h\to\Delta x_h}$ and $m_{C_h\to\Delta y_h}$ in (4.18) and (4.19) follow the positivity and negativity of the value of sign of $m_{\Delta x_h\to C_h}$ and $m_{\Delta y_h\to C_h}$, respectively.

In the TOA-based FG technique in [17], the iteration process is performed only between the nodes x, y, and C_h. After the modification of the functions at the original node C_h in [17] by adding additional Pythagorean function as in (4.16) and (4.17), the iteration is extended to between the nodes x, y, and $D_{i,j}$. However, we find that the value of the message

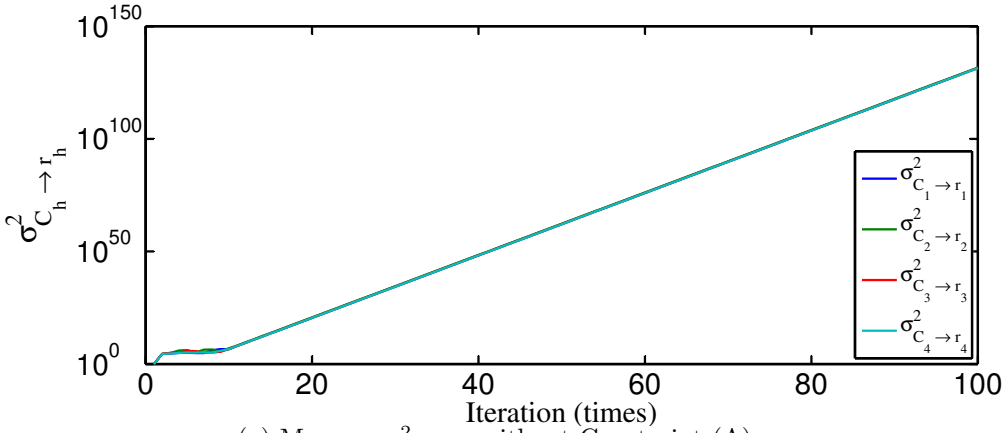

(a) Message $\sigma^2_{C_h \to r_h}$ without Constraint (A).

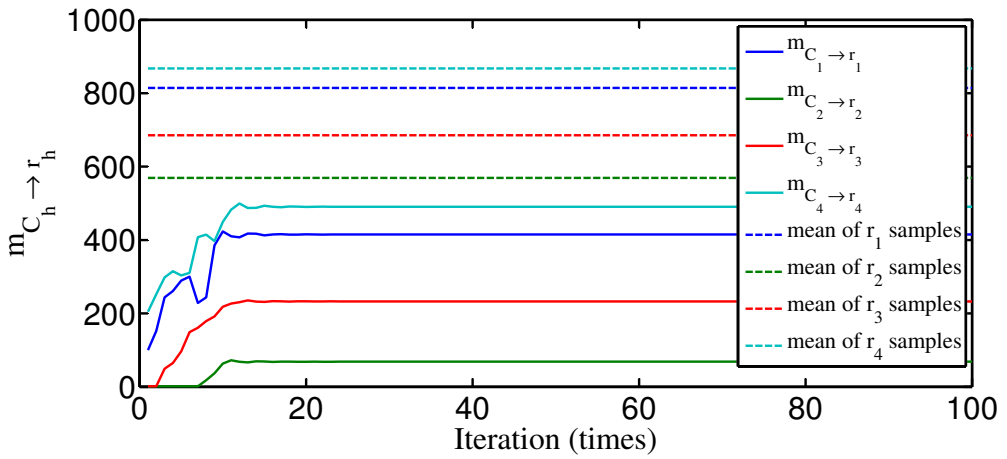

(b) Message $m_{C_h \to r_h}$ without Constraint (A).

Figure 4.5. The messages $m_{r_h \to C_h}$, $m_{C_h \to r_h}$ and $\sigma^2_{C_h \to r_h}$ without Constraint (A), target is at $(795, -457)$ m, 100 times iteration.

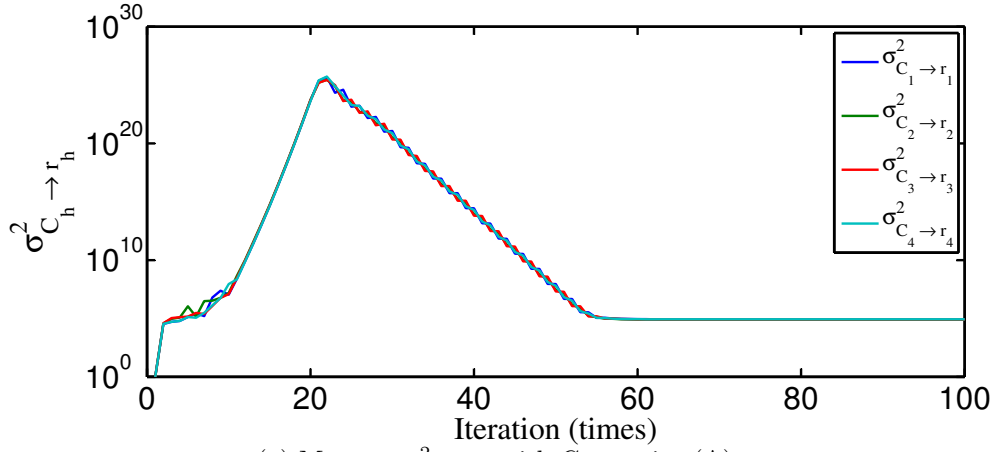

(a) Message $\sigma^2_{C_h \to r_h}$ with Constraint (A).

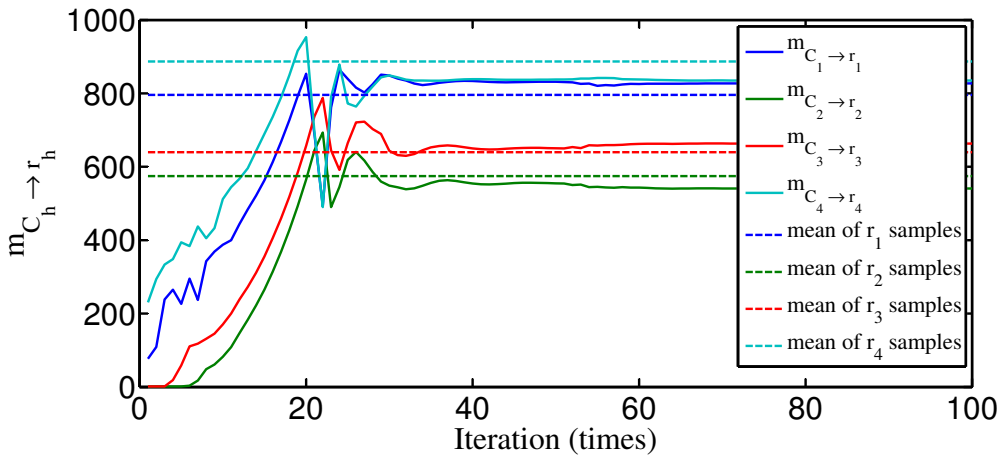

(b) Message $m_{C_h \to r_h}$ with Constraint (A).

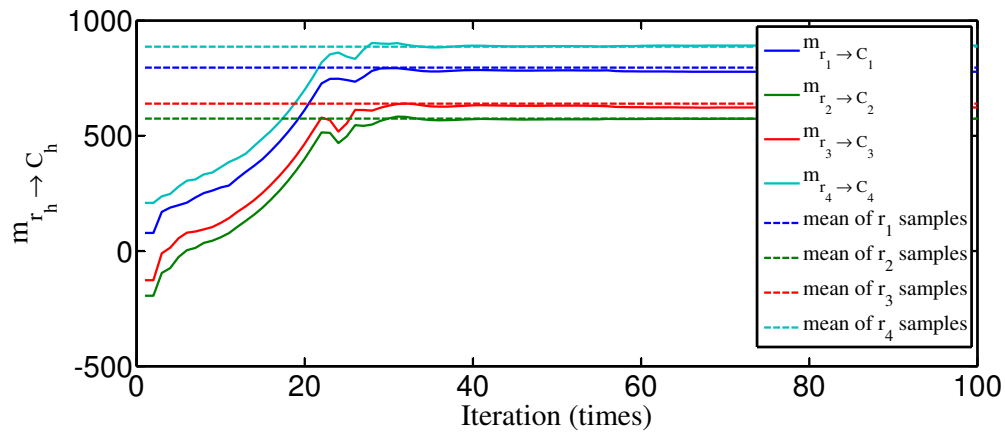

(c) Message $m_{r_h \to C_h}$ with Constraint (A).

Figure 4.6. The messages $m_{r_h \to C_h}$, $m_{C_h \to r_h}$ and $\sigma^2_{C_h \to r_h}$ with Constraint (A), target is at $(795, -457)$ m, 100 times iteration.

$\sigma^2_{C_h \to r_h}$ increases to infinity during the iteration as shown in Fig. 4.5(a). This is because the node C_h performs only additions, thereby the Euclidean distance messages $m_{C_h \to r_h}$ forwarded from the node C_h to the node r_h does not converge into the true value, as shown in Fig. 4.5(b). Since the variance $\sigma_{C_h \to r_h}$ appears in the denominator of (4.13) and (4.12), the messages $m_{C_h \to r_h}$ and $\sigma^2_{C_h \to r_h}$ can be ignored when $\sigma^2_{C_h \to r_h}$ becomes excessively large. Hence, the information of the known sensor positions in the Euclidean distance messages forwarded from the node D_h to the node r_h are not used effectively. To solve this problem, we propose Constraint (A), as

$$\begin{aligned} if \quad & \sigma^2_{C \to r} > max(\sigma^2_{D \to r}) \\ & \sigma^2_{C \to r} = max(\sigma^2_{D \to r}) \\ end. & \end{aligned} \tag{4.22}$$

With Constraint (A), the value of the messages $\sigma^2_{C_h \to r_h}$ can be kept close to the messages $\sigma^2_{D_{i,j} \to r_h}$ during the iteration. To verify the avoidance of the message to diverge, we tested using the parameters shown in Table. 5.1. Fig. 4.4 shows that the RMSE of the proposed technique has higher accuracy if we use the maximum value of $\sigma^2_{D \to r}$ for Constraint (A). The simulation for Fig. 4.5(a)–4.6(c) is used the minimum value of $\sigma^2_{D \to r}$ for Constraint (A).

Fig. 4.6(a) shows that the variance messages $\sigma^2_{C_h \to r_h}$ converge after around 60 times of iterations with the values around $8 \cdot 10^4$. It is shown in Figs. 4.6(b) and 4.6(c) that the Euclidean distance messages $m_{C_h \to r_h}$ and $m_{r_h \to C_h}$ converge after around 40 and 60 times of iteration, respectively, because the variance messages $\sigma^2_{C_h \to r_h}$ converge into a proper value with Constraint (A).

The nodes $D_{i,j}$ and r_h added to the TOA-based FG in [17] as well as the node function modifications in C_h guarantees the proper operability of the proposed P-TDOA-FG technique with Pythagorean function. However, we still need to improve the stability of the convergence property of the proposed technique by introducing other constraints, Constraints (B) and (C), as described before.

Constraint (B): The *equivalent* Euclidean distance value in the message $m_{r_h \to C_h}$ can be very small during iteration, which imposes numerical instability. To avoid the numerical instability, we need Constraint (B), as

$$\begin{aligned} if \quad & m_{r_h \to C_h} < \epsilon \\ & m_{r_h \to C_h} = \epsilon \\ end, & \end{aligned} \tag{4.23}$$

Table 4.1.
Simulation Parameters.

Parameter	Value
N	4
K	$10, 25, 100, 500, 1000$
Trial	10000
(X, Y)	$(100, 0)$, $(100, -1000)$, $(1100, 0)$, $(1100, -1000)$ m
ϵ	2
δ	1
Iteration	100
Target area	400×400 m^2
Sensor area	1000×1000 m^2
$\sigma_r = \sigma_d$	$\{10, 50, 100, 150, \cdots, 300\}$ m
Initial position (x, y)	$(0, 0)$ m

where the value of ad-hoc parameter ϵ is chosen empirically (according to the author's experience, $\epsilon \geq 1.0$).

Constraint (C): To avoid the case where the argument of Pythagorean function the becomes negative, we set the message value as:

$$\begin{aligned} if \quad & m^2_{r_h \to C_h} - m^2_a < 0 \\ & m_a = sign(m_a) \times (abs(m_{r_h \to C_h}) - \delta) \\ end, & \end{aligned} \tag{4.24}$$

where the value of another ad-hoc parameter δ is determined empirically. We found that $\delta = 1.0$ is reasonable. a represents $\Delta x_h \to C_h$ and $\Delta y_h \to C_h$. Constraint (C) provides the advantage that the initial point x and y for iteration can be at any position. It should be noticed that with the TOA-based FG technique in [17], the initial values have to be carefully chosen to avoid the case where the value calculated by the Pythagorean function becomes imaginary.

The other processes of exchanging the messages between the nodes C_h, x, and y, are in the same way as in [17], where we briefly describe the processes below. The node Δx_h directly forwards the messages from the node C_h to the node A_h and from the node A_h to the node C_h in opposite way, as

$$(m_{\Delta x_h \to A_h}, \sigma^2_{\Delta x_h \to A_h}) = (m_{C_h \to \Delta x_h}, \sigma^2_{C_h \to \Delta x_h}), \tag{4.25}$$

$$(m_{\Delta x_h \to C_h}, \sigma^2_{\Delta x_h \to C_h}) = (m_{A_h \to \Delta x_h}, \sigma^2_{A_h \to \Delta x_h}), \tag{4.26}$$

respectively, where the messages $m_{A_h \to \Delta x_h}$ and $\sigma^2_{A_h \to \Delta x_h}$ are described later in (3.19). The node Δy_h also directly forward the messages from the node C_h to the node B_h and also from the node B_h to the node C_h, as

$$(m_{\Delta y_h \to B_h}, \sigma^2_{\Delta y_h \to B_h}) = (m_{C_h \to \Delta y_h}, \sigma^2_{C_h \to \Delta y_h}), \tag{4.27}$$

$$(m_{\Delta y_h \to C_h}, \sigma^2_{\Delta y_h \to C_h}) = (m_{B_h \to \Delta y_h}, \sigma^2_{B_h \to \Delta y_h}), \tag{4.28}$$

respectively, where the messages $m_{B_h \to \Delta y_h}$ and $\sigma^2_{B_h \to \Delta y_h}$ are described below in (3.20).

The nodes A_h and B_h, taking into account the known sensor position, convert the relative distance messages $(m_{\Delta x_h \to A_h}, \sigma^2_{\Delta x_h \to A_h})$ and $(m_{\Delta y_h \to B_h}, \sigma^2_{\Delta y_h \to B_h})$ to the coordinate of target position messages $(m_{A_h \to x}, \sigma^2_{A_h \to x})$ and $(m_{B_h \to y}, \sigma^2_{B_h \to y})$, respectively, where the reverse process is also performed in the same nodes. The messages updating process in the node A_h and B_h are calculated with the equations similar as (3.19), (3.20), (3.21), and (3.22) in Chapter 3. The messages $(m_{A_h \to x}, \sigma^2_{A_h \to x})$ and $(m_{B_h \to y}, \sigma^2_{B_h \to y})$ are then forwarded by the nodes A_h and B_h to the nodes x and y, respectively.

In the nodes x and y, the reserve process having different means and variance has also Gaussian pdf, are invoked according to the message passing principle, where the fact that the product of independent multiple Gaussian variables is utilized. Hence, the messages $(m_{x \to A_h}, \sigma^2_{x \to A_h})$ and $(m_{y \to B_h}, \sigma^2_{y \to B_h})$, needed for calculation by (3.19) and (3.20), are sent back from the nodes x and y to the node A_h and B_h, respectively, by using sum-product algorithm in (2.5) and (2.4) in Chapter 2, where $(m_{z \to Z_i}, \sigma^2_{z \to Z_i})$ indicates $(m_{x \to A_h}, \sigma^2_{x \to A_h})$ and $(m_{y \to B_h}, \sigma^2_{y \to B_h})$.

The entire process described above is repeated. All messages from the nodes A_h and B_h are combined by the sum-product algorithm in the nodes x and y when the iteration converges, by using sum-product algorithm in (2.8) and (2.7). The final decision to obtain the position estimate of unknown radio emitter (x, y) is then made from the mean (m_x, m_y) in (2.8) after the iteration converges, where m_z indicates m_x and m_y. To provide more comprehensive understanding, all equations operating at each node of the FG are summarized in Table 4.2, where the directions of the message flow is shown in the left column.

4.2.3 Computational Complexity

In [17], the linear approximation of Pythagorean is derived to be used in the conventional TOA-FG. The proposed P-TDOA-FG follows the same

Table 4.2. The operations required for each node in the proposed P-TDOA-FG.

Messages flow	(Means, Variances)			
	Inputs	Outputs	Flops	Remarks
$E_{i,j} \to d_{i,j}$	$\hat{\tau}_{i,j}$	$\left(m_{\hat{d}_{i,j}}, \sigma^2_{\hat{d}_{i,j}}\right)$	$4K$	- Similar to [17]
$d_{i,j} \to D_{i,j}$	$\left(m_{\hat{d}_{i,j}}, \sigma^2_{\hat{d}_{i,j}}\right)$	$\left(m_{\hat{d}_{i,j}}, \sigma^2_{\hat{d}_{i,j}}\right)$	–	
$D_{i,j} \to r_i$	$\left(m_{\hat{r}_i}, \sigma^2_{\hat{r}_i}\right)$ $\left(m_{\hat{d}_{i,j}}, \sigma^2_{\hat{d}_{i,j}}\right)$	$\left(m_{\hat{d}_{i,j}} + m_{\hat{r}_i}, \sigma^2_{\hat{d}_{i,j}} + \sigma^2_{\hat{r}_i}\right)$	2	- New proposed - Sensor index is omitted in $r \to D$ and $r \to C$ for simplicity. The detailed equations are in (4.12)–(4.15)
$D_{i,j} \to r_j$	$\left(m_{\hat{r}_i}, \sigma^2_{\hat{r}_i}\right)$ $\left(m_{\hat{d}_{i,j}}, \sigma^2_{\hat{d}_{i,j}}\right)$	$\left(-m_{\hat{d}_{i,j}} + m_{\hat{r}_i}, \sigma^2_{\hat{d}_{i,j}} + \sigma^2_{\hat{r}_i}\right)$	2	
$r \to D$ $r \to C$	$\left(m_j, \sigma^2_j\right)$ $j \neq i$	$\left(\sigma_i^2 \sum_{j\neq i} \frac{m_j}{\sigma_j^2}, \sigma_i^2 = \frac{1}{\sum_{j\neq i} \frac{1}{\sigma_j^2}}\right)$	$4(N-1)$	
$C_i \to r_i$	$\left(m_i, \sigma_i^2\right)$ $\left(m_j, \sigma_j^2\right)$	$\left(\sqrt{m_i^2 + m_j^2}, \frac{m_i^2\sigma_i^2 + m_j^2\sigma_j^2}{m_i^2 + m_j^2}\right)$	13	
	σ_i^2 $\sigma^2_{\hat{r}_i}$	Constrain (A)	–	
$C_i \to \Delta y_i$ $C_i \to \Delta x_i$	$\left(m_i, \sigma_i^2\right)$ $\left(m_{\hat{r}_i}, \sigma^2_{\hat{r}_i}\right)$	Constrains (B) and (C)	–	
		$\left(\pm\sqrt{m^2_{\hat{r}_i} - m_i^2}, \frac{m^2_{\hat{r}_i}\sigma^2_{\hat{r}_i} + m_i^2\sigma_i^2}{m^2_{\hat{r}_i} - m_i^2}\right)$	13	- Similar to [17] - The sign $(\pm)$ is equal to the sign of the messages from the nodes Δy and Δx to the node C
$A_i \to \Delta x_i$ $A_i \to x$	$\left(m_i, \sigma_i^2\right)$	$\left(X_i - m_i, \sigma_i^2\right)$	1	
$B_i \to \Delta y_i$ $B_i \to y$	$\left(m_i, \sigma_i^2\right)$	$\left(Y_i - m_i, \sigma_i^2\right)$	1	
$\Delta x_i \to C_i$ $\Delta x_i \to A_i$ $\Delta y_i \to C_i$ $\Delta y_i \to B_i$	$\left(m_i, \sigma_i^2\right)$	$\left(m_i, \sigma_i^2\right)$	–	
$x \to A_i$ $y \to B_i$	$\left(m_j, \sigma_j^2\right)$ $j \neq i$	$\left(\sigma_i^2 \sum_{j\neq i} \frac{m_j}{\sigma_j^2}, \sigma_i^2 = \frac{1}{\sum_{j\neq i} \frac{1}{\sigma_j^2}}\right)$	$4(N-1)$	
x and y	$\left(m_i, \sigma_i^2\right)$	$\left(\sigma^2 \sum_i \frac{m_i}{\sigma_i^2}, \sigma^2 = \frac{1}{\sum_i \frac{1}{\sigma_i^2}}\right)$	$4N$	

linear approximation as in [17]. Furthermore, the proposed P-TDOA-FG only adds subtraction operation, and another Pythagorean function and sum-product algorithm. Hence, the computational complexity for arithmetic at the factor nodes is proportional to N. Similar to as described in Chapter 2, the computational complexity of sum-product algorithm in iteration process is proportional to N^2.

Even though the H-TDOA-FG technique in [6] has also used the approximation in [17], the technique in [6] needs high computational complexity as described above. It is shown in [6] that the conventional H-TDOA-FG technique achieves higher accuracy but requires heavier computational complexity over the Gauss-Newton technique. As described in Chapter 2, the computational complexity of Gauss-Newton algorithm is proportional to N^3. Hence, the proposed P-TDOA-FG has lower computational complexity compared to the conventional Gauss-Newton and H-TDOA-FG techniques.

4.3 Performance Evaluation

A series of computer simulations were conducted to confirm the performance superiority of the proposed P-TDOA-FG geolocation technique as shown in Table. 5.1, where $10,000$ trials were conducted, each having 1 target randomly chosen from the area of 400×400 m^2 in the middle of sensor area of $1,000 \times 1,000$ m^2 as shown in Fig. 4.7(a). We estimate only one target position in each trial, where the case to estimate the multiple-target of unknown radio emitter is left for the future work. The scenario assumption taken in the simulation is for monitoring of illegal radio wave emitter as one of the example of unknown radio emitter. It is assumed that the radio wave emitted by the target is strong enough to reach area width of $1,000 \times 1,000$ m^2.

Fig. 4.7(a) shows positions of the four sensors denoted by the Δ mark. The positions of sensors are set at $(100, 0)$, $(100, -1000)$, $(1100, 0)$, and $(1100, -1000)$ m in the $(X - Y)$ coordinate. Since the target positions are enough randomly chosen, relative to the sensor positions, we fixed the sensor positions in the simulations.

We evaluated the accuracy of proposed technique by using the 3 and 4 sensors. The standard deviation of measurement error were set at $\sigma_r = \sigma_d = \{10, 50, 100, 150, \cdots, 300\}$ m, where σ_r is for the TOA-based technique and σ_d is for the P-TDOA-FG technique. We set the same value for σ_r and σ_d to observe the improvement of the P-TDOA-FG technique over TOA-based technique as done in [6]. We also assume

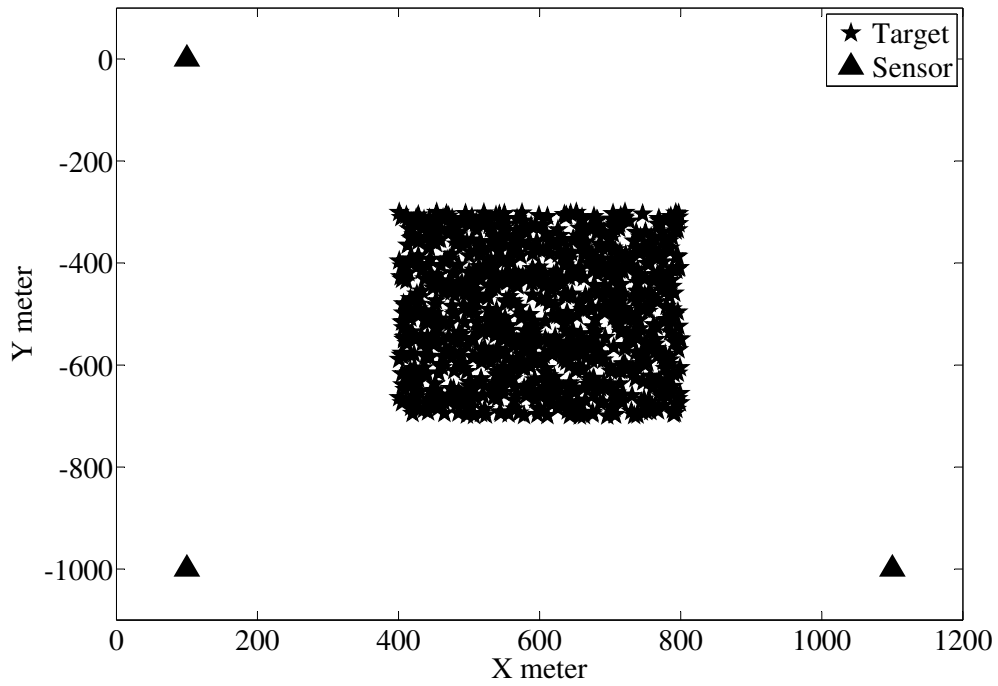

(a) 500 of 10,000 target positions.

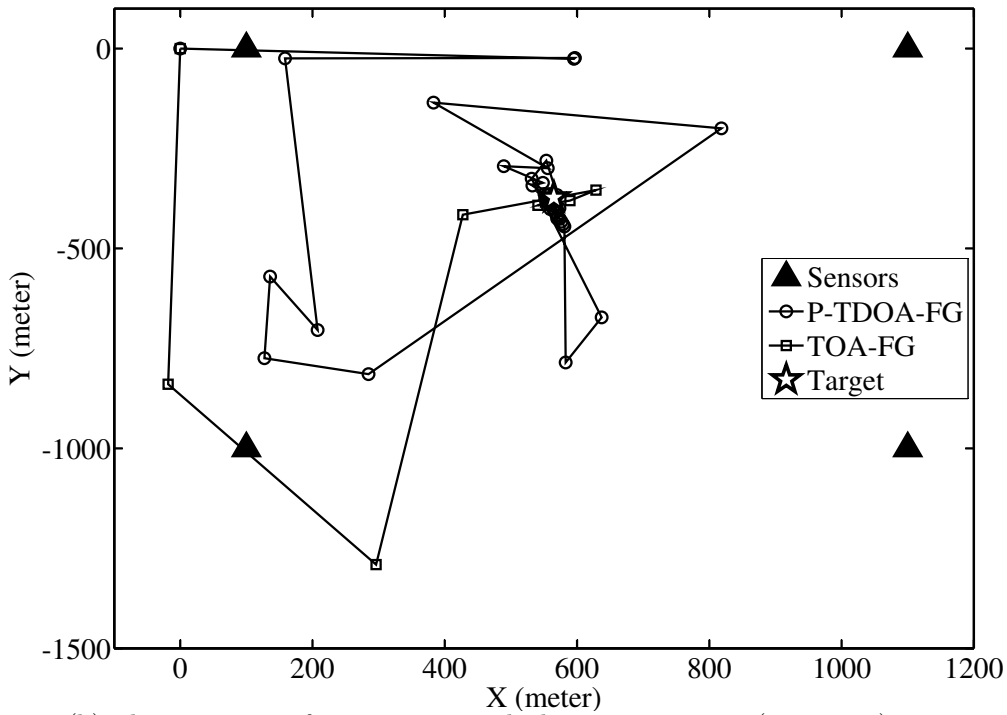

(b) The trajectory of iteration to reach the target position $(565, -373)$ m.

Figure 4.7. The configuration with 10,000 target positions of targets and 4 sensors in 400×400 m^2 width area, with $\sigma = 150$ m.

that the measurements error has the same σ_r values for all the sensors for the simplicity as we have mentioned in Chapter 2. We set the initial value in the simulation with 0 for the means $m_{r_h \to D_{i,j}}$, $m_{x \to A_h}$, $m_{y \to B_h}$, and $m_{C_h \to r_h}$. The initial value for variance $\sigma^2_{r_h \to D_{i,j}}$, $\sigma^2_{x \to A_h}$, $\sigma^2_{y \to B_h}$, and $\sigma^2_{C_h \to r_h}$ are set to 1. The small constant values of conditional constraint are set $\epsilon = 2$ and $\delta = 1$.

We create the TDOA samples model directly converted to difference Euclidean distance by using (4.6). After that, we add Gaussian noise with standard deviation of measurement error, σ_r, as mentioned above. The Gaussian noise is calculated by computer simulation in 10 up to $1,000$ samples. Finally, we utilize these samples to calculate mean and variance as the messages of the P-TDOA-FG.

Fig. 4.7(b) shows the trajectory indicating the algorithm behavior for each iteration to demonstrate the convergence property of the proposed technique. Fig. 4.7(b) also shows the trajectory of the TOA-based FG technique, for comparison where the absolute time stamp is assigned to be available. The proposed technique successfully reaches the true target position at $(x, y) = (497, -344)$ m in around 21 iterations, while the TOA-based FG technique exhibits faster convergence; around 6 iteration as needed, where iteration process is started from the initial point $(0, 0)$ m. However, it is shown in the Fig. 5.18 that even though the TOA-based FG technique is faster to converge in the both case. The fast convergence with the TOA-based technique is because the absolute time stamp information is available. The accuracy with the proposed technique is higher than the TOA-based technique when the algorithms converge. This is because with the proposed technique, the additional averaging process takes place both in the nodes $D_{i,j}$ and C_h, while in the TOA-based technique the averaging process takes place only in the node C_h.

Fig. 4.8(b) shows that the accuracy of the both techniques in term of RMSE. It is found that the standard deviation σ_r of the measurement error increases, the accuracy decreases, which is consistent to the tendency of the CRLB curve. It is also shown that the accuracy of CRLB has the same tendency. Fig. 4.8(b) also shows that the accuracy of the proposed technique is very close to the TDOA-based CRLB, where the curve of the proposed technique lies between the TOA-based CRLB and TDOA-based CRLB. Obviously, we can see in the Fig. 4.8(b) that the accuracy of the proposed technique outperforms the accuracy of the TOA-based FG technique. Fig. 4.8(c) shows that all the curves goes down by the increasing of the number of samples which means the accuracy increases with larger number of samples. It is shown also in Fig. 4.8(c) that the

proposed technique has reasonable high accuracy in the practical case where only a few samples is available.

4.4 Summary

A new FG-based geolocation technique using the TDOA measurement to detect the position of an unknown (anonymous) radio wave emitter has been in this paper. The uniqueness of the proposed technique compared to the conventional hyperbolic TDOA-based technique is the use of the simple Pythagorean function instead of the hyperbolic functions. Several sets of new nodes have been introduced to the conventional TOA-FG technique. Furthermore, the modification has been made on the node functions, so that it works with Pythagorean function where the input of the FG is TDOA measurement. Constraints are also introduced in this paper: (1) to allow the iteration to started at arbitrary point in the target area, and (2) to preserve the numerical stability of the algorithm. It is confirmed by the computer simulation results that our proposed technique provides high accuracy with better position estimate, RMSE lower than 5 m for $\sigma_r < 50$ m, even though it does not require high computational complexity. The accuracy proposed P-TDOA-FG outperforms the conventional TOA-FG. Furthermore, the achieved RMSE curve of the proposed technique is also close to CRLB curve.

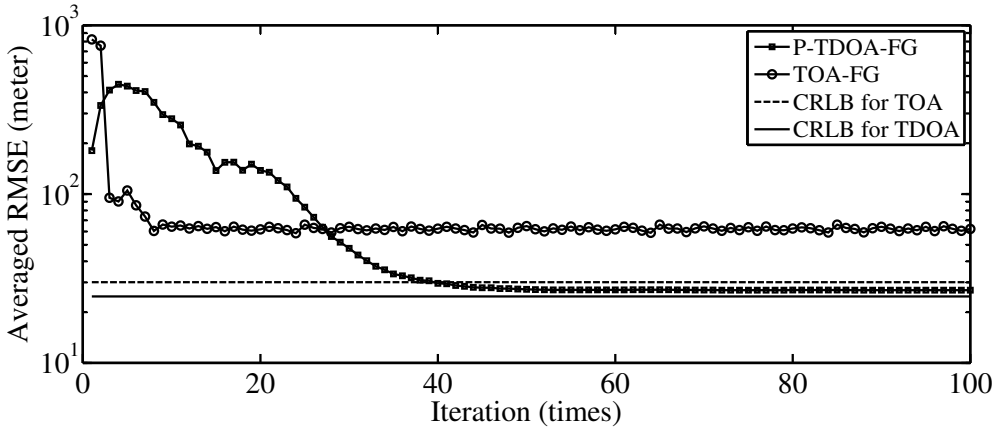

(a) RMSE vs. iteration times with $\sigma_r = 300$ m.

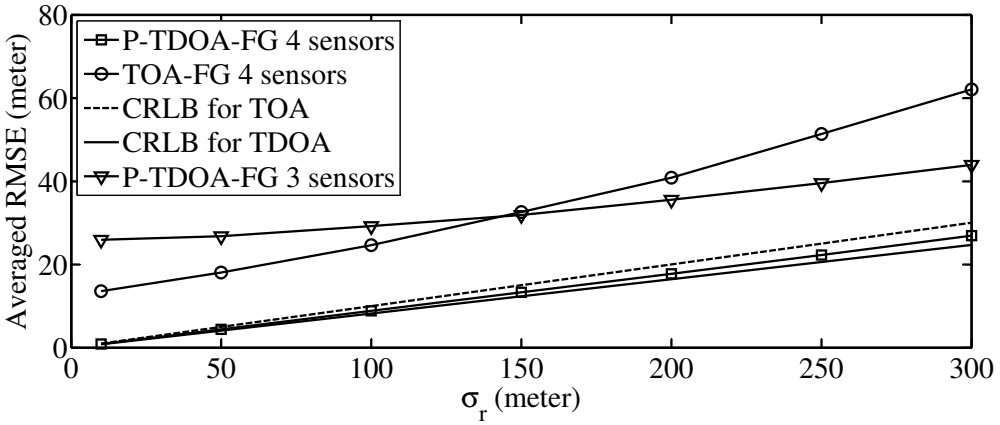

(b) The RMSE vs. σ_r with 100 samples.

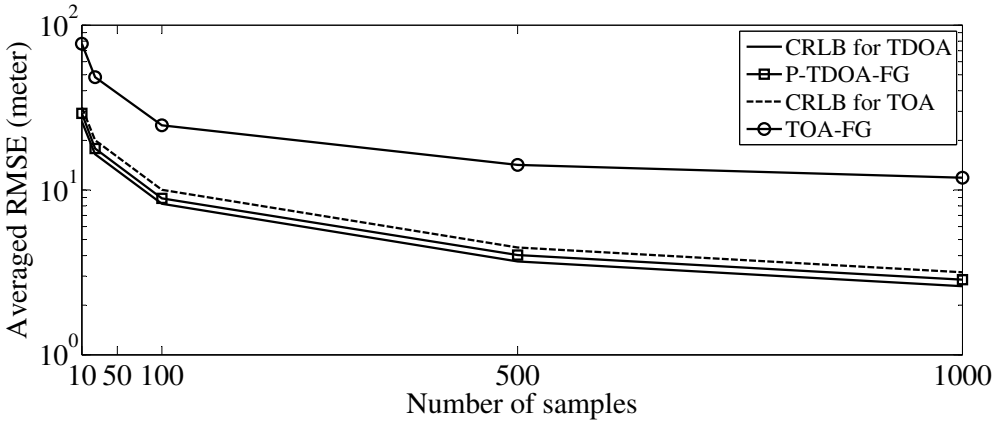

(c) The RMSE vs. number of samples with $\sigma_r = 100$ m.

Figure 4.8. RMSE of the proposed technique, TOA-based FG technique, and CRLBs for TOA and TDOA, averaged over 10,000 trials, with 4 sensors. The sensor positions for the case of 3 sensors the sensor positions are at $(100, 0), (1100, -1000), (600, 1000)$ m.

Chapter 5

DRSS-Based Factor Graph Geolocation

In this chapter, the joint use of the conventional RSS-V and RSS-FG techniques is proposed, where the RSS-V is used to select the appropriate four monitoring spots of the RSS-FG covering the target. The RSS-V also provides the initial value for iteration in the RSS-FG algorithm. The RSS-FG itself improves the accuracy of the RSS-V. The main objectives of this chapter are as follows: 1) The conventional RSS-V algorithm in [58] is modified with the opposite way, i.e., the sensors measure the RSS of the target and then forward it to fusion center, where the RSS-V algorithm is performed in fusion center. It is called as opposite way because, in the conventional RSS-V [58], the target measures the RSS of the signals sent from several beacons/transmitters for estimating own position. 2) The modified RSS-V with the RSS-FG are combined to improve the accuracy, where RSS-V is used to select four monitoring spots, which are covering the target, for RSS-FG. 3) We compare the performance of the proposed technique with number of sensors and signal to noise power ratio (SNR) as parameters. 4) The outdoor environment is assumed free space loss or long enough averaging range performed to eliminate the shadowing and instantaneous fading, hence the only path-loss still remains as in [53].

Furthermore, DRSS-based factor graph technique is proposed for outdoor environment with the aim of its application which detects the position of the unknown radio wave emitter, e.g., emergency signal sent by the victim of disaster, the signal sent by illegal radio emitter. The DRSS-FG is developed by modifying the RSS-FG in [18]. The modification is simply by the subtraction of RSS parameters between two sensors, hence the DRSS parameter is obtained to eliminate the necessity of transmit power

knowledge of unknown target. The DRSS-FG is able to detect the position of the unknown target, while the conventional RSS-FG fails because the absolute value of the transmit power is eliminated by the subtraction of the RSS samples between two sensors. This is clearly shown in the next section by analyzing the intersection of the approximated DRSS profile obtained by assuming a linear plane path-loss model around the target coordinate. The trajectory and the RMSE analysis results show that the DRSS-FG technique accurately estimates the unknown target.

5.1 Joint RSS-Based Voronoi and Factor Graph Geolocation Technique

5.1.1 Proposed Technique

The RSS-V-FG technique is a joint use of the RSS-V and RSS-FG techniques as shown in Fig. 5.1. The RSS-V is used to provide the RSS-FG algorithm with the initial point of the target and proper monitoring spots surrounding the target. Before performing the RSS-V and RSS-FG in the RSS-V-FG algorithm, the sensors measure the RSS samples using training signals sent by monitoring spots. The measurement is performed in a long range enough around the monitoring spots so that the measurement data contains only path-loss information. The RSS samples of training signal sent from monitoring spot are measured by the sensor over long duration to obtain the RSS value which is free from measurement error [18]. It should be noted that the RSS samples of the target still contain measurement error. All measured RSS samples in the sensor are sent to the fusion center, where the RSS-V-FG geolocation algorithm is performed. The error-free measured RSS samples of the training signals are used for establishing the equation in the *linear plane LS factor nodes* A_p, where RSS samples of the target is converted into the target position. The pseudo code of the proposed RSS-V-FG technique can be found at Algorithm 1.

Fig. 5.2 shows the Voronoi diagram with 23 sensors. One of the Voronoi region with the highest measured RSS value is assigned with its measured RSS value. After that, since the sensor having the highest measured RSS value is removed, there remain only 22 sensors. The Voronoi region of the sensor, with highest measured RSS value among 22 sensors, is added with its own RSS value. Hence, there is accumulation and overlapping between the first Vornoi region and the second Voronoi region. When all sensors are removed, we have the overlapping accumulation of RSS

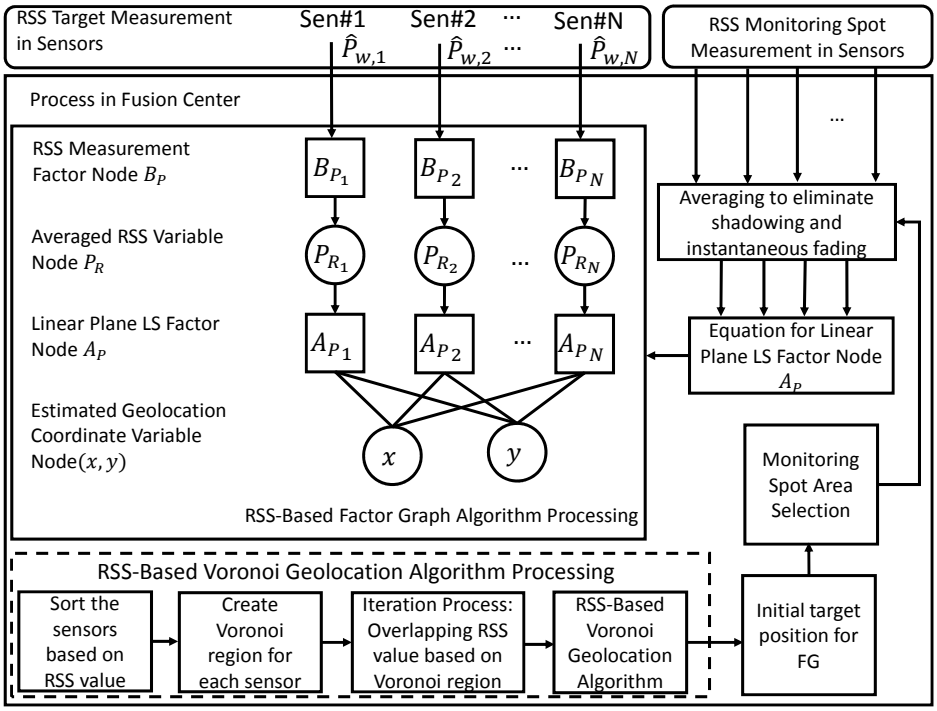

Figure 5.1. The proposed RSS-V-FG for Geolocation Technique

Algorithm 1 : RSS-V-FG

1: **procedure** RSS-V
2: **Input:** RSS samples and sensors position
3: calculate mean and variance k RSS samples
4: sort and make indexing the sensors
5: calculate meshgrid (xi, yi)
6: **for** $ii = 1$ until N sensors **do**
7: calculate $d_i(xi, yi)$ to each grid
8: **end for**
9: **for** $ii = 1$ until N sensors **do**
10: P_{RV} = maximum of $P_i \in N + 1 - ii$
11: **for** all $d_i(xi, yi)$ **do**
12: **if** $d_i(xi, yi)$ minimum to other sensors **then**
13: $P(xi, yi) = P(xi, yi) + P_{RV}$
14: **end if**
15: **end for**
16: remove the selected sensors, $i \in N - ii$
17: **end for**
18: select the grid (xi, yi) with maximum $P(xi, yi)$
19: **Output:** inital target of RSS-FG, $(x^0, y^0) = E[(xi, yi)]$
20: **end procedure**
21: **procedure** SELECT MONITORING SPOTS
22: **Input:** $(\Delta x_j, \Delta y_j) = (x^0 - x_j, y^0 - y_j)$
23: (x_r, y_r) = sort (x_j, y_j) based on $(\Delta x_j, \Delta y_j)$
24: **for** $si = 1$ until M monitoring spots **do**
25: **if** $si = 1$ **then**
26: $x_{s_1} = x_r(1)$, $y_{s_1} = y_r(1)$
27: **else**
28: **if** $x_r(si) = x_r(1)$ **then** do nothing
29: **else**
30: $x_{s_2} = x_r(si)$
31: **break**
32: **end if**
33: **repeat:** line 29 – 33 for y coordinate
34: **end if**
35: **end for**
36: **Output:** selected monitoring spots (x_{s_1}, y_{s_1}), (x_{s_2}, y_{s_1}), (x_{s_1}, y_{s_2}), (x_{s_2}, y_{s_2})
37: **end procedure**
38: **procedure** RSS-FG
39: **Input:** Sensors position, selected monitoring spots, and RSS samples
40: calculate the coefficients (5.3), (2.25)
41: **for** $ti = 1$ until T iteration **do**
42: calculate $\sigma^2_{A_{P_i} \to x}$, $m_{A_{P_i} \to x}$ (2.23),(2.21)
43: calculate $\sigma^2_{x \to A_{P_i}}$, $m_{x \to A_{P_i}}$ (2.4)
44: calculate $\sigma^2_{A_{P_i} \to y}$, $m_{A_{P_i} \to y}$ (2.24), (2.22)
45: calculate $\sigma^2_{y \to A_{P_i}}$, $m_{y \to A_{P_i}}$ (2.5)
46: **end for**
47: calculate σ^2_x, σ^2_y (2.7)
48: **Output:** target coordinate, (m_x, m_y) (2.8)
49: **end procedure**

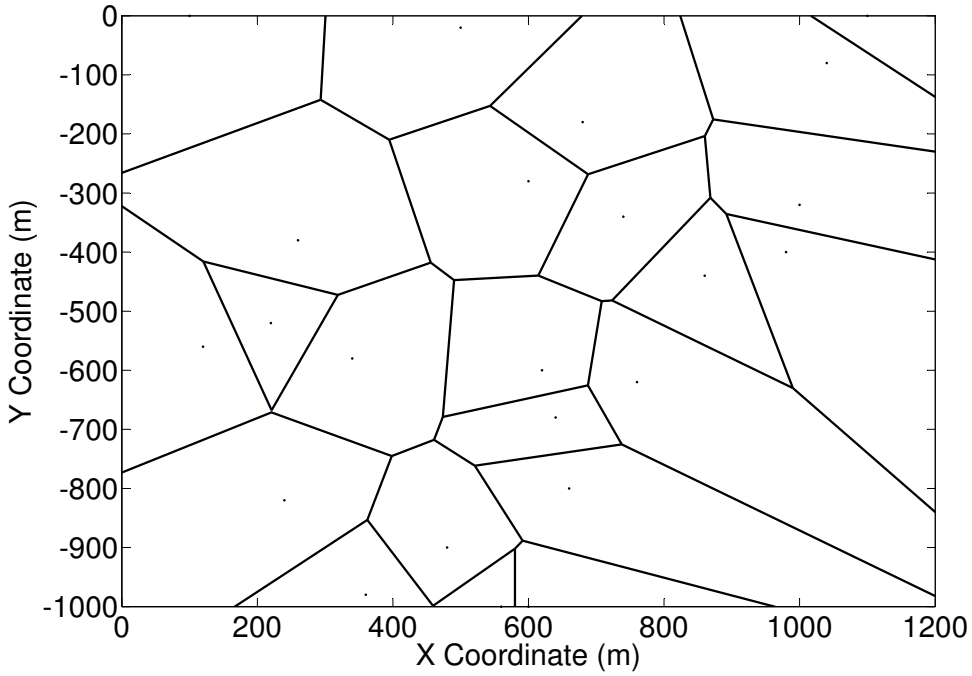

Figure 5.2. The Voronoi diagram with 23 sensors in $1,000 \times 1,000$ m^2.

value from 23 sensors, as shown in Fig. 5.3. It is found that the region having the highest accumulated RSS of target measured by 23 sensors are close to the true target position, which is at $(468, -838)$ m. The position estimate is obtained from the average of the coordinates having the highest accumulated RSS, which is at $(477, -840)$ m.

The computational complexity of the RSS value accumulation performed for the overlapped Voronoi region in the RSS-V depends on the resolution of the region. This means that higher resolution requires heavier computation, for example, the resolution with grid 10 m^2 has lower complexity compare to higher resolution with grid 1 m^2. We tested the computation time of the RSS-V-FG, RSS-FG, and RSS-V with parameter setting described in Table 5.2. The computation time of the RSS-V-FG, RSS-FG, and RSS-V is shown in Table. 5.1. The RSS-FG which is using only 3 sensors has much lower computation time over the RSS-V-FG and RSS-V. One of the schemes that can be used to solve the complexity issue is by using pre-computing for the RSS-V before using the technique for geolocation. The result of pre-computing of RSS is simply used as a look-up table. However, pre-computing of the RSS-V is not discussed in detail in this dissertation because we leave it as a future work.

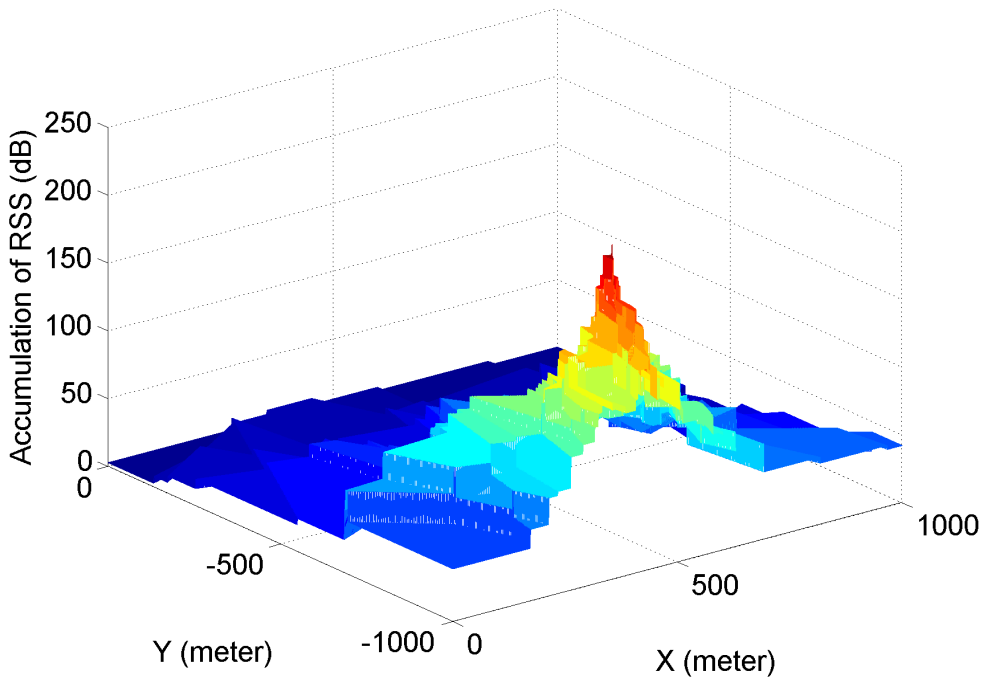

Figure 5.3. The RSS of target accumulation by the RSS-V algorithm with 23 sensors, where the target is at $(468, -838)$ m.

Table 5.1.
The Computation Time of RFVF, RSS-FG, and RSS-V techniques.

Sensor Number	Time Processing (second)		
	RSS-V-FG	RSS-FG	RSS-V
3	1.2036	0.0086	1.195
23	25.9462	–	25.93755

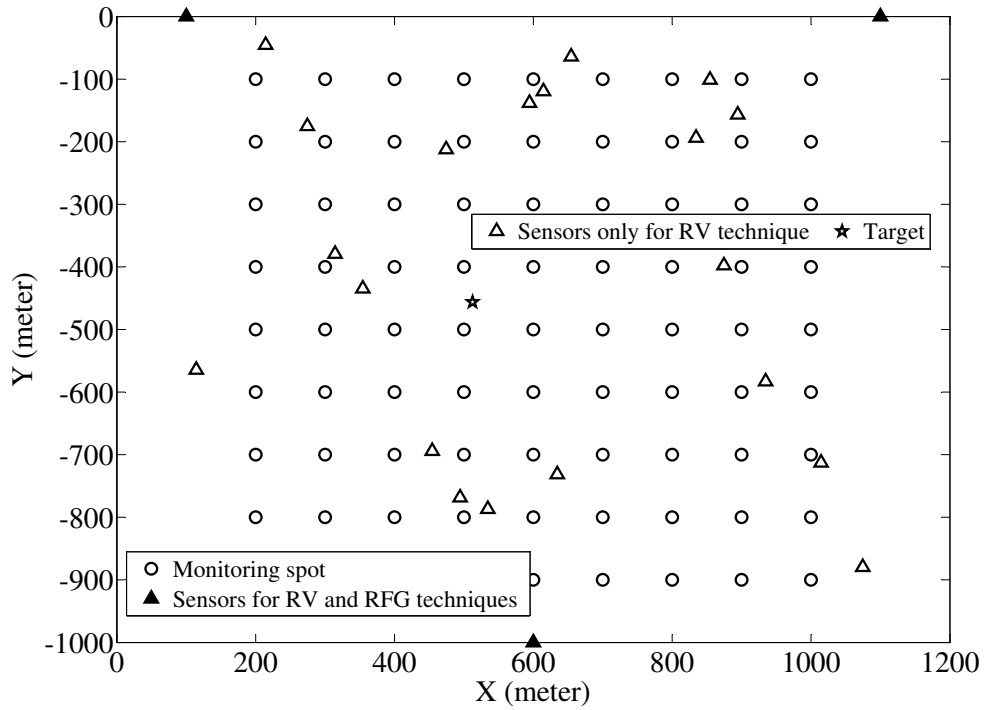

Figure 5.4. The simulation setup describing monitoring spots with grid 100×100 m^2, 23 sensors, 1 targets in total outdoor area of $1,000 \times 1,000$ m^2.

5.1.2 Simulation Results

A series of computer simulations was conducted to verify the performance of the proposed technique. The simulation round consists of 100 trials, each having one target randomly chosen from the area of 800×800 m^2. Three sensors used by RSS-FG technique are set at fixed the positions of $(100, 0), (100, -1000), (600, -1000)$ m in $(X - Y)$ coordinate as shown in Fig. 5.4. Each trial has also additional numbers of sensors, i.e, 0 to 20 sensors, randomly chosen from the area of $1,000 \times 1,000$ m^2, where all of the sensors in total are used by RSS-V.

The monitoring spot positions are set in a square area of $1,000 \times 1,000$ m^2 with grid step in 100×100 m^2 as suggested in [53]. The RSS-V is used to select one cell having four monitoring spots, covering the target position. The results are followed by the RSS-FG technique to obtain the accurate position estimate of the target by using the selected four monitoring spots and initial value provided by RSS-V technique. The RSS-FG technique also uses only three sensors which are set at the fixed positions.

The RSS values of target measured in sensors are made by path-loss exponent model because of the long enough averaging range assumption to eliminate the shadowing and instantaneous fading as in [53]. We set the path-loss exponent $n = 3$, reference distance $d_0 = 100$ m, and frequency carrier $f = 1$ GHz.

The following parameters were used to evaluate the accuracy of the proposed technique: a) 30 times of iterations for each trial, b) 100 samples, c) 3 to 23 sensors. The values of the measurement error is in SNR, i.e., 0 to 30 dB. We assume that the measurements are corrupted by the measurement error having the same variance in each sensor for simplicity. The summary of computer simulation setting can be found in Table. 5.2.

Table 5.2.
Simulation Parameters.

Parameters	Values
N Sensors	3 and 23
K Samples	100
Trial	100
(X, Y) fixed in meter	$(100, 0)$,$(100, -1000)$,$(600, -1000)$ Other sensor positions are random
n path-loss exponent	3
f GHz	1
d_0 meter	100
Iteration times	30
Target area in m^2	800×800
Sensor area in m^2	1000×1000 m^2
SNR in dB	0 to 30

Figs. 5.5 and 5.6 show the trajectory of the proposed technique with 23 sensors. The initial value provided by RSS-V is close to the target position at $(498, -463)$ m because of many sensors involved, hence the accumulation of the measured RSS value concentrated at averaged coordinate at $(500, -464)$ m, near to the target position. The trajectory of proposed technique is compared to the trajectory of the idealistic of RSS-FG curve where correct monitoring spots are always selected. The initial value is set at $(0, 0)$ m. The RSS-V with small number of sensors selects the wrong monitoring spots area as shown in Fig. 5.7, with the number of sensors of three. Therefore, the proposed technique can not reach close to the true target position.

Figs. 5.8 and 5.9 show the the accuracy of the proposed technique in term of RMSE with number of sensors as a parameter. It is shown that the

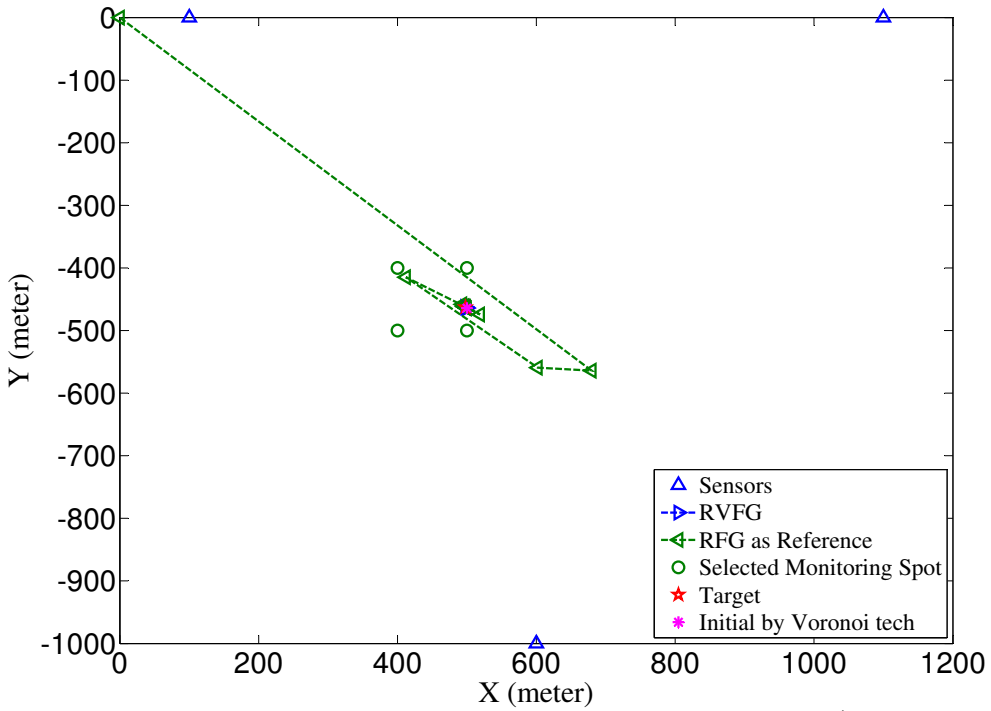

Figure 5.5. The trajectory of the RSS-V-FG technique with 23 sensors (in this figure only shown 3 sensors used by factor graph-based for simplicity in analysis) and target at $(498, -463)$m.

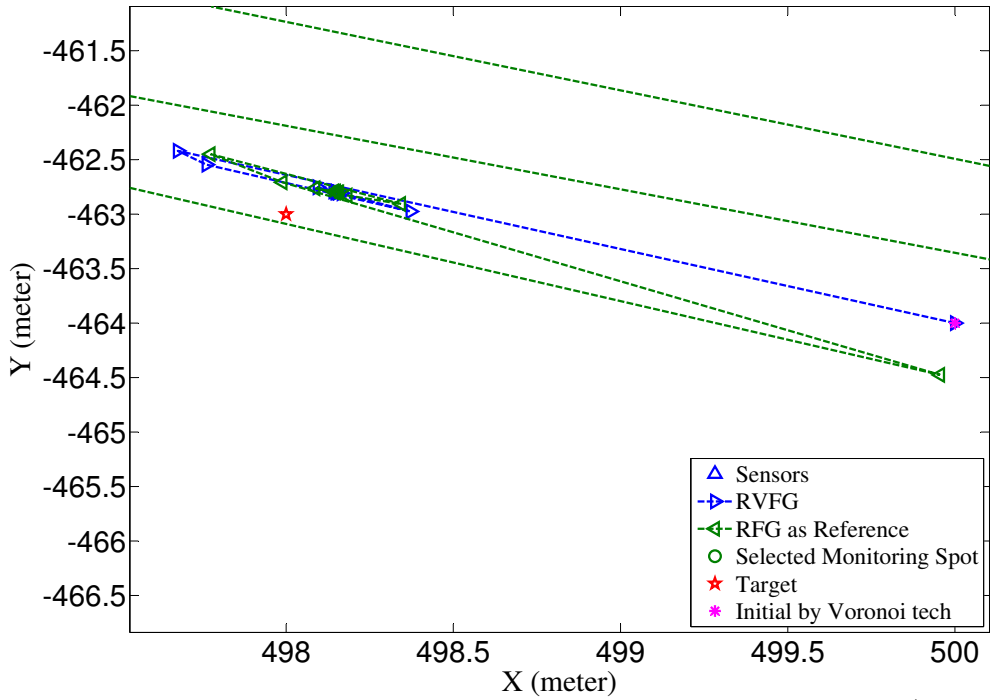

Figure 5.6. Zoom of the trajectory of the RSS-V-FG technique with 23 sensors (in this figure only shown 3 sensors used by factor graph-based for simplicity in analysis) and target at $(498, -463)$m.

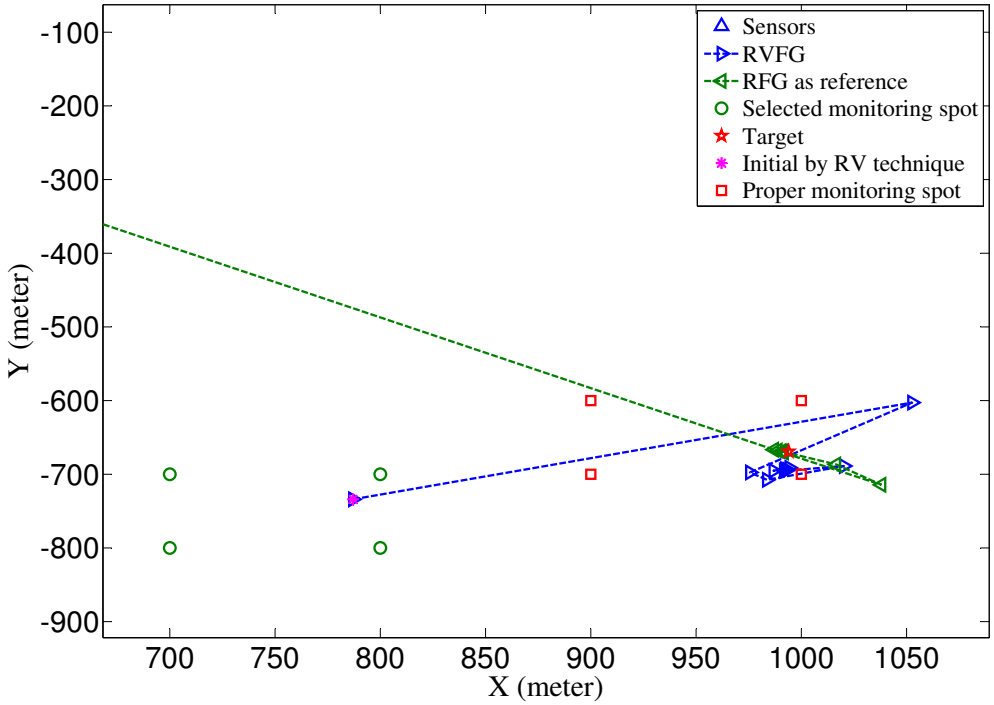

Figure 5.7. Zoom of the trajectory of the RSS-V-FG technique with 3 sensors (the sensors are now shown because of the zoom of the figure) and target at $(994, -669)$m.

accuracy with 23 sensors is better than that with three sensors because the larger the number of sensors the higher the accuracy of the initial value given by the RSS-V for selecting the appropriate four monitoring spots for the factor graph technique. It can be seen that when the iteration converges, the RMSE curve of the RSS-V-FG is asymptotically equal to the idealistic RSS-FG. This means that the RSS-V-FG having the initial point given by the RSS-V with 23 sensors in most cases correctly select the four appropriate monitoring spots. Fig. 5.8 shows that the RSS-V-FG is faster to converge, requiring around 5 iterations, while the RSS-FG alone requires around 10 iterations to converge. This is because the factor graph algorithm with RSS-V-FG has initial value much closer to the target rather than the RSS-FG alone which is set at $(0, 0)$ m.

The proposed technique outperforms the conventional RSS-V for SNR more than 7 dB with 23 sensors. For example, the improvement in estimation accuracy with the proposed technique over the conventional RSS-V is approximately 7.5 m at the SNR of 15 dB. Obviously, the tendency of the RMSE curve decreases with the increased SNR values as shown in Fig. 5.9.

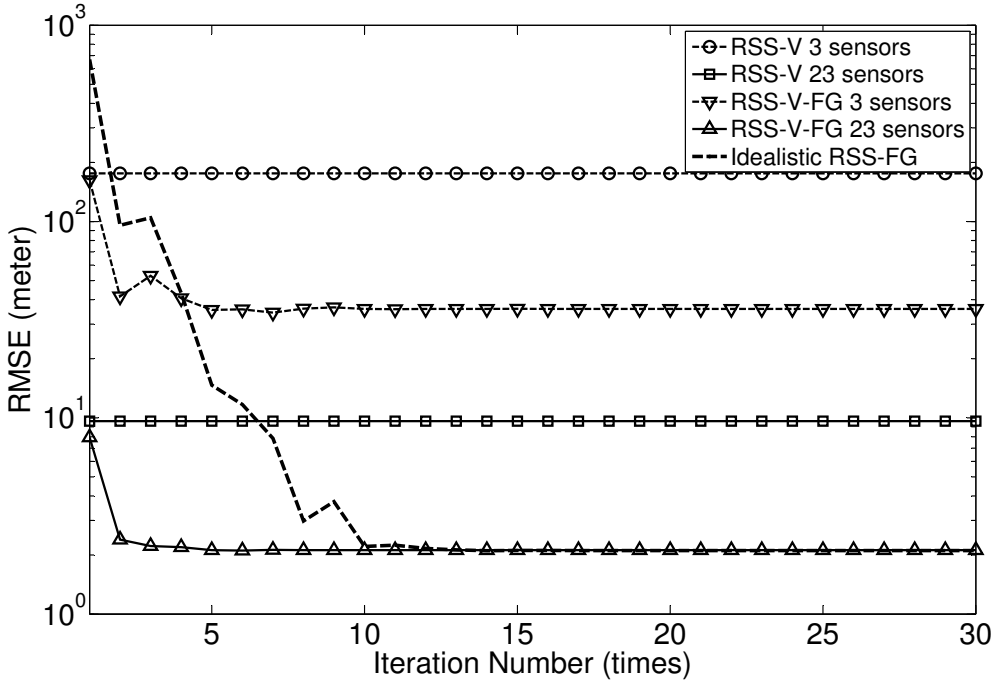

Figure 5.8. RMSE vs. iteration times with 3 sensors and 23 sensors over 100 trials, and SNR of 15 dB.

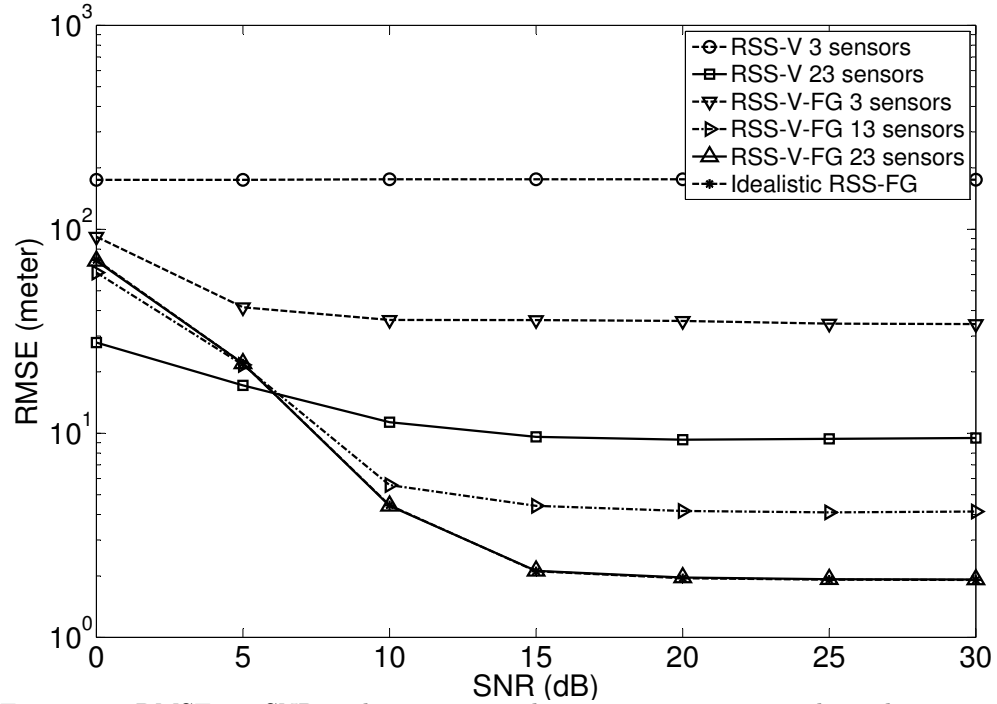

Figure 5.9. RMSE vs. SNR with 3 sensors and 23 sensors over 100 trials, and 30 times of iteration.

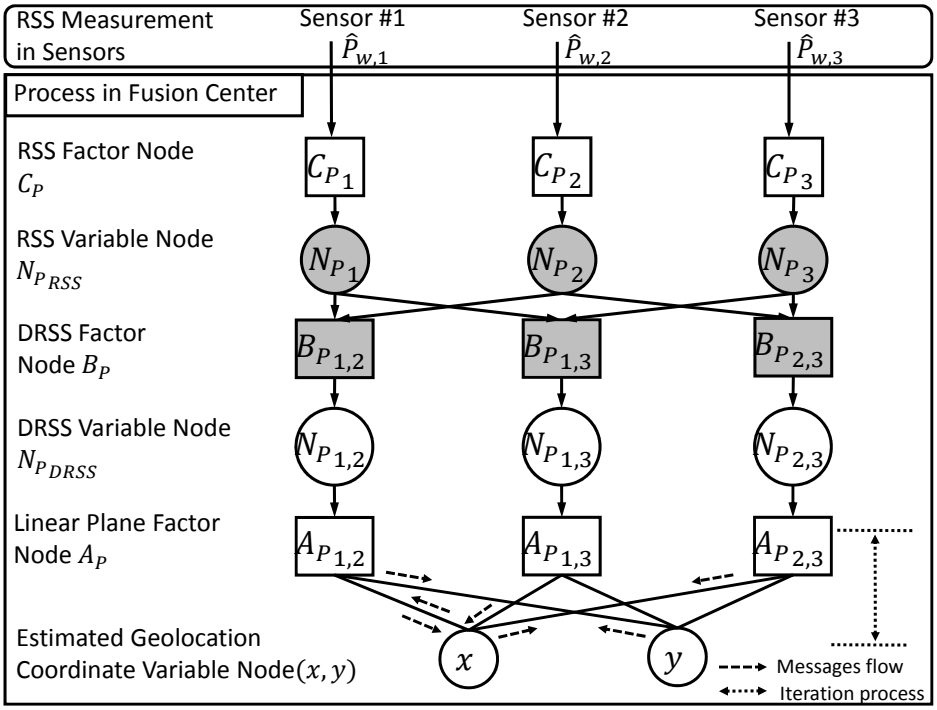

Figure 5.10. The proposed DRSS-FG for geolocation technique with $N = 3$ sensors and $\hat{P}_{w,t}$ being the input in units of watt. The new proposed nodes are marked by darkgray. The message flow arrows are shown in part to avoid over crowded of the figure.

5.2 DRSS-Based Factor Graph Technique

5.2.1 System Model

It is provided in this chapter, a new factor graph geolocation technique that utilizes DRSS information used as the input to the corresponding factor graph as shown in Fig. 5.10. The factor graph is composed of factor nodes denoted by square and variable nodes denoted by circle as shown in Fig. 5.10. The factor node contains formula to process the messages coming from several variable nodes, then forwards the output messages to the destination variable node. During the iteration process, each connected factor node into one variable nodes is the destination nodes. When one of connected factor nodes to variable node served as destination node, all other connected factor nodes are the incoming nodes. The variable node performs sum-product algorithm to all the incoming messages, then it forwards the output messages to the destination node. Finally in convergence process, all connected factor nodes to one variable node are the incoming

nodes, where there is no connected factor node assigned as destination node [17, 37].

The factor graph algorithm is performed in fusion center. The samples of RSS of unknown target and monitoring spots measured by each sensor are sent to the fusion center. The first process in the factor graph algorithm performed by the fusion center is to perform subtraction function to the RSS samples between two sensors to obtain the DRSS samples.

Due to the Gaussianity assumption, we can use the mean and variance as the messages in the factor graph processing, hence the computational complexity is very light. Before using the algorithm, it is assumed that sufficient amount of RSS samples of the training signal sent from monitoring spots are averaged by the fusion center to obtain both of the DRSS and RSS samples of the monitoring spots which are free from noise.

It is assumed that long enough averaging of the RSS samples sent by unknown radio emitter is sufficient to eliminate the instantaneous and shadowing fading. Hence, the RSS sample is modelled as path-loss exponent as (2.26). Figs. 5.11(a)–5.11(c) show the RSS of path-loss exponent model with f_c is 1 GHz, d_0 is 100 m, n is 3 for urban area, and sensor positions at $(100, 0), (1100, 0), (600, -1000)$ m.

The configuration of sensor, target, and monitoring spot locations are as follow, $\mathbf{X} = (X_i, Y_i)^T$ is sensor position, $\mathbf{x_T} = (x_T, y_T)^T$ is the unknown radio emitter (target) position, and $\mathbf{x_M} = (x_{M_j}, y_{M_j})^T$ is the coordinate of monitoring spot, where $j = 1, 2, ..., M$ is the monitoring spot number [18]. It is assumed that the four monitoring spots are always appropriate used in the simulation where the target is in the middle of monitoring spots. In this section, the selected four monitoring spots are the appropriate one without any help from other algorithm, even though our works in selecting the monitoring spots has been done in [51].

5.2.2 Proposed Technique

The proposed technique modifies the RSS-FG in [18] to solve the problem of conventional RSS-FG for estimating the location of unknown radio emitter position. The modification is simply by performing subtraction of the RSS samples between two sensors to obtain the DRSS samples as shown in Fig. 5.10. The subtraction of RSS sample is performed in *DRSS factor node* B_P. Hence, the other process after obtaining the DRSS samples follow the RSS-FG algorithm in [18]. In this section, the RSS-FG in [18] is summarized as the DRSS-FG, where the details of the RSS-FG refer to [18]. The analysis of the DRSS profile, which eliminates the

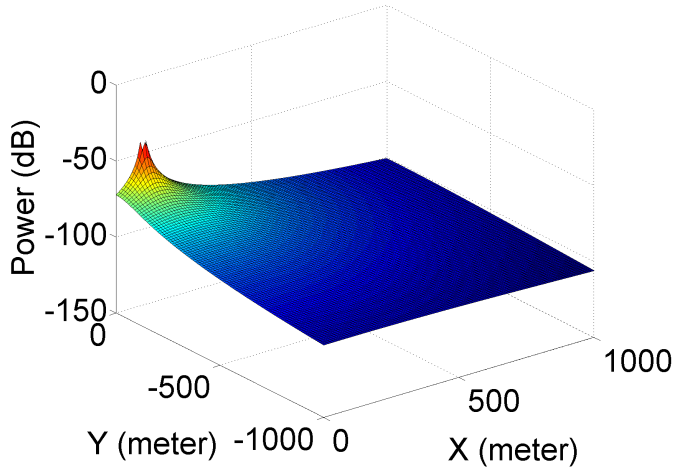

(a) at Sensor 1.

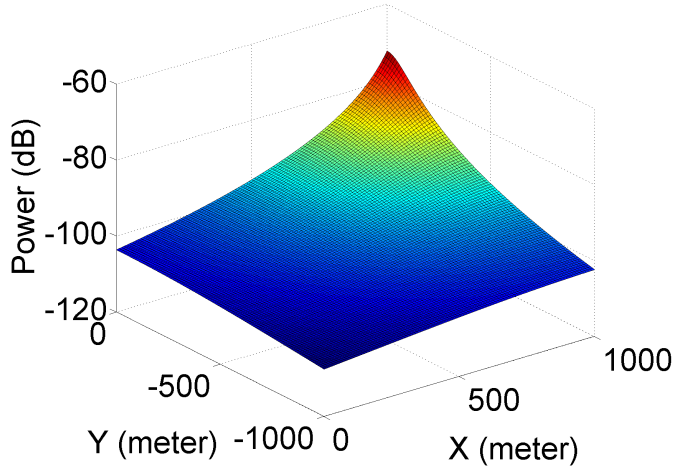

(b) at Sensor 2.

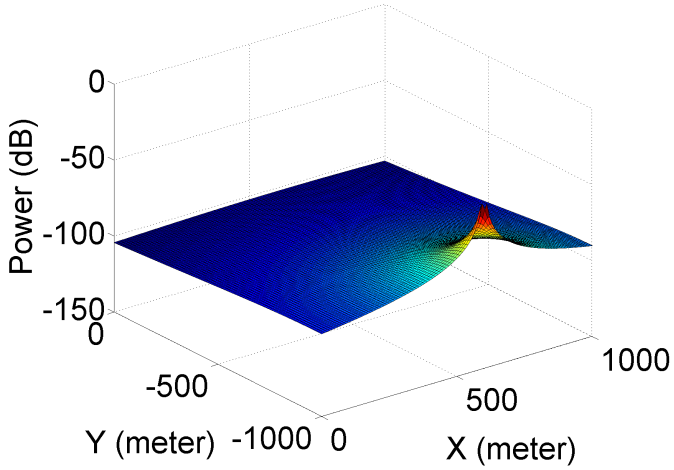

(c) at Sensor 3.

Figure 5.11. RSS profile from path-loss exponent model in each sensor.

necessity of knowledge of transmit power, is presented in this section.

The first process in the DRSS-FG is to receive the RSS samples, in units of watt, in *RSS measurement factor node* C_P. After that, the node C_P converts RSS samples $\hat{P}_{w,i}$ in units of watt to $\hat{P}_i$ dB. It should be notice that the distribution of RSS samples, $\hat{P}_i$, in units of dB, shows the similarity to Gaussian distribution. Hence, the proposed DRSS-FG and conventional RSS-FG still preserve the Gaussianity assumption as shown in [18]. The RSS samples, $\hat{P}_i$, in units of dB, are forwarded to the *Averaged RSS variable node* $N_{P_{RSS}}$. The node $N_{P_{RSS}}$ directly forwards $\hat{P}_i$ the node B_P. The RSS samples in units of dB from two sensors are subtracted in the node B_P resulting DRSS samples, $\hat{P}_{i,j}$, in units of dB, by performing the operation of (5.1), where $j, j = 2, 3, ..., N$, is the secondary sensor index. We obtain the DRSS samples dexpressed as

$$\hat{P}_{i,j} = \hat{P}_i - \hat{P}_j. \tag{5.1}$$

As shown in Fig. 5.10, there are three DRSS variables, i.e., $\hat{P}_{1,2}, \hat{P}_{1,3}$, and $\hat{P}_{2,3}$. It should be noticed that $\hat{P}_{2,3}$ is a linear combination of $\hat{P}_{1,2}$ and $\hat{P}_{1,3}$, however, $\hat{P}_{2,3}$ is not redundant. This is because $\hat{P}_{2,3}$ has different DRSS profile as shown in Fig. 5.13(b)–5.14(b). Hence, $\hat{P}_{2,3}$ is useful for detection position of the unknown target. After a set of the DRSS samples are obtained, the node B_P calculates the mean and variance messages, in units of dB, and then forward the messages to the *DRSS variable node* $N_{P_{DRSS}}$. After that, node $N_{P_{DRSS}}$ directly forward the messages to the *linear plane LS factor node* A_P. The iteration process starts from the node A_P.

Before the node A_P is used for the iterations, the function at the node A_P has to be set. The proposed DRSS-FG technique uses the error-free DRSS of four monitoring spots to obtain the variable coefficient of the linear plane equation at the node A_P, expressed as [18]

$$a_{x_{i,j}} \cdot x_m + a_{y_{i,j}} \cdot y_m + a_{P_{i,j}} \cdot P_{m,i,j} = c_{m,i,j}, \tag{5.2}$$

where $a_{x_{i,j}}$, $a_{y_{i,j}}$ denote the coefficient of coordinate variable x, y, respectively, x_m and y_m denote the position coordinate of monitoring spots, where $m = 1, 2, ..., M$ is the monitoring spot index. $P_{m,i,j}$ denotes the error-free DRSS of the signal sent from monitoring spot in units of dB. The error free of the DRSS is obtained by performing averaging over large enough of the amount of DRSS samples. The large amount of the samples are collected from the DRSS measurement over long enough in time duration. $a_{P_{i,j}}$ indicates the coefficient of variable $P_{m,i,j}$. $c_{mi,j}$ indicates

a constant with the value being always the unity. It is assumed that the four monitoring spots are always used in the simulations so that the target is in the middle of monitoring spots. In this paper, the selected four monitoring spots are the most suitable without any help from other algorithm, even though our recent work for selecting the monitoring spot surrounding the target [51] can be used for this purpose.

Due to the values of x_m, y_m, and $P_{m,i,j}$ are known, hence we can utilize the least square (LS) algorithm to obtain the coefficients of linear equations at the node A_P. The detailed explanation of the use of LS for obtaining the coefficients of the variables $a_{x_{i,j}}, a_{y_{i,j}}$, and $a_{P_{i,j}}$, can be found in [18]. Finally, the coefficients complete the final linear equations as

$$a_{x_{i,j}} \cdot x + a_{y_{i,j}} \cdot y + a_{P_{i,j}} \cdot P_{i,j} = c_{i,j}, \tag{5.3}$$

where x and y denotes the unknown target position, $P_{i,j}$ is the DRSS of unknown target in unit of dB, and $c_{i,j}$ is the constant with value being unity. The detail derivation formula of (5.3) in terms of mean and variance can be found in [18].

In this paper, we summarize the equations/operations used in this algorithm in Table. 5.3, with the most left column being the message flow between the nodes, h being general sensor index, m being the mean, and σ^2 being the variance. For example, m_x and m_y indicates the mean values from the nodes x and y, and $m_{\hat{P}}$ indicates the mean of the samples from measurement. It is also shown in Table. 5.3 that the proposed technique requires simple operations. Furthermore, the computational complexity of the proposed technique is linearly proportional to N similar as mentioned in [18]. The output of the last two rows in Table. 5.3 are the sum-product algorithm used to combine the messages coming to the nodes x and y. Finally, the final position estimate of the unknown target emitter is taken from the mean value, m_Λ.

We compare both the RSS the DRSS profiles at 3 sensors calculated (2.26) with transmit power gap between the target and monitoring spots, ΔP_T, being 5 dB. Both the approximated DRSS and RSS profiles are calculated by using (5.3). The simulation setup is detailed later in the Section III. As shown in Figs. 5.12(a) – 5.14(b), there are gaps between the RSS profile of path-loss mode and the approximated linear plane of RSS profile at all sensors, because there is the gap of transmit power between the unknown target and the monitoring spots. Hence, the conventional RSS-FG fails in estimating the position of unknown radio emitter. On the contrary, the path-loss plane has intersection with the approximated DRSS profile around the unknown target, because the necessity of the

Table 5.3. The Operations Required for Each Node in The Proposed DRSS-FG.

Message Flow (Nodes)	Samples ($\hat{}$) and/or (Means, Variances)		
	Inputs	Outputs	Remarks
$C_{P_h} \rightarrow N_{P_h}$	$\hat{P}_{w,h}$, $h = \{i,j\}$	$\hat{P}_h,\ h = \{i,j\}$	Similar to [17,18]
$N_{P_h} \rightarrow B_{P_{i,j}}$	$\hat{P}_h$, $h = \{i,j\}$	$\hat{P}_h,\ h = \{i,j\}$	New proposed
$B_{P_{i,j}} \rightarrow N_{P_{i,j}}$	$\hat{P}_i$ and $\hat{P}_j$	$\hat{P}_{i,j} = \hat{P}_i - \hat{P}_j$ $\left(m_{\hat{P}_{i,j}}, \sigma^2_{\hat{P}_{i,j}}\right)$	New proposed
$N_{P_{i,j}} \rightarrow A_{P_{i,j}}$	$\left(m_{\hat{P}_{i,j}}, \sigma^2_{\hat{P}_{i,j}}\right)$	$\left(m_{\hat{P}_{i,j}}, \sigma^2_{\hat{P}_{i,j}}\right)$	Similar to [17,18]
$A_{P_{i,j}} \rightarrow x$	$\left(m_{\hat{P}_{i,j}}, \sigma^2_{\hat{P}_{i,j}}\right)$ $\left(m_{y_{i,j}}, \sigma^2_{y_{i,j}}\right)$	$\left(\frac{c_{i,j} - a_{y_{i,j}} m_{y_{i,j}} - a_{P_{i,j}} m_{\hat{P}_{i,j}}}{a_{x_{i,j}}}, \frac{a^2_{y_{i,j}} \sigma^2_{y_{i,j}} + a^2_{P_{i,j}} \sigma^2_{\hat{P}_{i,j}}}{a^2_{x_{i,j}}}\right)$	Similar to [18]; Iteration process is only performed between nodes $A_{P_{i,j}}$ and x, y. Initial values are set for $m_{x_{i,j}}$, $m_{y_{i,j}}$, $\sigma^2_{x_{i,j}}$, $\sigma^2_{y_{i,j}}$
$A_{P_{i,j}} \rightarrow y$	$\left(m_{\hat{P}_{i,j}}, \sigma^2_{\hat{P}_{i,j}}\right)$ $\left(m_{x_{i,j}}, \sigma^2_{x_{i,j}}\right)$	$\left(\frac{c_{i,j} - a_{x_{i,j}} m_{x_{i,j}} - a_{P_{i,j}} m_{\hat{P}_{i,j}}}{a_{y_{i,j}}}, \frac{a^2_{x_{i,j}} \sigma^2_{x_{i,j}} + a^2_{P_{i,j}} \sigma^2_{\hat{P}_{i,j}}}{a^2_{y_{i,j}}}\right)$	
$x \rightarrow A_{P_{i,j}}$ $y \rightarrow A_{P_{i,j}}$	$\left(m_k, \sigma^2_k\right)$ $k \neq l$	$\left(\sigma^2_k \sum_{l \neq k} \frac{m_l}{\sigma^2_l}, \sigma^2_k = \frac{1}{\sum_{l \neq k} \frac{1}{\sigma^2_l}}\right)$	Similar to [17,18]; Iteration process; For simplicity, let replace $(\cdot)_{i,j}$ to $(\cdot)_k$
x and y	$\left(m_k, \sigma^2_k\right)$	$\left(\sigma^2_\Lambda \sum_k \frac{m_k}{\sigma^2_k}, \sigma^2_\Lambda = \frac{1}{\sum_k \frac{1}{\sigma^2_k}}\right)$	

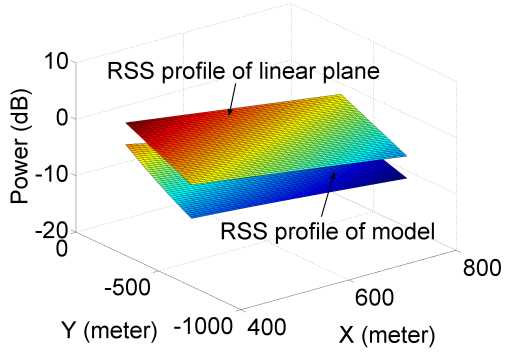

(a) RSS profile at sensor 1.

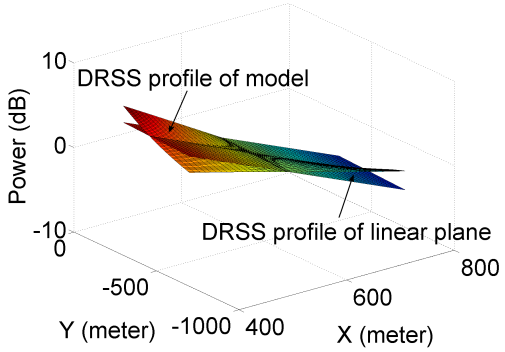

(b) DRSS profile at sensor 1.

Figure 5.12. RSS and DRSS profiles of linear plane and model in each sensor with the power transmit gap between the unknown target and monitoring spots are 5 dB. The sensor positions are at $(100, 0), (1100, 0), (600, -10000)$ m.

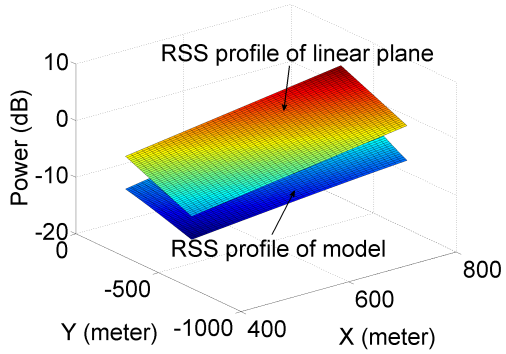

(a) RSS profile at sensor 2.

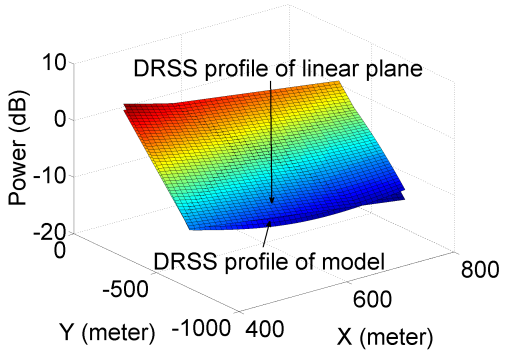

(b) DRSS profile at sensor 2.

Figure 5.13. RSS and DRSS profiles of linear plane and model in each sensor with the power transmit gap between the unknown target and monitoring spots are 5 dB. The sensor positions are at $(100, 0), (1100, 0), (600, -10000)$ m.

knowledge of transmit power is eliminated by the subtraction in the node B_P. Hence, the DRSS-FG successfully estimates the position of unknown target radio emitter.

5.2.3 Computational Complexity

The proposed DRSS-FG [43] follows [18] which allows us to use the linear approximation. The DRSS-FG only adds one additional subtraction function, which is a simple arithmetic operation, to the conventional RSS-FG. Hence, as stated in Chapter 2, that the computational complexity of the conventional RSS-FG is proportional to N. Hence, the computational complexity of the proposed DRSS-FG technique is also proportional to N. It means that the DRSS-FG has low computational complexity. As

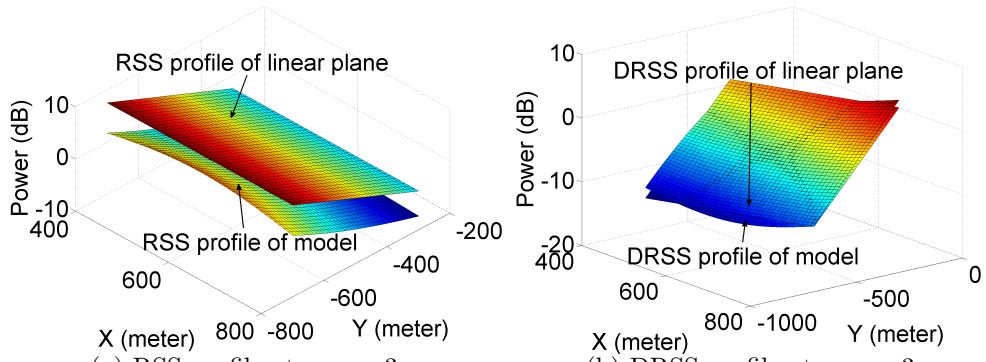

(a) RSS profile at sensor 3. (b) DRSS profile at sensor 3.

Figure 5.14. RSS and DRSS profiles of linear plane and model in each sensor with the power transmit gap between the unknown target and monitoring spots are 5 dB. The sensor positions are at $(100, 0), (1100, 0), (600, -10000)$ m.

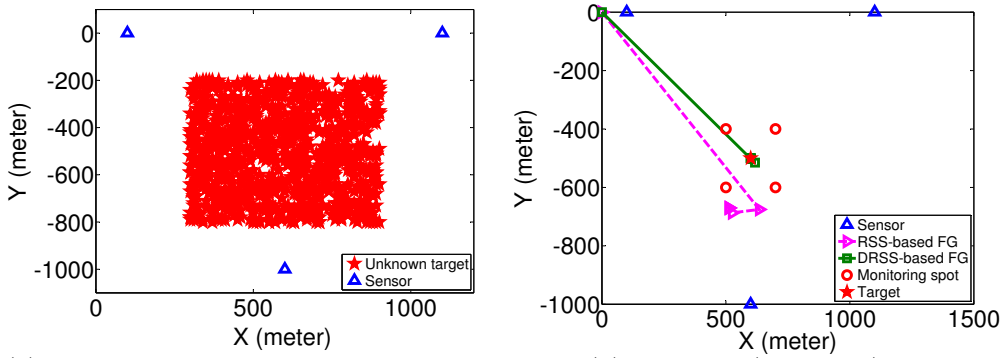

(a) $1,000$ of $10,000$ targets and 3 sensors. (b) Target at $(650, -500)$ m.

Figure 5.15. Accuracy of the unknown target detection for many locations confirmed by the trajectory analyses.

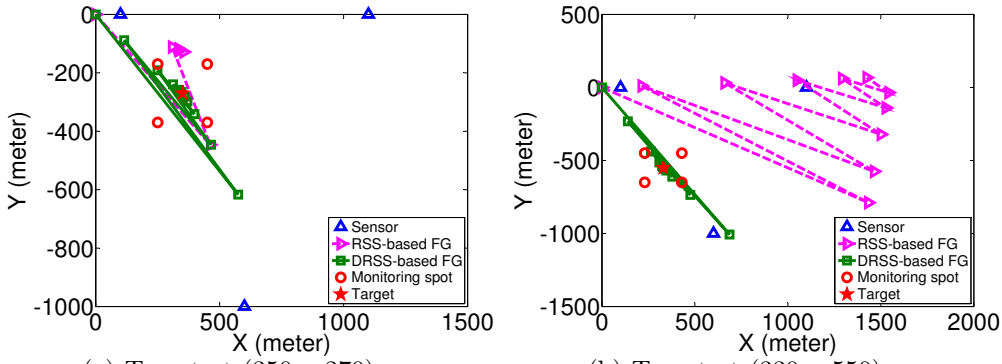

(a) Target at $(350, -270)$ m. (b) Target at $(330, -550)$ m.

Figure 5.16. Accuracy of the unknown target detection for many locations confirmed by the trajectory analyses.

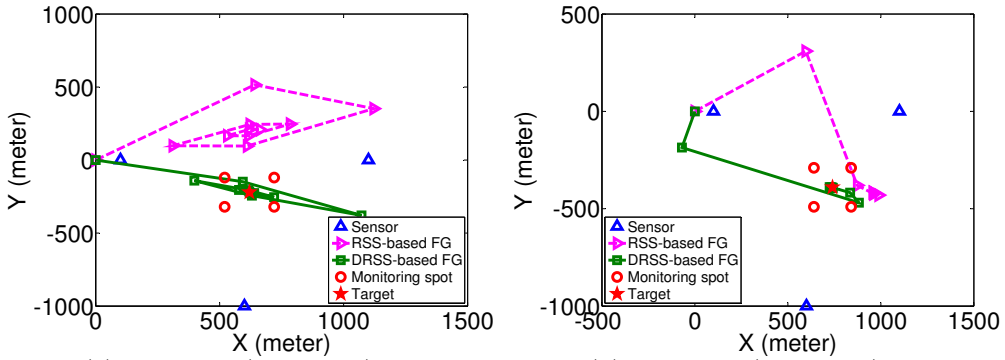

(a) Target at $(620, -220)$ m. (b) Target at $(740, -390)$ m.

Figure 5.17. Accuracy of the unknown target detection for many locations confirmed by the trajectory analyses.

described in Chapter 3, the computational complexity of sum-product algorithm is proportional to N^2 during iteration process. However, It is still lower than computational complexity of Gauss-Newton algorithm which is proportional to N^3.

5.2.4 Numerical Results

To verify the performance of the proposed technique, we conducted a series of computer simulations. One target is randomly chosen from area width of 600×600 m^2 in each $10,000$ target positions performed in the computer simulations. 100 samples of RSS and DRSS are processed in 30 times of iteration for each trial. The sensors position are at $(100, 0), (1100, 0), (600, -1000)$ m in (X, Y) coordinate, where the sensors area width is $1,000 \times 1,000$ m^2 as shown in Fig. 5.15(a). The root-mean-square error (RMSE) performance is evaluated by the signal-to-noise power ratio (SNR) from 0 to 45 dB. The gap of transmit power between the unknown target radio emitter and the monitoring spots is 5 dB. For simplicity, the RSS and DRSS measurements are assumed to be corrupted by the measurement error having the same variance in each sensor. The path-loss exponent model in (2.26) is used to create the RSS profile, where the set-up of the exponent path-loss variables are set in Section II. The monitoring spots area set in this simulation is 200×200 m^2 according to [53].

Figs. 5.15(b) – 5.16(b) show how the proposed DRSS-FG is very accurate in detection, even though the location of the unknown target is changed many times. The accuracy is confirmed via the trajectory analy-

sis shown in the figures. The initial point can be set from arbitrary value, however we set the initial value of nodes x and y at $(0, 0)$ m. It is shown in Figs. 5.15(b) – 5.16(b) that the conventional RSS-FG fails to reach the unknown target radio emitter. This is because as we discuss in Section III that the RSS profile of exponent path-loss model has a gap $\Delta P_T = 5$ dB to the approximated RSS profile created by linear plane of (5.3). On the other hand, the trajectories of the DRSS-FG shows that the proposed technique successfully reach the unknown target.

The Figs. 5.18 and 5.19 show that the proposed technique for any ΔP_T values is not only able to detect the location of unknown target radio emitter, but it also provides very accurate detection after it converges around 50 iterations with RMSE of around 4.5 and 3.7 m, at SNR of 10 dB and above, respectively. It is also shown that the high accuracies with RMSE of around 5 and 4 m even have been achieved in 30 and 40 iterations, respectively, at SNR of 15 dB. Hence, the proposed DRSS-FG technique achieves high and stable accuracy for any transmit power gap values between the target and monitoring spots, but it requires more iteration. The proposed technique does not taken into account the difference of transmit power between the unknown target and the monitoring spots because the subtraction of RSS samples to obtain DRSS samples in the node B_P eliminates the necessity of transmit power.

On the other hand, Figs. 5.18 and 5.19 show that when the target and monitoring spots have equal transmit power, the accuracy of conventional RSS-FG technique, with RMSE of 1.9 and 1.6 m, at SNR of 15 dB and above, respectively, outperforms the proposed DRSS-FG technique. This is because the linear plane approximation of RSS parameter has better shape than the DRSS parameter as shown in Figs. 5.12(a) – 5.14(b). However, when there are transmit power gaps, $1, 3$, and 5 dB, the accuracy of the conventional RSS-FG technique drop significantly to $57, 171$, and 286 m, respectively, at SNR of 15 dB. Opposite to the DRSS-FG curve, the RSS-FG curve shows the best accuracy in SNR of 0 dB because the gap 5 dB of transmit power is very big. Hence, the high noise power in 0 dB helps the RSS-FG for better accuracy than other SNR values even tough the overall accuracy is still low.

5.3 Summary

A new wireless geolocation technique using joint RSS-based Voronoi and factor graph (RSS-V-FG) has been proposed. The RSS-V geolocation is used to select the area of monitoring spots for RSS-FG geolocation algo-

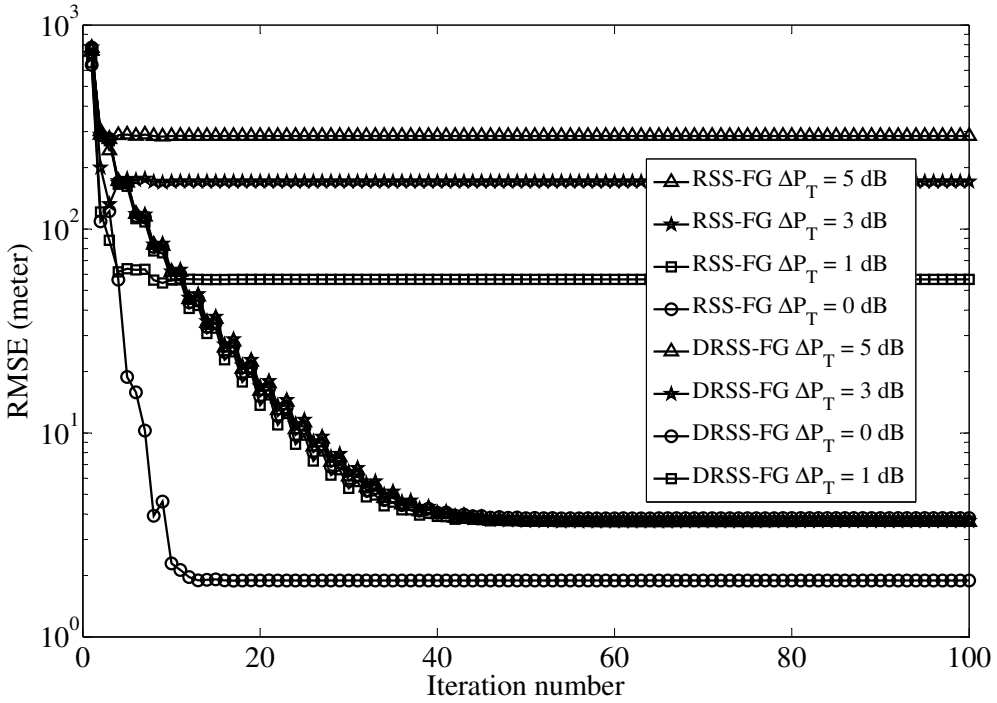

Figure 5.18. RMSE vs. iteration number with 10,000 target positions, SNR of 15 dB, and 100 samples.

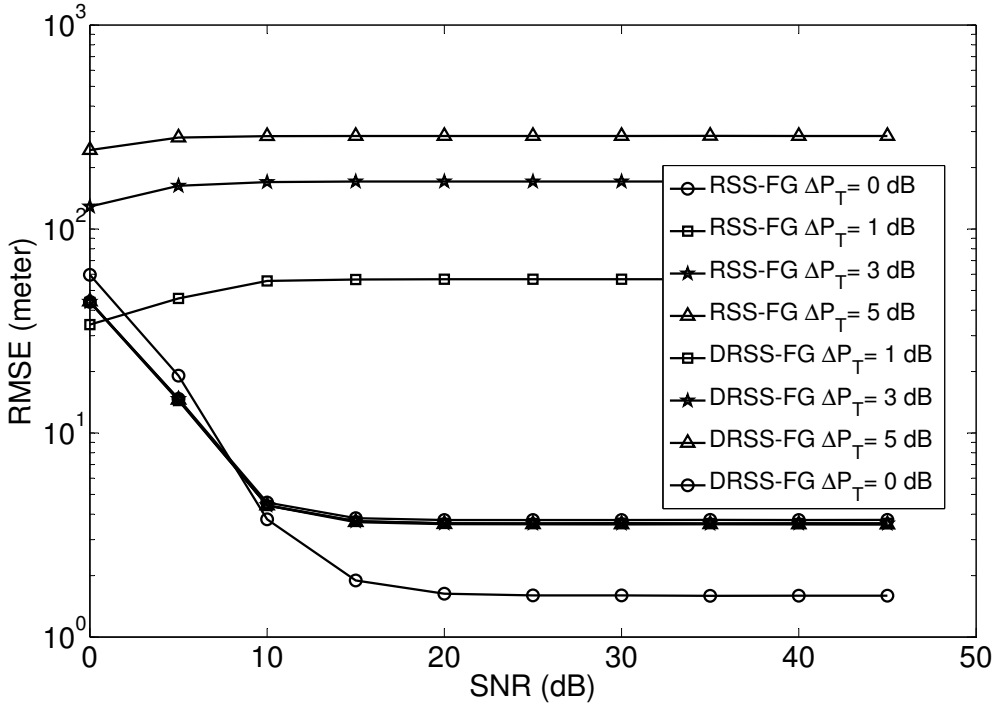

Figure 5.19. RMSE vs. SNR with 10,000 target positions, 100 samples, and 30 iterations.

rithm, as well as to provide its inital value. The simulation results confirmed that our proposed technique provides higher accuracy compared to the conventional RSS-V technique. This technique is suitable for outdoor environment in the future location based applications. The RSS-based factor graph geolocation technique is successfully evaluated in outdoor environment. The smaller area of monitoring spot around the target, the higher accuracy is obtained. Reducing the complexity due to the RSS-V technique by using pre-computing processing is left as a future study.

The new technique of DRSS-based factor graph (DRSS-FG) geolocation algorithm has been presented in this paper. It is shown in this paper that when the transmit power of target and monitoring spots are unequal, the proposed technique successfully estimates the unknown radio emitter with high accuracy around RMSE of 3.7 m, while the conventional RSS-FG fails to detect the location of the unknown target. The transmit power information of the unknown target is no longer required because it can be replaced by performing subtraction of one sensor's RSS samples from another sensor's RSS samples. This technique provides high accuracy and low computational complexity detection, which is suitable for future geolocation technique.

Chapter 6

Conclusions and Future Work

6.1 Conclusions

In Chapter 3, a new factor graph-based geolocation technique using DOA information for a single static unknown (anonymous) radio emitter with accuracy improvement of the position estimate has been proposed. A set of new approximated expression for the mean and variance of the tangent and cotangent functions has been derived based on the first-order TS to hold the Gaussianity assumption. The simulation results confirmed that the proposed technique provides: (a) better accurate position estimate with number of samples and sensors, and standard deviation of measurement error, as parameters, (b) fast convergence, and (c) keep low computational complexity, which are suitable for the future geolocation techniques requiring high accuracy and low complexity in imperfect synchronization condition.

In Chapter 4, a new factor graph-based geolocation technique using the TDOA measurement to detect the position of an unknown (anonymous) radio wave emitter has been in this paper. The uniqueness of the proposed technique compared to the conventional Hyperbolic TDOA-based technique is the use of the simple Pythagorean function instead of the Hyperbolic functions. Several sets of new nodes have been introduced on the conventional TOA-based factor graph technique. Furthermore, the modification has been made on the node functions, so that it works with Pythagorean function where the input of the factor graph is TDOA measurement. Constraints are also introduced in this paper: (1) to allow the iteration to started at arbitrary point in the target area, and (2) to preserve the numerical stability of the algorithm. It is confirmed by the computer simulation results that our proposed technique provides high

accuracy with better position estimate, even though it does not require high computational complexity.

In Chapter 5, a new wireless geolocation technique using joint RSS-based Voronoi and factor graph (RSS-V-FG) has been proposed. The RSS-V geolocation is used to select the area of monitoring spots for RSS-FG geolocation algorithm, as well as to provide its inital value. The simulation results confirmed that our proposed technique provides higher accuracy compared to the conventional RSS-V technique. This technique is suitable for outdoor environment in the future location based applications. The RSS-based factor graph geolocation technique is successfully evaluated in outdoor environment. The smaller area of monitoring spot around the target, the higher accuracy is obtained. Reducing the complexity due to the RSS-V technique by using pre-computing processing is left as a future study.

A new technique of factor graph-based geolocation algorithm utilizing the DRSS (DRSS-FG) has been presented in this chapter. It is shown in this chapter that the proposed technique successfully estimates the unknown radio emitter with high accuracy, while the conventional RSS-FG fails to detect the location of the unknown target. The DRSS-FG is developed by modifying the conventional RSS-FG with simply subtraction of RSS samples between two sensor to obtain the DRSS samples for the factor graph. The transmit power information of the unknown target is no longer required because it can be replaced by performing subtraction of one sensor's RSS samples from another sensor's RSS samples. All the proposed techniques provide high accuracy and low computational complexity detection, which is suitable for future geolocation technique. Fig. 6.1 shows the flow chart of the use of the proposed measured parameter-based factor graph geolocation technique for position detection of unknown target emitter.

6.2 Future Work

The development action points listed below are left for future work.

1. The development of location detection of *multiple moving* unknown radio emitter takes into account the Doppler effect and frequency difference of arrival (FDOA). Hence, the technique can perform tracking of the moving target. In multiple target, we have to distinguish more than one signal measured by the sensors.

2. The development of joint RSS-V and DRSS-FG technique, as well as

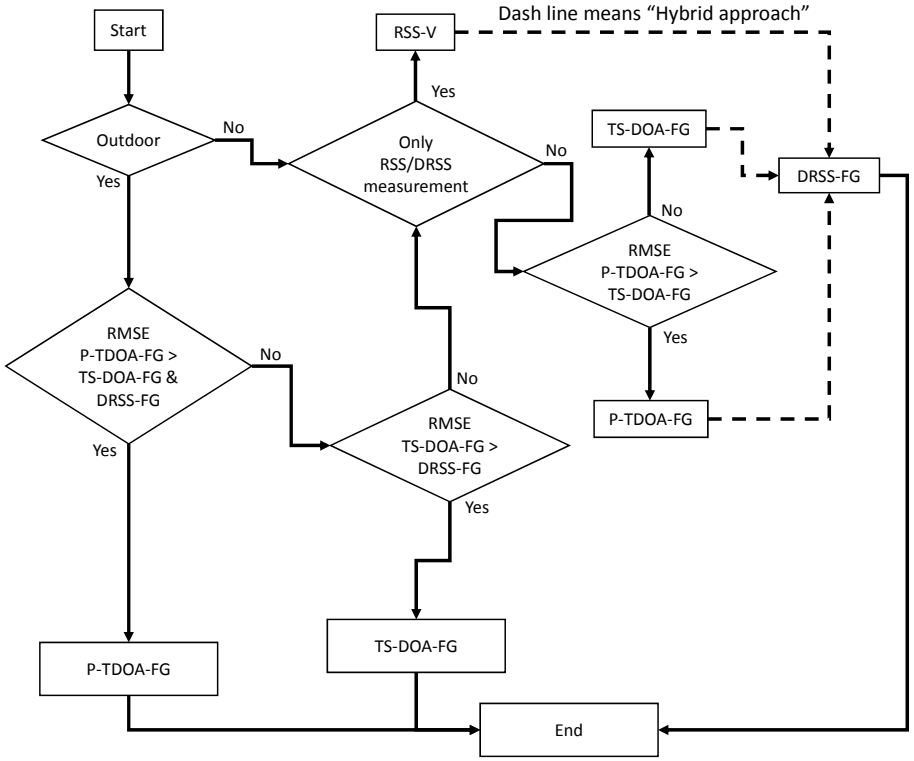

Figure 6.1. Flow chart of the use of the proposed measured parameter-based geolocation technique.

joint P-TDOA-FG and DRSS-FG technique are important for selecting the appropriate monitoring spots for the DRSS-FG technique. It is also required to increase the accuracy of the detection where the RSS-V and the P-TDOA-FG provide rough position estimate.

3. Derivation of CRLB for TDOA-, RSS-, and DRSS-based technique is required for theoretical limit or the bound of the accuracy of geolocation technique.

4. Fully mathematical analysis of the convergence property of the factor graph techniques is required to ensure that the proposed techniques always converge.

5. The evaluation of the accuracy of the proposed techniques are verified by utilizing the field measurement data.

Appendix A

CRLB Derivations for DOA-based Geolocation

The sensor index i is omitted in this derivation for simplicity. By taking the expectation of (2.36), we have

$$E\left[\frac{\partial^2}{\partial\theta^2}\ln p(\hat{\theta})\right] = -\frac{K}{\sigma_\theta^2}. \tag{A.1}$$

Since

$$E\left[\left(\frac{\partial}{\partial\theta}\ln p(\hat{\theta})\right)^2\right] = -E\left[\frac{\partial^2}{\partial\theta^2}\ln p(\hat{\theta})\right], \tag{A.2}$$

as shown in [64]

$$E\left[\left(\frac{\partial}{\partial\theta}\ln p(\hat{\theta})\right)^2\right] = \frac{K}{\sigma_\theta^2}. \tag{A.3}$$

The FIM [10, 64, 65]

$$\mathbf{F}(\mathbf{x}) = \frac{\partial\theta}{\partial\mathbf{x}}^T E\left[\left(\frac{\partial}{\partial\theta}\ln p(\hat{\theta})\right)^T\left(\frac{\partial}{\partial\theta}\ln p(\hat{\theta})\right)\right]\frac{\partial\theta}{\partial\mathbf{x}} \tag{A.4}$$

is found to

$$\mathbf{F}(\mathbf{x}) = \frac{\partial\theta}{\partial\mathbf{x}}^T E\left[\left(\frac{\partial}{\partial\theta}\ln p(\hat{\theta})\right)^2\right]\frac{\partial\theta}{\partial\mathbf{x}}. \tag{A.5}$$

Substituting (A.3) into (A.5) yields

$$\mathbf{F}(\mathbf{x}) = \frac{\partial\theta}{\partial\mathbf{x}}^T\left[\frac{K}{\sigma_\theta^2}\right]\frac{\partial\theta}{\partial\mathbf{x}}. \tag{A.6}$$

Now, we replace θ by a vector $\theta = (\theta_1, \ldots, \theta_N)$. Then, the variance (σ_θ^2) is replaced by the Gaussian covariance matrix Σ_θ, as

$$\mathbf{F}(\mathbf{x}) = K\mathbf{J}^T\Sigma_\theta^{-1}\mathbf{J}. \tag{A.7}$$

Finally, by substituting (A.7) into the CRLB expression (2.37), as in [6,64], and [4], we obtain the CRLB for DOA-based geolocation that takes into account the measured sample number K, as expressed below

$$\text{CRLB}_{\text{DOA}} = \sqrt{\text{trace}\left(\left(\mathbf{J}^T\Sigma_\theta^{-1}\mathbf{J}\right)K\right)^{-1}}.$$

Bibliography

[1] Q. Bi, G. L. Zysman, and H. Menkes, "Wireless mobile communications at the start of the 21st century," *IEEE Communications Magazine*, vol. 39, pp. 110–116, Jan 2001.

[2] K. Pahlavan and P. Krishnamurthy, *Principles of Wireless Networks A Unified Approach*. Prentice Hall, 2002.

[3] J.-C. Chen, C.-S. Maa, and J.-T. Chen, "Mobile position location using factor graphs," *IEEE Commun. Lett.*, vol. 7, pp. 431–433, September 2003.

[4] B. Omidali and S. A.-A. B. Shirazi, "Performance improvement of AOA positioning using a two-step plan based on factor graphs and the gauss-newton method," in *14th International CSI Computer Conference (CSICC 2009)*, pp. 305–309, September 2009.

[5] H.-L. Jhi, J.-C. Chen, and C.-H. Lin, "A factor-graph-based TOA location estimator," *IEEE TWC*, vol. 11, pp. 1764–1773, May 2012.

[6] C. Mensing and S. Plass, "Positioning based on factor graphs," *EURASIP Journal on Advances in Signal Processing*, vol. 2007, pp. 1–11, April 2007.

[7] S. Cai, H. Pan, Z. Gao, N. Yao, and Z. Sun, "Research of localization algorithm based on weighted voronoi diagrams for wireless sensor network," *EURASIP Journal on Wireless Communications and Networking*, 2014.

[8] I. Progri, *Geolocation of RF Signals: Principles and Simulations*. Springer, 2011.

[9] R. Chellappa and S. Theodoridis, *Array and Statistical Signal Processing*. Academic Press Library in Signal Processing, 2014.

[10] C. Gentile, N. Alsindi, R. Raulefs, and C. Teolis, *Geolocation Techniques, Principles and Applications*. New York: Springer, 2013.

[11] F. Yin, C. Fritsche, F. Gustafsson, and A. M. Zoubir, "TOA-based robust wireless geolocation and Cramer-Rao lower bound analysis in harsh LOS/NLOS environments," *IEEE Transaction of Signal Processing*, vol. 61, pp. 2243–2255, May 2013.

[12] S. Hara, D. Anzai, T. Yabu, K. Lee, T. Derham, and R. Zemek, "A perturbation analysis on the performance of TOA and TDOA localization in mixed LOS/NLOS environments," *IEEE Transactions on Communications*, vol. 61, pp. 679–689, February 2013.

[13] G. Wang, Y. Li, and N. Ansari, "A semidefinite relaxation method for source localization using tdoa and fdoa measurements," *Vehicular Technology, IEEE Transactions on*, vol. 62, pp. 853–862, Feb 2013.

[14] J. James J. Caffery and G. L. Stuber, "Overview of radiolocation in CDMA cellular systems," *IEEE Communications Magazine*, vol. 36, pp. 38–45, April 1998.

[15] S. Tekinay, "Wireless geolocation systems and services," *IEEE Communications Magazine*, vol. 36, p. 28, April 1998.

[16] X. Li, K. Pahlavan, M. Latva-aho, and M. Ylianttila, "Comparison of indoor geolocation methods in DSSS and OFDM wireless LAN systems," in *Proc. IEEE-VTS Fall Vehicular Technology Conference (VTC) 2000*, vol. 6, pp. 3015–3020, 2000.

[17] J.-C. Chen, Y.-C. Wang, C.-S. Maa, and J.-T. Chen, "Network side mobile position location using factor graphs," *IEEE Trans. on Wireless Comm.*, vol. 5, pp. 2696–2704, October 2006.

[18] C.-T. Huang, C.-H. Wu, Y.-N. Lee, and J.-T. Chen, "A novel indoor RSS-based position location algorithm using factor graphs," *IEEE Trans. on Wireless Comm.*, vol. 8, pp. 3050–3058, June 2009.

[19] H. Liu, F. K. W. Chan, and H. C. So, "Non-line-of-sight mobile positioning using factor graphs," *IEEE Trans. on Vehicular Technology*, vol. 58, pp. 5279–5283, November 2009.

[20] B. T. Sieskul, F. Zheng, and T. Kaiser, "On the effect of shadow fading on wireless geolocation in mixed los/nlos environments," *IEEE Transaction of Signal Processing*, vol. 57, pp. 4196–4208, Nov. 2009.

[21] M. Kanaan and K. Pahlavan, "CN-TOAG: a new algorithm for indoor geolocation," in *Proc. 15th IEEE International Symposium on Personal, Indoor and Mobile Radio Communications (PIMRC)*, pp. 1906–1910, September 2004.

[22] E. Tzoreff, B. Z. Bobrovsky, and A. J. Weiss, "Single receiver emitter geolocation based on signal periodicity with oscillator instability," *IEEE Transaction of Signal Processing*, vol. 62, pp. 1377–1385, March 2014.

[23] J.-C. Chen, P. Ting, C.-S. Maa, and J.-T. Chen, "Wireless geolocation with TOA/AOA measurements using factor graph and sum-product algorithm," in *IEEE VTC 2004*, vol. 5, pp. 3526–3529, September 2004.

[24] C. Mensing and S. Plass, "TDOA positioning based on factor graphs," in *Proc. The 17th Annual IEEE International Symposium on Personal, Indoor and Mobile Radio Communications (PIMRC'06)*, 2006.

[25] T. Jia and R. M. Buehrer, "A new cramer-rao lower bound for TOA-based localization," in *Proc. IEEE Military Communications Conference (MILCOM 2008)*, pp. 1–5, Nov 2008.

[26] L. Sun, J. Li, Y. Chen, and H. Zhu, *Wireless Sensor Network*. Beijing: Tsinghua University Press, 2005.

[27] I. Akyildiz, W. Su, Y. Sankarasubramaniam, and E. Cayirci, "A survey on sensor networks," *Communications Magazine, IEEE*, vol. 40, pp. 102–114, Aug 2002.

[28] N. Patwari, J. Ash, S. Kyperountas, A. Hero, R. Moses, and N. Correal, "Locating the nodes: cooperative localization in wireless sensor networks," *Signal Processing Magazine, IEEE*, vol. 22, pp. 54–69, July 2005.

[29] S. Salari, S. Shahbazpanahi, and K. Ozdemir, "Mobility-aided wireless sensor network localization via semidefinite programming," *Wireless Communications, IEEE Transactions on*, vol. 12, pp. 5966–5978, December 2013.

[30] K. Ho, "Bias reduction for an explicit solution of source localization using tdoa," *Signal Processing, IEEE Transactions on*, vol. 60, pp. 2101–2114, May 2012.

[31] E. Ackerman, "Wireless power takes charge," *IEEE Spectrum*, vol. 53, pp. 13–14, Jan 2016.

[32] J. V. Stafford, *Precision Agriculture '05*. Wageningen Academic Publishers, 2005.

[33] E. Koden. Land Based Radio Monitoring System. [Online]. Available: https://www.koden-electronics.co.jp/en/ennetwork/musen-e/enhanced/.

[34] S. Guo, "Performance analysis of wireless intruder geolocation in campus wireless networks," in *Proc. Militray Communications Conference (MILCOM) 2012*, pp. 1–6, Oct-Nov 2012.

[35] Y. Wang and K. Ho, "TDOA source localization in the presence of synchronization clock bias and sensor position errors," *Signal Processing, IEEE Transactions on*, vol. 61, pp. 4532–4544, Sept 2013.

[36] Q. Liang, B. Zhang, C. Zhao, and Y. Pi, "TDoA for passive localization: Underwater versus terrestrial environment," *Parallel and Distributed Systems, IEEE Transactions on*, vol. 24, pp. 2100–2108, Oct 2013.

[37] F. R. Kschischang, B. J. Frey, and H.-A. Loeliger, "Factor graphs and the sum-product algorithm," *IEEE Trans. on Information Theory*, vol. 47, pp. 498–519, February 2001.

[38] E. Serpedin, T. Chen, and D. Rajan, *Mathematical Foundations for Signal Processing, Communications, and Networking*. CRC Press, 2012.

[39] J.-C. Chen, C.-S. Maa, and J.-T. Chen, "Factor graphs for mobile position location," in *Proc. IEEE International Conference on Acoustics, Speech, and Signal Processing (ICASSP) 2003*, vol. 2, pp. 393–396, April 2003.

[40] G. Giorgetti, A. Cidronali, S. K. S. Gupta, and G. Manes, "Single-anchor indoor localization using a switched-beam antenna," *Communications Letters, IEEE*, vol. 13, pp. 58–60, January 2009.

[41] J. Wang, J. Chen, and D. Cabric, "Cramer-rao bounds for joint RSS/DOA-based primary-user localization in cognitive radio networks," *IEEE Transaction on Wireless Communications*, vol. 12, pp. 1363–1375, March 2013.

[42] M. R. K. Aziz, K. Anwar, and T. Matsumoto, "A new DOA-based factor graph geolocation technique for detection of unknown radio wave emitter position using the first-order Taylor series approximation," *EURASIP Journal on Wireless Communications and Networking*. Conditional Accepted with Major Revision, Revision Submitted 4 Feb 2016.

[43] M. R. K. Aziz, K. Anwar, and T. Matsumoto, "DRSS-based factor graph geolocation technique for position detection of unknown radio emitter," *International Workshop on Advanced PHY and MAC Layer Design for 5G Mobile Networks and Internet of Things in conjunction with European WIRELESS 2016*. Accepted.

[44] G. Wang and H. Chen, "An importance sampling method for tdoa-based source localization," *Wireless Communications, IEEE Transactions on*, vol. 10, pp. 1560–1568, May 2011.

[45] T. Qiao, S. Redfield, A. Abbasi, Z. Su, and H. Liu, "Robust coarse position estimation for tdoa localization," *Wireless Communications Letters, IEEE*, vol. 2, pp. 623–626, December 2013.

[46] N. Okello, F. Fletcher, D. Musicki, and B. Ristic, "Comparison of recursive algorithms for emitter localisation using tdoa measurements from a pair of uavs," *Aerospace and Electronic Systems, IEEE Transactions on*, vol. 47, pp. 1723–1732, July 2011.

[47] R. H. Wu, "Alternative terminal navigation based on modified airport multilateration system," in *Digital Avionics Systems Conference (DASC), 2012 IEEE/AIAA 31st*, pp. 5B4–1–5B4–13, Oct 2012.

[48] Y.-P. Lei, F.-X. Gong, and Y.-Q. Ma, "Optimal distribution for four-station TDOA location system," in *Biomedical Engineering and Informatics (BMEI), 2010 3rd International Conference on*, vol. 7, pp. 2858–2862, Oct 2010.

[49] Y. S. Cho, J. Kim, W. Y. Yang, and C.-G. Kang, *MIMO-OFDM Wireless Communications with MATLAB*. Wiley, 2010.

[50] P. Bahl and V. Padmanabhan, "Radar: an in-building rf-based user location and tracking system," in *INFOCOM 2000. Nineteenth Annual Joint Conference of the IEEE Computer and Communications Societies. Proceedings. IEEE*, vol. 2, pp. 775–784 vol.2, 2000.

[51] M. R. K. Aziz, Y. Lim, and T. Matsumoto, "A new wireless geolocation technique using joint RSS-based Voronoi and factor graph," *9th Asia Modelling Symposium (AMS) 2015*, pp. 132–136, Sep 2015.

[52] M. R. K. Aziz, Y. Lim, and T. Matsumoto, "A new RSS-based wireless geolocation technique utilizing joint Voronoi and factor graph," *International Journal of Simulation: Systems, Science and Technology (IJSSST)*. Accepted on 23 March 2016.

[53] M. R. K. Aziz, K. Anwar, and T. Matsumoto, "Monitoring spot configuration of RSS-based factor graph geolocation technique in outdoor WSN environment," in *IEICE General Conference 2015*, March 2015.

[54] M. P. Wylie and J. Holtzman, "The non-line of sight problem in mobile location estimation," *IEEE Transactions on Signal Processing*, p. 827831, 1996.

[55] D. Gregoire and G. Singletary, "Advanced ESM AOA and location techniques," in *Aerospace and Electronics Conference, 1989. NAECON 1989., Proceedings of the IEEE 1989 National*, pp. 917–924 vol.2, May 1989.

[56] S. Kang and Z. Ming, "Passive location and tracking using DOA and TOA measurements of single nonmaneuvering observer," in *Aerospace and Electronics Conference, 1988. NAECON 1988., Proceedings of the IEEE 1988 National*, pp. 340–344 vol.1, May 1988.

[57] J. C. Peterson, *Technical Mathematics, 4th Edition*. Delmar, Cengage Learning, 2013.

[58] J. C. Wang, L. S. Huang, H. L. Xu, B. Xu, and S. L. Li, "A novel range free localization scheme based on voronoi diagrams in wireless sensor networks," *Journal of Computer Research and Development*, vol. 45, no. 1, pp. 119–125, 2008.

[59] S. Cai, H. Pan, Z. Gao, N. Yao, and Z. Sun, "Research of localization algorithm based on weighted voronoi diagrams for wireless sensor network," *EURASIP Journal on Wireless Communications and Networking*, vol. 50, pp. 1–5, 2014.

[60] L. Ni, Y. Liu, Y. C. Lau, and A. Patil, "Landmarc: indoor location sensing using active rfid," in *Pervasive Computing and Communications, 2003. (PerCom 2003). Proceedings of the First IEEE International Conference on*, pp. 407–415, 2003.

[61] P. Kulakowski, J. Vales-Alonsob, E. Egea-Lopez, W. Ludwin, and J. Garca-Haro, "Angle-of-arrival localization based on antenna arrays for wireless sensor networks," *Computers and Electrical Engineering*, vol. 36, pp. 1181–1186, April 2010.

[62] F. Gustafsson and F. Gunnarsson, "Mobile positioning using wireless networks," *IEEE Signal Processing Magazine*, vol. 22, pp. 41–53, July 2005.

[63] T. Qiao and H. Liu, "An improved method of moments estimator for toa based localization," *IEEE Communications Letters*, vol. 17, pp. 1321–1324, July 2013.

[64] S. M. Kay, *Fundamentals of Statistical Signal Processing: Estimation Theory*. Prentice Hall, 1993.

[65] G. Mao and B. Fidan, *Localization Algorithms and Strategies for Wireless Sensor Networks: Monitoring and Surveillance Techniques for Target Tracking*. New York: IGI Global, 2009.

[66] F. Yin, C. Fritsche, F. Gustafsson, and A. Zoubir, "Em- and jmap-ml based joint estimation algorithms for robust wireless geolocation in mixed los/nlos environments," *Signal Processing, IEEE Transactions on*, vol. 62, pp. 168–182, Jan 2014.

[67] J. Shen, A. Molisch, and J. Salmi, "Accurate passive location estimation using TOA measurements," *Wireless Communications, IEEE Transactions on*, vol. 11, no. 6, pp. 2182–2192, 2012.

[68] R. Kaune, "Accuracy studies for TDOA and TOA localization," in *15th International Conference on Information Fusion (FUSION) 2012*, July 2012.

[69] N. O'Donoughue and J. Moura, "On the product of independent complex gaussians," *IEEE Transactions on Signal Processing*, vol. 60, no. 3, pp. 1050–1063, 2012.

[70] G. Casella and R. L. Berger, "Statistical inference, 2nd edn. Duxbury," 2002.

[71] G. H. Golub and C. F. V. Loan, *Matrix Computations, 3rd edition*. Johns Hopkins University Press, 1996.

[72] M. S. Grewal and A. P. Andrews, *Kalman Filtering: Theory and Practice Using MATLAB, 2nd edition*. John Wiley and Sons, 2001.

[73] W. Liu and X. Huang, "Enhanced DOA tracking based on the PASTd algorithm with outlier rejection," in *2011 3rd International Conference on Signal Processing Systems (ICSPS 2011)*, pp. 29–36, 2011.

Publications

Journal Articles

[1] **M. R. K. Aziz**, K. Anwar, T. Matsumoto, "A New DOA-based Factor Graph Geolocation Technique for Detection of Unknown Radio Wave Emitter Position Using The First-Order Taylor Series Approximation," *EURASIP Journal on Wireless Communications and Networking (JWCN)*, Conditionally Accepted with Major Revision on 17 December 2016.

[2] **M. R. K. Aziz**, Y. Lim, and T. Matsumoto, "A New RSS-based Wireless Geolocation Technique Utilizing Joint Voronoi andFactor Graph." *International Journal of Simulation: Systems, Science and Technology (IJSSST)*, Accepted on 23 March 2016.

[3] **M. R. K. Aziz**, K. Anwar, T. Matsumoto, "A Pythagorean TDOA-based Factor Graph Geolocation Technique for Position Detection of An Unknown Radio Emitter," *IEEE Transactions on Vehicular Technology (TVT)*, (to be submitted).

Conference Proceedings

[4] **M. R. K. Aziz**, K. Anwar, T. Yamaguchi, S. Arata, T. Matsumoto, "Monitoring Spot Configuration of RSS-based Factor Graph Geolocation Technique in Outdoor WSN Environments," *IEICE General Conference*, Kusatsu, Kyoto, Japan, March 2015. – *Non-refeered*

[5] **M. R. K. Aziz**, K. Anwar, T. Matsumoto, "A New Wireless Geolocation Technique Using Joint RSS-based Voronoi and Factor Graph," *Asia Modelling Symposium (AMS) 2015)* , Kuala Lumpur, Malaysia, September 2015, **Best Paper Award**. – *Refereed*

[6] S. N. Karimah, **M. R. K. Aziz**, and T. Matsumoto, "A Hybrid TOA and RSS-based Factor Graph for Wireless Geolocation Technique". *CSPA2016: 12th IEEE Colloquium on Signal Processing and its Applications*, Malacca, Malaysia, March 2016. – *Refereed*

[7] **M. R. K. Aziz**, K. Anwar, and T. Matsumoto, "DRSS-based Factor Graph Geolocation Technique for Position Detection of Unknown Radio Emitter". *International Workshop on Advanced PHY and MAC Layer Design for 5G Mobile Networks and Internet of Things in conjunction with European WIRELESS 2016*, Oulu, Finland, May, 2016. – *Refereed*

Newsletter

[8] **M. R. K. Aziz**, K. Anwar, and T. Matsumoto, Joint RSS-DOA Factor Graphs based Geo-location Technique, *COST IC1004 Newsletter*, No.4, p.4, March 2013, Half A4 Page Paper.

Achievements

[9] Best Paper Award in Asia Modelling Symposium (AMS) 2015, September 2015, Kuala Lumpung, Malaysia.

[10] Selected Technical Document (TD) from total 87 presented TD in 6th Meeting COST IC1004, Feb 2013, Malaga, Spain, to be summarized in COST IC1004 News Letter March 2013 Edition.

Biography

Muhammad Reza Kahar Aziz received B.S. and M.S. (*cum laude*) degrees in Electrical Engineering (Telecommunications) from Institut Teknologi Bandung (ITB), Bandung, Indonesia, in 2004 and 2012, respectively. He is currently holding Doctor Research Fellow (DRF), while pursuing his PhD degree in Japan Advanced Institute of Science and Technology (JAIST). From 2004–2005, he was Microwave Service Engineer with Siemens Indonesia (PT. DGE). From 2005–2010, he had been with Ericsson Indonesia as Broadband Solution Engineer. Since 2012, he has joined to Institut Teknologi Sumatera (ITERA), Indonesia. He received 10% top performer Ericsson Indonesia employee in 2009 and ITB Voucher Scholarship in 2011. He also received Overal Best Paper Award in Asia Modelling Symposium (AMS) 2015. His research interests include wireless communication system, signal processing, and radio geolocation using graph.